Development of Algorithms to Analyze Electrogastrography (EGG) for Neonatal Gastrointestinal Development and Electroencephalography (EEG) for Effects of LED-based Pre-frontal Light Stimulation

by

AKHIL CHAUDHARI

DISSERTATION

Presented to the Faculty of the Graduate School of

The University of Texas at Arlington in Partial Fulfillment

Of the Requirements

For the Degree of

DOCTOR OF PHILOSOPHY

THE UNIVERSITY OF TEXAS AT ARLINGTON

MAY 2022

ACKNOWLEDGMENTS

First, I would like to acknowledge and thank my advisor, Dr. Hanli Liu for her unrelenting guidance, mentorship, and support towards completing the degree. Her advice and mentorship have proved to be invaluable.

Second, I would like to thank my committee members, Dr. Alexandrakis, Dr. Papadelis, Dr. Ortigoza for their time and guidance on this work. In particular, Dr. Ortigoza has also mentored my research and encouraged collaboration and discussion with his lab.

Third, I would like to extend my appreciation to fellow doctoral, post-doctoral colleagues for their assistance and support in my research including Dr. Wang, Dr. Nghi Troung, Dr. Wu, Dr. Yudhajit Das, Dr. Hashini Wanniarachchi, Dr. Tyrell Pruitt, Devarshi Desai, Gauri Kathote, Saurabh Nair and Shruti Naik.

Finally, and most importantly, I would like to thank my family for always supporting me in every possible way. I especially would like to thank my dad, Dr. Mahendra Chaudhari, for providing me unconditional love and support for having a good education and a good life.

TABLE OF CONTENTS

LIST OF FIGURES

LIST OF TABLES

ABSTRACT

Development of Algorithms to Analyze Electrogastrography (EGG) for Neonatal Gastrointestinal Development and Electroencephalography (EEG) for Effects of LED-based Pre-frontal Light Stimulation

Akhil Chaudhari

The University of Texas at Arlington, 2022

Supervising Professor: Dr. Hanli Liu

Algorithm development, and biological signal processing are the key components for new applications of successful medical diagnosis that can provide physiological and functional information to better understand human condition for either patients with certain diseases or healthy human beings. Neuroimaging tools, such as functional near infrared spectroscopy (fNIRS), and electrogastrography (EGG) have been used to investigate the gut maturity in diseased and healthy state; and electroencephalogram (EEG) have been used to investigate brain functions in response to neuromodulated or task-based interventions. Accordingly, my dissertation focused on algorithm development and signal processing for two major topics: (1) to outline EGG response to gastrointestinal maturity in preterm, term neonates under different feeding intervention conditions. (2) to map electrophysiological responses in healthy human brain in response to transcranial photobiomodulation (tPBM) using Light Emitting Diode (LED). Furthermore, LED-tPBM is an important neuromodulation tool for treating several neurological disorders, as well for enhancement of cognition, hence it is essential to monitor electrophysiological changes induced by LED-tPBM on healthy human head.

Enteral feeding can be challenging in preterm neonates because of gastrointestinal (GI) immaturity leading to feeding intolerance. Current techniques to monitor feeding intolerance are non-specific and poor predictors of GI maturity and feeding readiness. Objective measures of GI maturity are needed for accurate assessment of feeding readiness. Electrogastrography (EGG) is a non-invasive technology that can be used to measure gastric myoelectrical activity in neonates of different gestational ages (GA). Hence in this aim we characterized different parameters of gastric myoelectrical activity such as mean power spectral density, % time in bradygastria, % time in normogastria, and % time in tachygastria by EGG in neonates of different GA before, during and post feeding.

Transcranial photobiomodulation (tPBM) is a novel optical neuromodulation method that uses lasers or light emitting diodes (LED) to improve human cognitive functions for various brain disorders in the human brain. However, there is a lack of investigations on the improvement of cognitive and electro-physiological functions in the healthy human brains. This work addresses the knowledge gap of electro-physiological responses while performing a vigilance based task induced by LED-based tPBM in healthy human head.

Specifically, chapter 2 depicts the characterization of different parameters of gastric myoelectrical activity by EGG in neonates of different GA before, during and post feeding. The EGG signals were analyzed for respective mean Power spectral density (PSD) at the three gastric rhythms (GR; i.e. bradygastria (0.5-2 cpm), normogastria (2-4 cpm), tachygastria (4-9 cpm)). These results suggest that feeding dependent mean PSD values in normogastria (2-4 cpm) and tachygastria (4-9 cpm) increased significantly with increase of GA. The percent time spent in normogastria was also found to increase with increased GA.

In Chapter 3, the effects of tPBM applied on right forehead is investigated while performing vigilance based task (PVT) as measured by EEG. To help understand the eletro-physiological changes induced by LED-based tPBM, acute changes in power in scalp were quantified. These findings imply that LED-based stimulation for ten minutes significantly affect brain activity. The Delta (0.5-4 Hz) and alpha (7-13 Hz) band power significantly increased under LED stimulation while performing PVT task. Further EEG power at the temporal lobe and motor regions was found to increase in delta band, and parieto-occipital, left-temporal lobes in the healthy human brain.

Chapter 4 further expands on the effect of LED-based stimulation on reaction time and electro-physiological changes induced by four weeks of stimulation. To help understand the effect of LED-based stimulation on reaction time, the reaction time was compared across time (weeks) for both LED and sham treated groups. The electro-physiological changes after four weeks of LED-based stimulation were quantified by comparing the power changes across four weeks for both LED and sham treated groups. Further source localization was performed to identify the brain networks activated under LED-based stimulation. These findings suggests that reaction time significantly decreases over four weeks suggesting improvement in vigilance. The Power in Theta (4-7 Hz), Beta (13-30 Hz), and Gamma (30-70 Hz) frequency bands significantly increases after four weeks under LED-based stimulation. Furthermore, power increment was also found in default mode network, executive control network, fronto-parietal network, and visual network. These results may help understand the underlying mechanisms of LED-based tPBM modulated brain networks while performing vigilance tasks.

Chapter 1

Introduction

Biological signal processing, algorithm development are key components for new applications of successful medical diagnosis that can provide functional and physiological information to better understand human condition for either patients with certain diseases or healthy human beings. In particular, neuroimaging tools, such as electrogastrography (EGG) and functional near infrared spectroscopy (fNIRS), have been used to investigate the gut maturity in healthy and diseased state, and electroencephalogram (EEG) have been used to investigate brain functions in response to neuromodulated or task-based interventions. Accordingly, my dissertation focused on signal processing and algorithm development for two specific topics: (1) to outline EGG response to gastrointestinal maturity in preterm, term neonates under feeding conditions. (2) to map electrophysiological responses in healthy human brain in response to transcranial photobiomodulation (tPBM) using Light Emitting Diode (LED). Furthermore, since LED-tPBM is an important neuromodulation tool for treating several neurological disorders, as well for enhancement of cognition, it is essential to monitor electrophysiological enhancement by LED-tPBM.

One of the most challenging tasks in neonatal intensive care is feeding preterm neonates via the enteral route. Because of gastrointestinal (GI) immaturity, preterm neonates can develop feeding intolerance, which leads to significant health problems including malnutrition and poor neurodevelopment outcomes (1-3). If a sensing methodology is available to measure the GI maturity in preterm neonates non-invasively and effectively, it will enable pediatric clinicians to gain insight and predict whether a preterm neonate will tolerate feed or develop intolerance.

However, current clinical methods used to sense feeding intolerance are dependent on direct observations with non-specific parameters such as abdominal circumference, bowel sounds, and stool patterns. All these parameters are poor biomarkers to predict GI maturity and success of enteral feeding.

EGG has been used in adult population in the past decade to investigate gastric dysfunctions such as gastroparesis (4, 5), gastroesophageal reflux (6, 7), delayed gastric emptying, abnormalities of central nervous system (8, 9), and functional dyspepsia (10, 11). Feeding compositions, prokinetic agents, and gut hormones' effect on gastric motility have been studied extensively using EGG (12, 13). The information and characterization on the gastric development of preterm neonates during feeding were inadequate and with highly dispersed results in the literature. Hence my first aim is to develop a novel time frequency methodology to characterize EGG data and identify biomarkers for sensing GI maturity in preterm neonates. The novelty of this aim included the following three aspects: (i) We applied continuous wavelet transform (CWT) to EGG time series taken from a cohort of perterm (47) and term (4) neonates. CWT enabled the non-stationary, time-frequency analysis for quantification of EGG spectral powers in different frequency bands such as bradygastria (0.5 – 2 cpm), normogastria (2 – 4 cpm), and tachygastria (4 – 9 cpm). The advantage of utilizing CWT was the ability to analyze changes in gastric myoelectrical activity that occurred as a result of enteral feeding and the changes that occurred with maturity. (ii) We investigated frequency-specific mean PSD values and percentage of time spent at each of the three frequency bands at all three feeding periods (i.e., pre-, during-, and post-feeding) for both preterm and term neonates. (iii) We obtained the significant and

linear dependance of (1) feeding-associated mean PSD in tachygastria and (2) percent time spent in normogastria on the increasing gestational age.

Photobiomodulation (PBM) is a novel method used for modulating cellular function and mitochondrial respiration using light (14, 15). It involves the absorption of high-energy photons photo-oxidizes the mitochondrial respiratory enzymes to produce a higher amount of cellular ATP. Vargas et al. presented that brain oxygenation increases with a higher tPBM laser light dosage (16). Wang et al. have non-invasively measured the increase in CCO concentration during and after laser tPBM (17, 18). Many 1064-nm infrared laser studies have reported improvements in cognitive performance in healthy individuals (19, 20). One of our previous neurophysiological studies has shown that tPBM using a 1064-nm laser stimulation could result in acute increase in alpha (7-13 Hz), and beta (13-30 Hz) EEG oscillations in the resting state of the human brain (21). Previous EEG studies have investigated various neurophysiological effects for LED based tPBM, such as visual size (22), luminance contrast (23), and chromatic contrast (24). LED-based tPBM also has applications in treatment of various conditions such as dementia (25), and anxiety control (26). However, all these studies focus on studying patients with neurological or psychological disorders. Hence my second aim is to study the electrophysiological effects induced by LED-based tPBM on healthy human brain. This aim is significant as it allows to study the electrophysiological effects induced by LED-tPBM on healthy human brain.

LED-based tPBM has been of interest because of its various advantages like easy-to-use, cheap, having low dose, and being harmless makes it a preferable choice for conducting tPBM. LED-based tPBM has been used in the past to treat various diseases and patients with brain injury (27). Nine months of LED-based tPBM on traumatic brain-injured subjects showed significant

improvement in executive function and memory (27). LED-based tPBM for twelve weeks on dementia patient showed improvement in functions like fewer angry outbursts, less anxiety, and better sleep patterns (28). However, these physiological effects of LED-based tPBM have never been studied on healthy human head while performing cognitive tasks. Hence, my third aim is to study the longitudinal effect of LED-based tPBM stimulation. This study is important as it would help to replace the conventionally used lasers with harmless LED-based tPBM to improvement cognition in healthy human.

The scope of my dissertation focuses on signal processing and algorithm development for two specific topics: (1) to outline EGG response to gastrointestinal maturity in preterm, term neonates under feeding conditions. (2) to map electrophysiological responses in healthy human brain in response to LED-based tPBM. There are three specific aims, as follows:

Aim 1: Time-frequency analysis to investigate/characterize gastrointestinal development in pre-term and full-term neonates measured by EGG and NIRS.

- Aim 1a: PSD (power spectral density)-based analysis to quantify/characterize averaged EGG power density for bradygastria, normogastria, and tachygastria frequency bands in the pre, during, and post-feeding periods for early, mid, and full-term neonates followed by finding a significance differences among them;
- Aim 1b: CWT (continuous wavelet transform)-based, time-frequency analysis to identify percentage time spent in each of bradygastria, normogastria, and tachygastria frequency bands in the pre, during, post-feeding periods for early, mid and full-term neonates, followed by find significance differences among them;

Aim 2: Alternations of electroencephalogram (EEG) oscillation powers induced by LED-based, right-forehead, 10-min tPBM measured by 64-channel EEG.

- Aim 2a: Experimental protocol, setup, and participants recruitment for LED-based tPBM;
- Aim 2b: Global analysis of power spectral density (PSD) across all 64-channels for all five frequency bands under both sham and tPBM intervention, followed by statistical comparisons between the two (sham and tPBM) intervention conditions;
- Aim 2c: Channel-wise analysis for PSD topography for all five frequency bands under both sham and tPBM intervention, followed by statistical comparisons between the two (sham and tPBM) intervention conditions (with cluster-wise statistical analysis using Fieldtrip).

Aim 3: Alterations of electroencephalogram (EEG) oscillation powers induced by LED-based, right-forehead, 10-min tPBM measured by 64-channel EEG.

- Aim 3a: Behavioral effects caused by 4-week repeated LED-tPBM stimulation;
- Aim 3b: Global PSD analysis for all five bands under both sham and tPBM intervention, followed by statistical comparisons between the tPBM-induced net changes in PSD in week 1 vs. week 4 for all frequency bands;
- Aim 3c: Channel-wise analysis for PSD topography for all five bands under both sham and tPBM intervention, followed by statistical comparisons between the tPBM-induced net changes in PSD topography in week 1 vs. week 4 for all frequency bands;

- Aim 3d: Leading to potential sources of EEG signals affected by LED-tPBM using e-LORETA.

Chapter 2

Time-frequency Analysis to investigate gastrointestinal development in pre-term and full-term neonates measured by EGG and NIRS:

Authorship: Akhil Chaudhari, Xinlong Wang, Lindsay Roblyer, Rina Sanghavi, Hanli Liu, and Eric B. Ortigoza.

2.1 INTRODUCTION

One of the most challenging tasks in neonatal intensive care is feeding preterm neonates via the enteral route (Figure 1(a)). Because of gastrointestinal (GI) immaturity, preterm neonates can develop feeding intolerance, which leads to significant health problems including malnutrition and poor neurodevelopmental outcomes [1-3]. If a sensing methodology is available to measure the GI maturity of preterm neonates non-invasively and effectively, it will enable pediatric clinicians to gain insight and predict whether a preterm infant will tolerate feeds or develop intolerance. However, current clinical methods used to sense feeding intolerance are primary, mainly depending on direct observations with non-specific parameters such as abdominal circumference, bowel sounds, and stool patterns. All these parameters are poor biomarkers to predict GI maturity and success of enteral feeding. Thus, it is highly desirable and necessary to develop or adapt a non-invasive device and methodology to quantify GI maturity for more accurate assessment of feeding readiness for preterm babies.

Electrogastrography (EGG) is a noninvasive technique used to record gastric myoelectrical activity using cutaneous electrodes placed on the abdominal skin over the stomach. Figure 2-1(b)

shows an example of EGG setting on a model infant. Gastric myoelectrical activity consists of slow waves and spike potentials. EGG measures gastric slow waves or gastric rhythms (GR), which determine the frequency and propagation of stomach smooth muscle contractions. While EGG records time series, the frequency-domain analysis is often used exhibiting three major frequency bands for three gastric rhythms between 0.5-9 cycles per minute (cpm), namely, bradygastria ($0.5 \leq GR < 2$ cpm), normogastria ($2 \leq GR < 4$ cpm), and tachygastria ($4 \leq GR < 9$ cpm). Accordingly, spectral-power-related parameters were widely used to characterize the development or health conditions of the GI tract, such as dominant frequency, dominant power, power ratio, % bradygastria, % normogastria, % tachygastria, instability coefficient (29, 30).

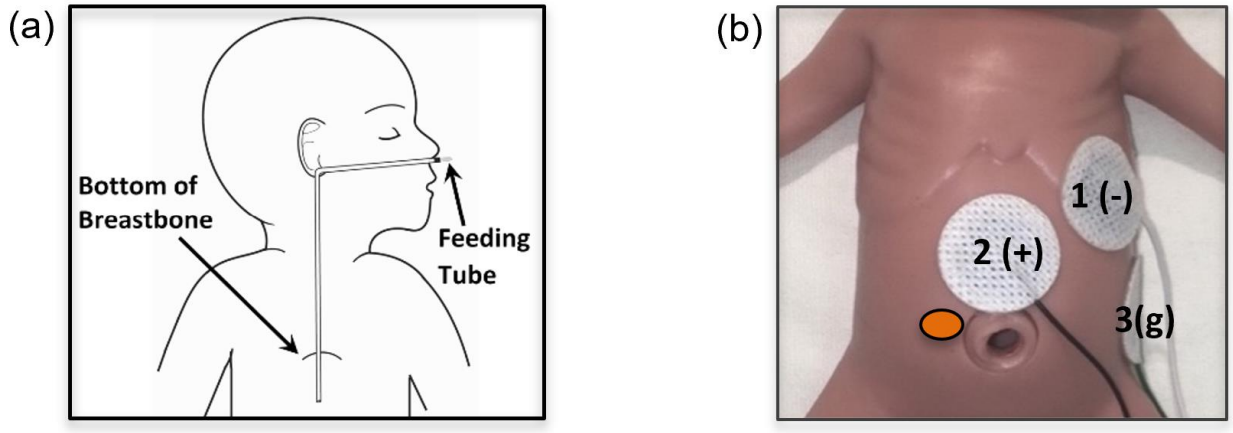

Figure 2-1: (a) A cartoon to show the tube setup and anatomical geometry of enteral feeding. (b) Setup of three EGG electrodes. The negative electrode (marked by '1 (-)') is placed on the left upper quadrant, near the mid-clavicular line. The positive electrode (marked by '2 (+)') is placed midway between the bottom of breastbone and the belly button, slightly below the level of the negative electrode. The ground electrode (marked by '3(g)') is placed at the mid-axillary line,

below the left costal margin. The orange spot next to the belly button marks the location of a NIRS sensor.

Because of its non-invasive nature, EGG has been used to monitor preterm infants with a setup as shown in Figure 1(b) on a model infant. However, the use of EGG to characterize GI maturity in preterm babies during or post-feeding is sparce with dispersed results in the literature. Lange et. al. showed no significant difference in the EGG dominant frequency between pre- and post-feeding and in the EEG power ratio between post-feeding power vs. pre-feeding power (30). Precioso et. al. reported no significant difference in % normogastria between term and preterm neonates in the pre- and Post-feed periods (11). Ortigoza et. al. reported a significant increase in Post-feed dominant power across the gastric spectrum (i.e., 0.5-9 cpm) (31). Moreover, most of the studies were limited to the comparisons between the pre- and post-feeding period, not during the actual feeding period. In particular, most of reported and analyzed parameters focused on dominant frequency, dominant power, power ratio, % bradygastria, % normogastria, % tachygastria, and instability coefficient. All these parameters were introduced several decades ago and may lack of updated development on its mathematical or computational algorithms, which may partially account for the dispersed results in the literature.

To better understand the rigor and derivation of these parameters, we performed a brief literature review and found that most of frequency-domain analyses used for EGG temporal data processing were different from the power spectral density (PSD) analysis. The latter is a well-accepted, signal-processing tool for decades in the engineering field and in the field of electroencephalogram (EEG), in particular, for analyses of multi-channel EEG time series. In definition, PSD quantifies the distribution of rhythm power over frequency components of the

signal and facilitates essential analyses of time series in many engineering and biomedical applications.

Thus, one goal of this study was to quantify and characterize PSD of EGG in preterm infants at three respective GR bands (i.e., mPSDGR) during three sub-feeding periods (pre-, during, and post-feed). The specific hypotheses in this study were that (i) mPSD increases during enteral feeding regardless of the GR frequency range, (ii) mPSD in the regular gastric rhythm (i.e., mPSDnormo) increases during feeding with increasing gestational age, and (iii) percent normogastria ($2 \leq GR < 4$ cpm) increases linearly with increasing gestational age for preterm infants. The overall goal was to develop and update the time-frequency analysis methodology to characterize EGG data and identify non-invasive biomarkers for sensing GI maturity in preterm infants at all 3 sub-feeding periods (pre-, during, and post-feed) instead of only pre-and Post-feed as customary.

The novelty of our study included the following three aspects:

(1) Technically, we applied continuous wavelet transform (CWT) (instead of fast Fourier transform) to EGG time series taken from a cohort of preterm (61) and term (5) neonates. CWT enabled the non-stationary, time-frequency analysis for quantification of EGG spectral powers in bradygastria, normogastria, and tachygastria. The advantage of utilizing CWT was the ability to analyze changes in gastric myoelectrical activity that occurred as a result of enteral feeding and the changes that occurred with maturation.

(2) We investigated frequency-specific mean PSD values and percentage of time spent at each of the three frequency bands (bradygastria, normogastria, and tachygastria) at all three feeding periods (i.e., pre-, during, and post-feeding) for each of both preterm and term neonates.

(3) We obtained the significant and linear dependance of (i) feeding-associated mean PSD in tachygastria and (ii) percent time spent in normogastria (2-4 cpm) on the increasing gestational age.

2.2 MATERIAL AND METHODS

2.2.1 Study Design

The study design was a longitudinal, prospective cohort study from 2017-2020 in which participants underwent weekly EGG monitoring until 40 weeks Gestational age (GA), discharge, or death, whichever came first.

2.2.2 Neonates

Sixty-six neonates (61 preterm and 5 term) from the neonatal intensive care unit (NICU) at Parkland Health and Hospital System and Children's Health in Dallas, Texas, were included in the study from 2017-2020 after parental consent. The Institutional Review Board at the University of Texas Southwestern Medical Center approved the study.

Inclusion and exclusion criteria: Participants were preterm neonates $<$ 34 weeks' of gestational ages (GA) and term neonates $\geq$ 37 weeks of GA at birth. Term neonates were enrolled as a study reference. Neonates were excluded if they had a known congenital or chromosomal disorder, significant clinical instability, or major skin abnormalities that would preclude placement of skin electrodes. Neonates were stratified by GA as early (<29 weeks of GA), mid (29-33 weeks of GA), and term (≥37 weeks of GA).

Electrogastrography data from this pilot study was obtained from a larger longitudinal study of GI development to investigate coherent features between gastric myoelectrical activity (by EGG) versus abdominal oxygenation (by near infrared spectroscopy; NIRS). Infants without NIRS data were excluded from EGG analysis in this study to avoid any bias due to un-identical experimental setups. Thus, we included 51 (47 preterm and 4 term) infants, who had concurrent EGG and NIRS readings, for the data analysis in this study.

2.2.3 Setup and Experimental Paradigm

2.2.3.1 *Electrogastrography (EGG)*

Neonatal EGG electrodes were placed onto each neonate's abdominal skin as validated and described in Chen et al. 1999 and others (31-34). The setup was limited to 3 electrodes (see Figure 2-1(b)) due to the abdominal size of neonates. Data acquisition was carried out using the data acquisition unit (BIOPAC Systems, Inc., Goleta, CA) of the BIOPAC(R) MP36 System.

2.2.3.2 *Near-Infrared Spectroscopy (NIRS)*

Neonatal INVOS™ Infant Regional Saturation Sensor (Covidien Ltd., Minneapolis, MN) was placed to the right of the belly button (marked by the orange spot in Figure 2-1(b)), while the control probe was placed on the baby's forehead. A cardiorespiratory monitor and an INVOS system took recordings concurrently from the participating neonates via a Vital Sync™ 5000 System (Covidien Ltd., Minneapolis, MN) for time synchronization between the two devices. However, the recorded NIRS signal was not the topic of this study and thus excluded for further analysis.

2.2.3.3 *Feeding*

Feeding was at the discretion of the clinical team. Because most babies in the NICU were fed every 3 hours, the timing of EGG recording was 6 hours to ensure that 2 pre-, 2 during, and 2

Post-feed periods were included. EGG recordings included the 3 sub-feeding periods (pre-, during, and post-feed). The EGG data were further analyzed, presented, and discussed in following sections.

2.2.4 Data processing

2.2.4.1 *EGG Data Preprocessing*

Raw EGG data were collected at a sampling frequency of 2000 Hz and then preprocessed using MATLAB (Mathworks®, Natick, Massachusetts) as follows: (1) data were down sampled to 500 Hz using MATLAB function “downsample”; (2) a 3rd order polynomial fit was performed with MATLAB function “polyfit” for data detrending to obtain a temporal trend for the down-sampled time series; (3) the fitted trend was subtracted from the down-sampled data (35, 36); (4) the detrended time series was filtered using a low-pass filter at 1 Hz with the “filtfilt” filter in MATLAB to avoid any filtering-induced phase shift.

2.2.4.2 *Selections of Sub-feeding Periods*

We divided the pre-processed data into pre-, during, and post-feed periods. Divisions of sub-feeding periods are demonstrated in Figure 2-2. Each infant’s EGG recording included two major feeding periods, namely, Feeding 1 and Feeding 2, each of which was further divided into Pre-, During-, and Post-feed. During-feed 1 and During-feed 2 were extracted within Feeding 1 and Feeding 2, respectively, based on the actual duration of administration of the enteral feed. The time for Pre-feed 1 was chosen to be no greater than 30 min. Similarly, the Post-feed 2 would be no greater than 30 min long. The time interval between the end of During-feed 1 and the start of During-feed 2 was then divided into two equal-time halves. The first temporal half (no longer

than 30 minutes) was labeled as Post-feed 1; the second temporal half (no longer than 30 minutes) was labeled Pre-feed 2, as illustrated schematically in Figure 2-2.

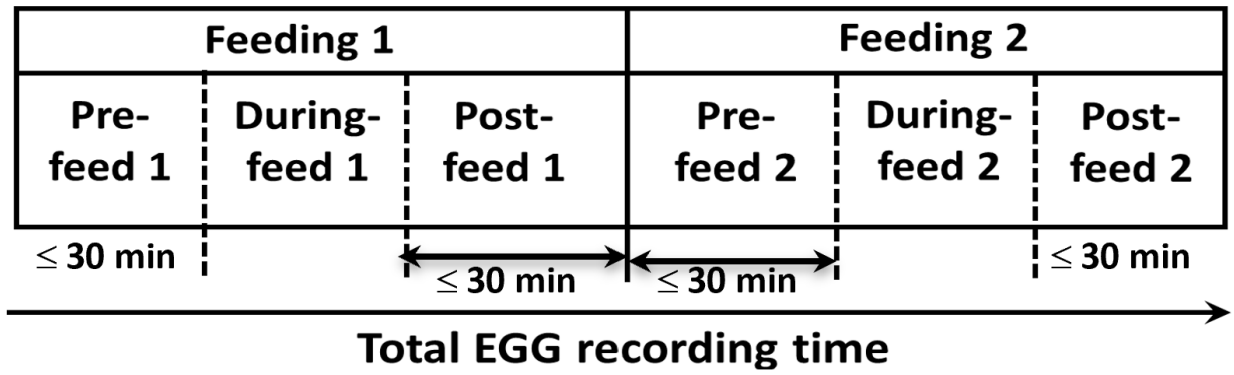

Figure 2-2: EGG data were first sectioned into two feeding periods. Then, Feeding 1 included Pre-feed 1, During-feed 1, and Post-feed 1, followed by Feeding 2 with Pre-feed 2, During-feed 2, and Post-feed 2.

2.2.4.3 *Mean Power Spectral Density (PSD) of EGG at three Gastric Frequencies*

There were several steps taken in this processing routine.

Step 1: The PSD across the entire gastric frequency band (0.5-9 cpm) during each of the six feeding periods (i.e., Pre-feed 1, During-feed 1, Post-feed 1, Pre-feed 2, During-feed 2, and Post-feed 2) was calculated using the native MATLAB function of "pwelch" (with the down-sampled frequency of 500 Hz, 4-min window and 2-min overlap) for each neonate. The 4-min window resulted in a frequency resolution of 0.004 Hz (or 4 mHz) in PSD calculation between 0 to 1 Hz.

Step 2: Mean PSD values over three sub-feeding periods were quantified by averaging them between Pre-feed 1 and Pre-feed 2, During-feed 1 and During-feed 2, and Post-feed 1 and Post-feed 2.

Step 3: Spectral means of PSD across each band were performed for all three gastric rhythm bands of interest, $m\text{PSD}_{GR}$, where "GR" represents Bradygastria ($0.5 \leq f < 2$ cpm; $0.008 \leq f < 0.033$ Hz), or Normogastria ($2 \leq f < 4$ cpm; $0.033 \leq f < 0.067$ Hz), or Tachygastria ($4 \leq f < 9$ cpm, $0.067 \leq f < 0.15$ Hz) during each sub-feeding period.

Step 4: group-level values of $m\text{PSD}_{brady}$, $m\text{PSD}_{normo}$, and $m\text{PSD}_{tachy}$ were calculated across three GA infants, namely, early GA (<29 weeks), mid GA (29-33 weeks), and term GA (≥37 weeks) infants for each of the three sub-feeding periods (i.e., pre-, during, and post-feed).

Step 5: Statistical analysis: the group-level $m\text{PSD}_{brady}$, $m\text{PSD}_{normo}$, and $m\text{PSD}_{tachy}$ were compared among three sub-feeding periods for each of the three neonate groups at each GR band separately using one-way ANOVA, followed by Tukey's post-hoc test. Also, linear regression was performed to determine the relationship between GA versus $m\text{PSD}_{GR}$ at each GR frequency band for each GA group.

2.2.4.4 *Continuous wavelet transform for non-stationary EGG signal processing*

Because EGG signal is non-stationary, CWT would be a rigorous processing method for its time-frequency analysis, in particular, to quantify its time-dependent spectral features. To perform CWT, we first filtered EGG data between 0.5-15 cpm using a zero-phase bandpass butterworth filter in MATLAB. Next, each filtered EGG time series was analyzed to achieve a time-frequency spectrogram per each of the sub-feeding periods including both Feeding 1 and Feeding 2 (see Figure 2-3) using a native MATLAB function "cwt" for each neonate. Figure 2-3(a) shows an example of CWT-derived spectrogram from one of the neonates during Feeding 1 period (96 min), while Figure 2-3(b) is a zoomed spectrogram within 9-10 min. Gray areas in this figure, are

called Cone of Inference (COI) that results from the edge effect of CWT (37). Values within COI are considered highly non-reliable and thus excluded from the analysis.

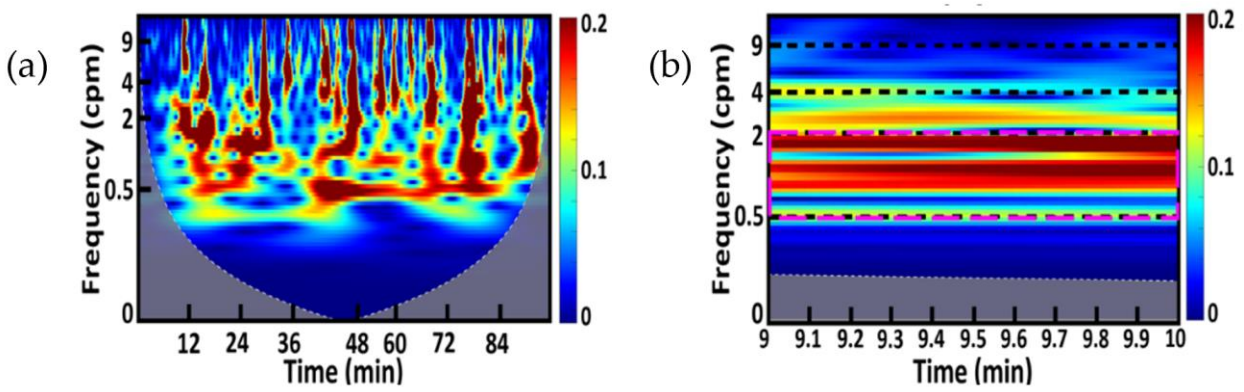

Figure 2-3: (a) A CWT-derived spectrogram from one of the neonates during Feeding 1, including 30-min pre-feed, 30-min during feed, and 36-min post-feed. The horizontal x-axis represents time in min over 96 min; the vertical y-axis denotes the frequency in cpm between 0-9 cpm plotted in log scale; and the color bar represents wavelet transform power of an EGG time series. (b) A zoomed spectrogram at 9-10 min from panel (a). Several horizontal lines mark the three frequency bands of interest (bradygastria: 0.5-2 cpm; normogastria: 2-4 cpm; tachygastria: 4-9 cpm). The pink dashed box indicates the dominant frequency band for this particular minute being considered (see text in Section 2.4.5 for details).

2.2.4.5 Percentage of time spent in each gastric rhythm during each sub-feeding period

Another characteristic feature of EGG signal from preterm neonates was percentage time spent in each gastric rhythm (GR) during three sub-feeding periods. Term babies are expected to have higher % normogastria, than early and mid GA preterm infants. Preterm infants (early and mid GA) are expected to have a higher % bradygastria and % tachygastria, than term infants, suggesting GI immaturity.

To determine the % time that each GA infant group spent on at each of the three GR bands, several steps were executed:

Step 1: Three EGG GR frequency bands, as marked in Figure 2-3(a), were identified. Accordingly, spectral and temporal averaging over each minute of respective CWT power values for each GR band were performed.

Step 2: The dominant frequency band per minute among the three GR-specific band (i.e., bradygastria, normogastria, and tachygastria) was determined by choosing the largest ratio between each of the three GR-specific CWT powers versus the total power over the entire 0.5-9 cpm band at the respective time. As an example, the pink box in Figure 2-3(b) outlines the GR band for bradygastria, which had the highest CWT power ratio and thus was considered the dominant frequency for the 9-10 minute interval. In general, the ratios at the three GR bands reflected frequency distributions of gastric myoelectrical activity of the infant in that minute.

Step 3: The two steps described above were repeated to identify the dominant frequency band for each minute over each of the six sub-feeding periods (i.e., Pre-feed 1, During-feed 1, Post-feed 1, Pre-feed 2, During-feed 2, and Post-feed 2). In this way, we created a time-dependent dominant frequency distribution and partition map for each sub-feeding period, as demonstrated in Figure 2-4(a). Each red box represents the dominant frequency band during each minute, and only one box appears per minute.

Step 4: The total number of rex boxes in each GR band shown in Figure 4(a) represents the total time, T_{GR}, during which the corresponding GR was dominant for the selected time

period, such as pre-, during, or Post-feed (within Feeding 1 or Feeding 2). Only one T_{GR} was chosen per minute among bradygastria, normogastria, and tachygastria.

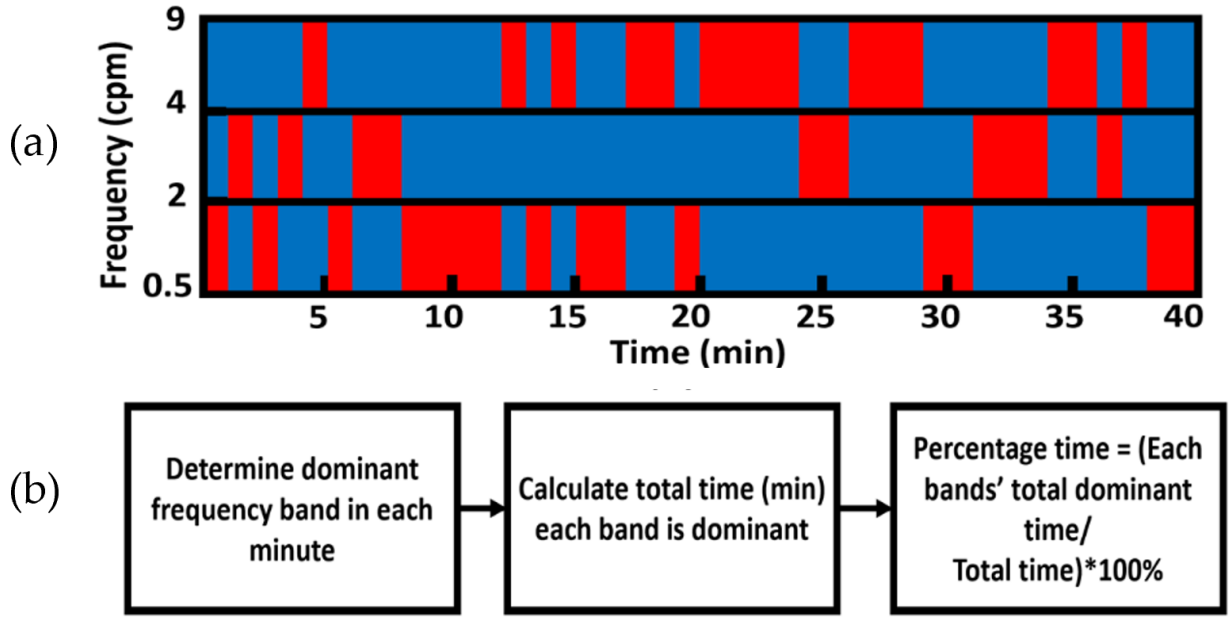

Figure 2-4: (a) Dominant frequency band partition map for each minute across a whole time period (0-40 min). X-axis denotes the time in minutes; Y-axis represents EGG rhythm frequency in cycles per minute (cpm). Red boxes indicate the dominant frequency band for each minute. (b) A flow chart of the procedure to calculate the % time spent in each GR band for each sub-feeding period.

Step 5: The percentage of time spent in each GR band during a selected time period (such as Pre-feed 1, During-feed 1, Post-feed 1, Pre-feed 2, During-feed 2, and Post-feed 2) was quantified by dividing T_{GR} (= number of red boxes in the respective frequency band) by the total minutes during the chosen feeding period, as outlined in Figure 4(b). Using this method, we obtained respective % bradygastria, % normogastria, and % tachygastria for each neonate in all sub-feeding periods.

Step 6: Then we averaged % bradygastria, % normogastria, and % tachygastria, respectively, over two Feeding periods for each sub-feeding period of each neonate (i.e., Pre-feed 1, Pre-feed 2; During-feed 1, During-feed 2; Post-feed 1, Post-feed 2). This was done to examine whether the percentage time spent on each GR band depended on feeding conditions.

Step 7: The percentage time spent in each GR frequency band during each sub-feeding period was plotted against the GA of each neonate. Linear regression was performed to determine the linear relationship between GA versus percentage time spent at each GR band. The significance level was set to be $p<0.05$.

2.3 RESULTS

2.3.1 Study Cohort

Sixty-six participants consented to participate in the study during the enrollment period (2017-2020). Fifteen participants were excluded (1 was too unstable for EGG recording, 1 had poor skin integrity, 3 had missing or poor data quality, and 10 did not have identical experimental setup because of missing NIRS measurements). Five subjects withdrew prior to completion of the protocol because of reasons unrelated to the study. For all withdrawn subjects, parental permission was obtained to analyze and include any data that was acquired prior to the date of withdrawal. Thus, 51 neonates (47 preterm, 4 term) were included in the study. None of the subjects developed any study-related skin complications.

2.3.2 Quantification of mPSD at three gastric frequency bands

After following the four steps given in Section 2.2.4.3, we were able to obtain group-level PSD of EEG in the GR frequency range of 0.5–9 cpm during different feeding periods. Figure 2-5 shows a set of such PSD plots from (a) early GA (n=25), (b) mid GA (n=22), and (c) term (n=4) infants in the During-feed period averaged between Feeding 1 and Feeding 2. By taking spectral average across each of the three GR bands (as marked in the Figure), we were able to obtain *m*PSD$_{brady}$, *m*PSD$_{normo}$, and *m*PSD$_{tachy}$, respectively, for each GA infant group and then for each of the three sub-feeding periods (i.e., pre-, during, and post-feed).

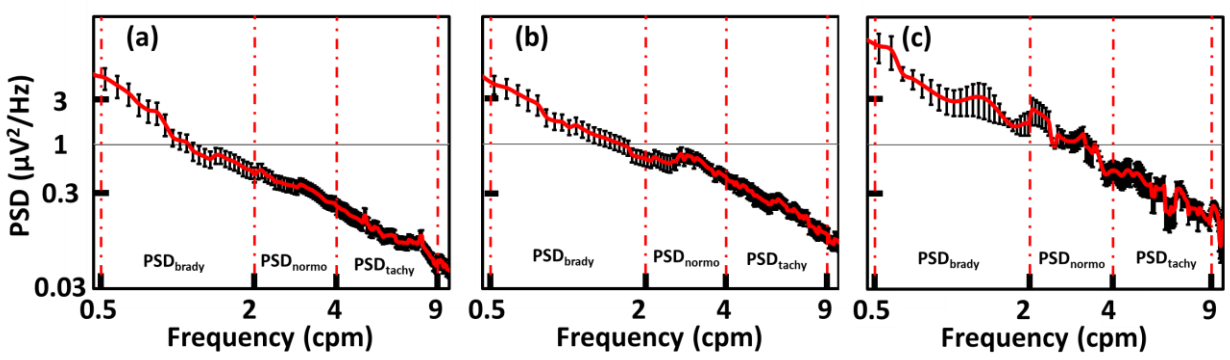

Figure 2-5: An example of group-level PSD taken from (a) early GA (n=25), (b) mid GA (n=22), (c) term infants (n=4) in the During-feed period averaged between Feeding 1 and Feeding 2. X-axis is the GR frequency of EGG in cpm, and y-axis is the power spectral density in μV2/Hz. The red, dashed vertical lines mark the GR frequency bands of bradygastria (Brady), normogastria (Norm), and tachygastria (Tachy). The error bars represent the standard error of the mean from four term infants.

2.3.3 GA-dependent *m*PSD$_{GR}$ values during the feeding periods

Figures 2-6(a) and 2-6(b) show among-group comparisons of GA-dependent *m*PSD values at all three GR (bradygastria, normogastria, and tachygastria) bands, respectively. The most consistent

and noticeable feature among these three panels is the significant increase in *m*PSD values in the During-feed period as the GA of infants increased. Corresponding p values for different pairs of comparisons are listed in Table 1.

		Pre-feed	During-feed	Post-feed
Bradygastria	Early vs. Mid GA	0.43	0.62	0.11
	Mid GA vs. Term	0.13	**0.04**	0.49
	Early GA vs. Term	0.2	**0.01**	0.85
Normogastria	Early vs. Mid GA	0.11	**0.01**	**0.02**
	Mid GA vs. Term	0.21	**0.04**	0.42
	Early GA vs. Term	0.22	**3.5×10^{-5}**	0.61
Tachygastria	Early vs. Mid GA	**0.01***	**0.004**	**0.006**
	Mid GA vs. Term	**0.03***	0.32	0.36
	Early GA vs. Term	0.08	**2.4×10^{-4}**	0.46

Note: The p values were derived by one-way ANOVA followed by Tukey's test. The bold font indicates the significance level with $p < 0.05$.

Table 1: List of p values for comparisons among different pairs of mPSD values at three GR bands during three feeding periods.

To better understand this feature, Figures 2-6(d) to 2-6(f) plot a linear regression between the GA of the infants versus *m*PSD during feeding in each GR case, revealing that the $m\text{PSD}_{\text{normo}}$ and $m\text{PSD}_{\text{tachy}}$ values during feeding are significantly higher for more mature preterm infants (mid) than less mature (early). We acknowledged that the sample size for term babies was limited; however, these several points served as a reference to demonstrate the overall trend for comparison. Furthermore, during the Post-feed period, significant increases in $m\text{PSD}_{\text{normo}}$ (p =

0.02; see Table 1) and in *m*PSD$_{tachy}$ (p = 0.006; see Table 1) were observed between the early and mid GA infants.

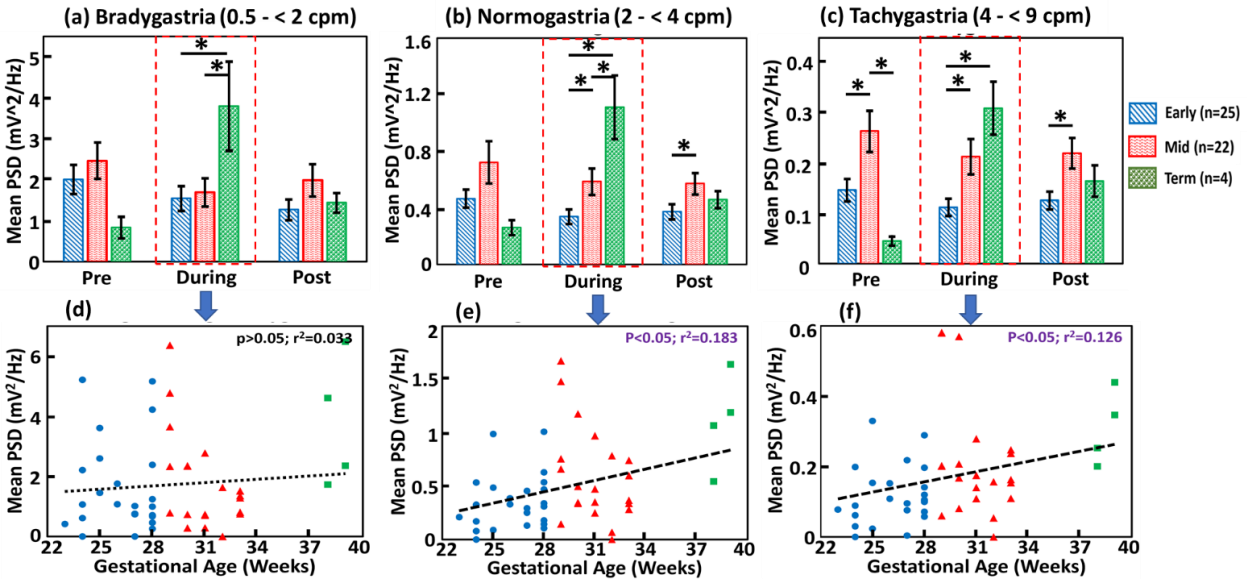

Figure 2-6: Group-level comparisons of GA-dependent *m*PSD values (mV^2/Hz) taken pre-, during, and post-feeding period in (a) bradygastria, (b) normogastria, and (c) tachygastria, respectively. "*" indicates the statistical significance with p < 0.05; the red boxes mark the During-feed periods. (d) – (f) show the corresponding linear regressions of (a) to (c) between GA of infants and *m*PSD, respectively, in the During-feed periods.

2.3.4 No alteration in *m*PSD$_{GR}$ in preterm neonates across three feeding periods and three GR bands

We examined within-group differences in *m*PSD across the three feeding periods for each of the GR bands in each GA group, as shown in Figures 2-7(a), 2-7(b), and 2-7(c), respectively. According to the one-way ANOVA results, there was no significant difference across the three sub-feeding periods in both early GA and mid GA infants (marked by the red dashed boxes in the three panels

of Figure 2-7) at all three GR bands. The ANOVA followed by Tukey's post-hoc test revealed that *m*PSD values of term babies had highly significant differences between During-feed versus Pre-feed and in all three GR bands (bradygastria with p=0.03; normogastria with p=0.01; tachygastria with p=0.002). Furthermore, for the term infants, the group-level values of $m\text{PSD}_{\text{normo}}$ altered significantly between Pre-feed vs. Post-feed (p = 0.04) and between During-feed and Post-feed (p = 0.03); similarly, the values of $m\text{PSD}_{\text{tachy}}$ altered significantly between Pre-feed vs. Post-feed (p = 0.01). Even though term babies were limited in number (n=4), the overall inability of preterm infants to alter EGG PSD across all three GR bands would still be a qualitative reflection of gastric immaturity because the term infants showed significant increases in PSD regardless of GR band during the feeding period.

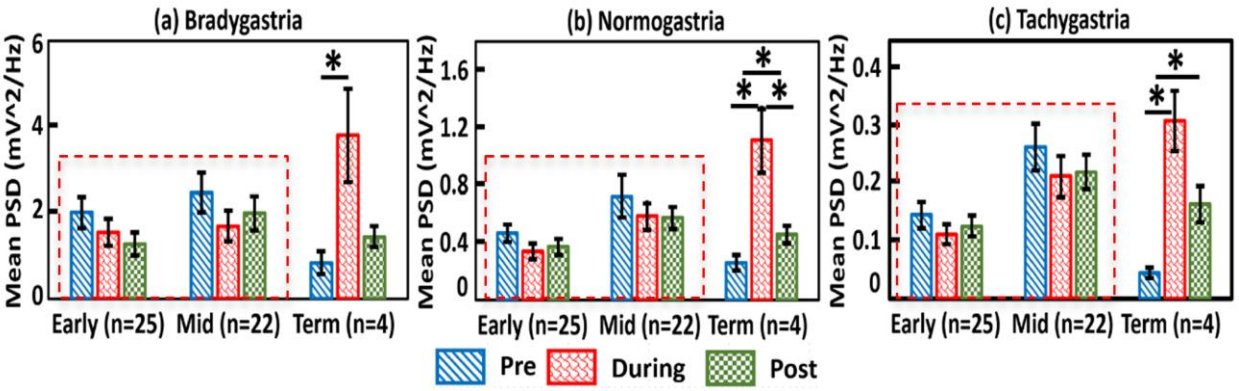

Figure 2-7: Group-level comparisons within each of the three GA groups of the *m*PSD values across the three feeding periods in (a) bradygastria, (b) normogastria, and (c) tachygastria, respectively. In each panel, the y-axis denotes the *m*PSD, and the x-axis represents the neonate GA groups. The red dashed boxes outline no significant difference in *m*PSD across the three feeding phases in both early GA and mid GA infants at all three GR bands. A significant increase

in *m*PSD is marked by "*" and determined by p<0.05. Error bars denote the Standard Error of the Mean for the respective *m*PSD values across three GA groups and in each GR band.

2.3.5 Increases in percent time in normogastria with increasing GA in all three sub-feeding periods

The percentage time spent in each GR band was quantified following 7 steps described in Section 2.2.4.5 for each GA group during three feeding periods and in three separate GR bands. Figure 2-8 demonstrates the relationship between percentage time (in each GR) versus GA for each of the three sub-feeding periods (along rows) in each of the three GR bands (along columns). Linear regression analysis showed a positive and significant linear correlation between % normogastria and GA in the Pre-feed (p<0.01, r^2=0.14), During-feed (p<0.01,r^2=0.25), and Post-feed (p<0.01,r^2=0.18) periods, as outlined by the red box in the middle row. In addition, negative correlations between % bradygastria versus GA During-feed (p<0.01,r^2=0.13) and between % tachygastria and GA Post-feed (p<0.05, r^2=0.08) were observed, as indicated by the blue boxes in Figure 2-8.

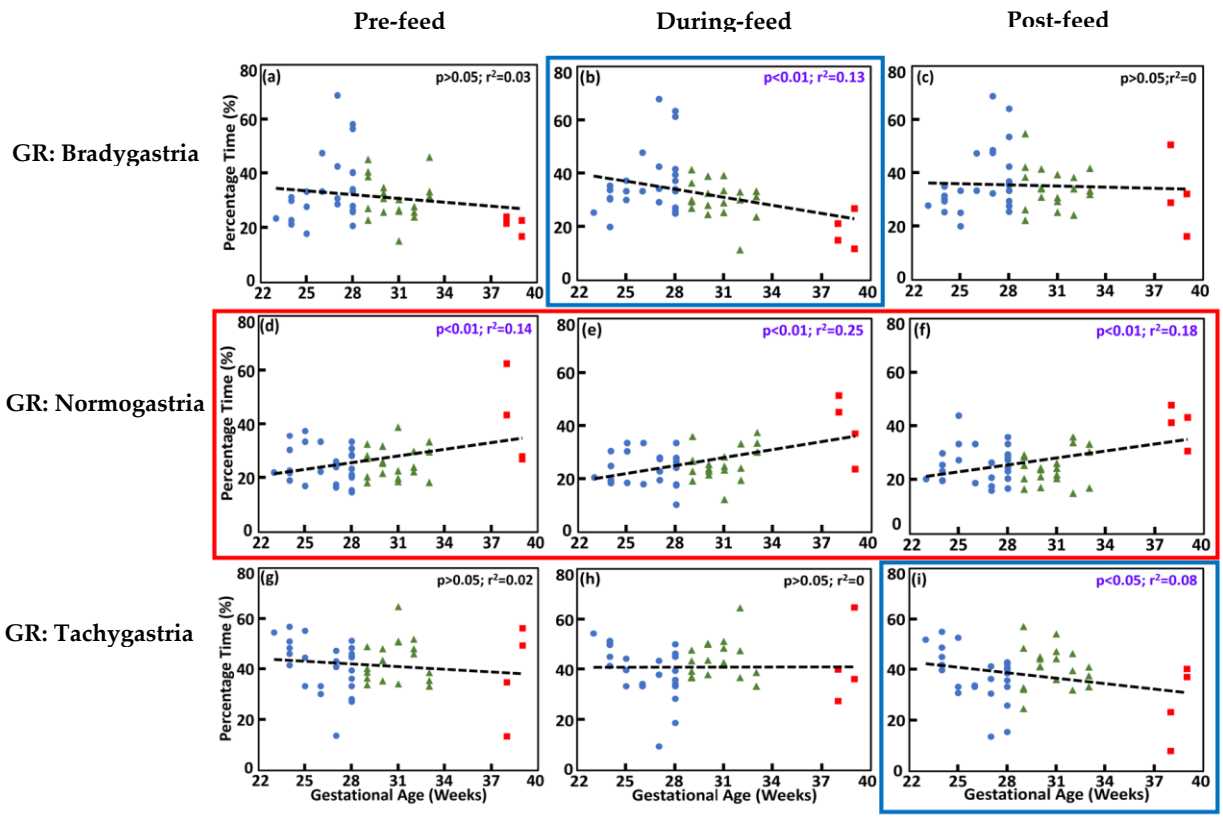

Figure 2-8: Percentage time spent in each GR band, namely, % bradygastria (top row), % normogastria (mid row), and % tachygastria (bottom row) for all the three sub-feeding periods. Panels (a)-(c) on the top row depict the % bradygastria in the 3 sub-feeding periods (pre-feed, During-feed, and post-feed, respectively). Panels (d)-(f) on the middle row show the % normogastria in the respective three sub-feeding periods. Panels (g)-(i) on the bottom row illustrate the % tachygastria during the respective three sub-feeding periods. A positive correlation was observed between the % normogastria and GA during each of the three sub-feeding periods, as outlined by the red box. A negative correlation was demonstrated between % bradygastria and GA in the During-feed period and between % tachygastria and GA in the Post-feed period (blue boxes).

2.4 DISCUSSION

EGG is a non-invasive, practical, and safe method to measure gastric myoelectrical activity in neonates. It is highly desirable that EGG could facilitate development of characteristic biomarkers/features to identify and estimate GI maturity in preterm infants. We hypothesized in the study that (i) spectral *m*PSD increases during enteral feeding regardless of the GR frequency range, (ii) *m*PSD in the regular gastric rhythm (i.e., $m\text{PSD}_{normo}$) increases during feeding with increasing gestational age, and (iii) percent normogastria ($2 \leq \text{GR} < 4$ cpm) increases linearly with increasing gestational age for preterm infants. To support our hypothesis, we conducted the study from a longitudinal cohort of preterm infants (n=51) born at early, mid, and term GA of <29, 29-33, and ≥37 weeks, respectively. After careful and thorough data analyses, we obtained several key findings, as discussed in more detail as follows.

2.4.1 Methodology-driven development in this study

First, we facilitated a novel and thorough approach to perform EGG time-frequency analysis of a longitudinal cohort of 51 neonates across three gastric rhythms, namely, bradygastria, normogastria, tachygastria and across three sub-feeding periods. Specifically, we quantified spectral means of EGG power spectral densities at the three GR bands for preterm infants and found distinct features that were linearly associated with gastric immaturity. In this way, we characterized novel and frequency-specific GR features of EGG, namely, $m\text{PSD}_{\text{brady}}$, $m\text{PSD}_{\text{normo}}$, and $m\text{PSD}_{\text{tachy}}$. Second, we utilized and implemented CWT for determination of percentage time of non-stationary EGG rhythms spent in the three GR frequencies across three sub-feeding periods (i.e., pre-feed, during-feed, and post-feed) for preterm and term neonates. The

advantage of utilizing CWT was the ability to analyze changes in gastric myoelectrical activity that occurred as a result of enteral feeding and the changes that occurred with maturation.

2.4.2 Feeding-dependent *m*PSD increases with maturation of preterm babies

The results shown in Section 2.3.3 demonstrated that *m*PSD values during the feeding period increased significantly in all three GR bands with increases of gestational age (Figures 2-6(a)- 2-6(c)). In particular, a significant and positive linear relationship between the $m\text{PSD}_{\text{normo}}$ and GA at the normal gastric rhythm (Figure 2-6(e)) during feeding is expected because it suggests developmental process and functional growth of the GI system of preterm babies. Also, changes in $m\text{PSD}_{\text{tachy}}$ (Figure 2-6(f)) were linearly in proportion to GA. Because both $m\text{PSD}_{\text{normo}}$ and $m\text{PSD}_{\text{tachy}}$ are absolute values and thus can be comparable among different infants, they may have great potential to be developed as biomarkers for assessing the GI maturity of preterm neonates.

2.4.3 Inability to alter *m*PSD in preterm neonates regardless of feeding conditions or gastric rhythms

The results shown in Section 2.3.4 revealed that preterm neonates at the GA of < 33 weeks were unable to alter/change their *m*PSD at any of the three GR frequencies across the three sub-feeding periods (Figure 2-7). The absence of change in gastric myoelectrical activity in response to feeding reflects GI immaturity. To-date, the comprehensive relationship between *m*PSD values versus three feeding periods (i.e., pre-, during, and post-feeding) at three GR bands has not been established until the present study, particularly for preterm infants. EGG has been utilized to study myoelectric changes only during postnatal maturation (38-43). In older children and adults,

EGG dominant power is expected to increase in response to feeding (44-47). These observations can be interpreted as follows: With an increase in GA, gut muscles during the period of feeding and post-feeding operate more and thus exert more myoelectrical power than that during pre-feed, indicating a normal developmental process. The absence of change in the *m*PSD of preterm infants in all 3 sub-feeding periods regardless of GR frequency band suggests immature or dysfunctional myoelectrical activity.

2.4.4 Novel method to quantify percentage time in GR using continuous wavelet transform

In this study, we have implemented a unique and novel method for quantifying the % time spent in each GR frequency band during each sub-feeding period using continuous wavelet transform, CWT. Previous literature has suggested the use of running spectral analysis methods, such as short-term Fourier transform (FT) analysis (11, 48-51). CWT is useful in analyzing the non-stationary signal and also allows to filter out stationary and non-stationary signals (52, 53). Because the EGG measurement is obtained from preterm babies longitudinally, the signal is expected to be highly non-stationary, and thus CWT is a more appropriate means used for time-frequency analysis. A brief literature review in the field of EGG (54-61) confirmed that this is the first research report to utilize and implement CWT for determination of percentage time of non-stationary EGG rhythms spent in different gastric rhythm frequencies across three sub-feeding periods.

2.4.5 Increases in % normogastria with maturation of preterm babies

In Section 2.3.5, we observed a positive correlation between % normogastria and GA during all 3 sub-feeding periods (Figure 2-8). This positive correlation between % normogastria and GA might

suggest normal gastric maturity of the gut with increase in gestational age. Furthermore, our results demonstrated that % bradygastria during feed and % tachygastria post-feed had a negative correlation with GA. Children with functional dyspepsia have been reported to have a higher % tachygastria when compared to normal healthy children (38, 62). An increase in % tachygastria may suggest delayed gastric emptying (51). A decrease in % tachygastria with the increasing GA suggests a developmental process and a decrease in gastric dysrhythmias with maturation. To-date, this is the first thorough investigation in preterm infants to report linear and significant changes between the increasing GA and in percentage time spent in different GR during all three sub-feeding periods (inclusive of during feed). Moreover, because of the linear and significant correlation between GA and the % normogastria, the latter (as denoted by $\%T_{normo}$) is also possible to be further developed as a biomarker because $\%T_{normo}$ is independent of sub-feeding period.

2.4.6 Confirmation of our hypothesis and summary of potential biomarkers

Our results shown in Section 2.3 revealed that *m*PSD values during enteral feeding regardless of the GR frequency range increased significantly with increases in gestational age (Figures 2-6), suggesting maturation of myoelectrical signal. Next, we reported that *m*PSD in the regular gastric rhythm (i.e., $m\text{PSD}_{normo}$) increased linearly during feeding with increasing gestational age. Furthermore, preterm infants < 34 weeks' GA were unable to alter/change their *m*PSD values across the three sub-feeding periods (Figure 2-7), suggesting GI immaturity. Last, % normogastria increased with increasing GA regardless of sub-feeding period for preterm infants. All these observations supported and confirmed the hypotheses proposed in the beginning of the study. Based on the results and discussions, we conclude that several EGG-derived parameters, such as

*m*PSD$_{normo}$, *m*PSD$_{tacky}$, and %T$_{normo}$, have potential to be further developed as tools to assess GI maturity and predict feeding readiness. However, further investigations need to be explored with a larger cohort of preterm and term infants.

2.4.6 Limitations and future work

This study had several limitations. First, the sample size for the term neonates was too small, preventing us from drawing more reliable conclusions for the term babies. Second, the time separations between two feedings should be more clearly defined as the post-feed for Feeding 1 and the pre-feed for Feeding 2. More investigations with appropriate methods to classify post-feed and pre-feed are desirable. Third, EGG is also sensitive to motion artifacts. Thus, additional hardware, such as electromyogram, and/or advanced algorithms for motion artifact identification, removal, and denoising for achieving higher quality of EGG data are a few future directions before EGG can serve as a non-invasive tool to measure GI maturity in preterm babies.

2.5 CONCLUSION

Electrogastrography is a non-invasive bedside tool that has the potential to become a non-invasive means to assess GI maturity in preterm infants. In this study, we confirmed that (1) gastric myoelectrical activity of preterm infants had no alteration of its EGG power spectral density in response to feeding or in the post-feeding period, (2) *m*PSD values in normogastria ($2 \leq GR < 4$ cpm) and tachygastria ($4 \leq GR < 9$ cpm) increased linearly and significantly with increases of gestational age, and (3) % normogastria increased linearly with increasing gestational age regardless of sub-feeding period. All of these quantified parameters may have promising potential to serve as biomarkers for assessment of feeding readiness in preterm infants, and thus

decreasing morbidity in this population. However, the findings in this study are relatively new with a limited sample size, particularly for term babies. Further clinical investigations with a larger sample size of both preterm and term babies are necessary for clinically meaningful conclusions.

Chapter 3

Alterations of electroencephalogram (EEG) oscillation powers induced by LED-based, right-forehead, 10-min tPBM measured by 64-channel EEG:

Authorship: Akhil Chaudhari, Xinlong Wang, Anqi Wu, Hanli Liu

3.1 INTRODUCTION

Photobiomodulation (PBM) is a novel method for modulating cellular function and mitochondrial respiration using light (14, 15). PBM has been used for pain management and wound healing purposes (63, 64). Transcranial photobiomodulation (tPBM) refers to the delivery of PBM on the human brain (65). Many sham-controlled studies have reported that the 1064-nm infrared laser improves cognitive performance on diseased and healthy individuals (19, 20). Furthermore, one of our previous neurophysiological studies has shown that tPBM using a 1064-nm laser stimulation could result in an acute increase in alpha (7-13 Hz) and beta (13-30 Hz) EEG oscillations in the resting state of human brains (21).

Besides lasers, Light-emitting Diode (LED) has been safely used since the 1980s because of its ability to noninvasively penetrate the human skull (66-69). Previous electroencephalogram (EEG) studies have investigated various neurophysiological effects for LED based tPBM, such as visual size (22), luminance contrast (23), and chromatic contrast (24). Treatment of dementia patients with 1064 to 1080 nm LEDs shows an acute improvement in the patient's executive function (25). LED stimulation also helps in depression control and anxiety control (26). Moreover, the LED treatment is known to improve executive function and memory consolidation.

Ali et al. reported an acute improvement in reaction time after LED tPBM on healthy subjects (70). A study conducted by Naesar et al. demonstrated improvements in executive function and memory after nine months of LED stimulation on two brain-injured participants (27). However, most of the LED studies are focused on studying patients with neurological or psychological diseases, no study has investigated the LED-induced prolonged effects on cognitive functions in healthy subjects.

The physiological mechanism of tPBM involves the absorption of high-energy photons by cytochrome c oxidase (CCO), which modulates the metabolic process in neurons. The high-energy photons photo-oxidizes the mitochondrial respiratory enzymes to produce a higher amount of cellular ATP. Vargas et al. presented that brain oxygenation increases with a higher tPBM laser light dosage (16). Wang et al. have non-invasively measured the increase in CCO concentration during and after laser tPBM (17, 18). In addition, electrophysiological activation in anterior and posterior regions was recently reported during and after tPBM conducted by laser (21). However, these physiological effects have never been studied under LED stimulation while the human subjects are performing cognitive tasks.

Psychomotor Vigilance Task (PVT) is a sustained attention game that has been used for measuring the speed of response to a visual stimulus, which has been recognized as an effective tool for the evaluation of sustained attentional performance (71). Jungyun et al. showed acute improvement in reaction time after laser stimulation (72). Vargas et al. also showed improvement in reaction time over five weeks under laser stimulation (16).

In this study, we designed a PVT task to evaluate the prolonged improvement of human cognitive performance over four weeks under active and sham LED-tPBM. Moreover, we recorded and quantified the acute enhancement of power in scalp EEG signal, during the first session of tPBM or sham. We hypothesize that LED based tPBM can induce an immediate increase of the EEG power, similar to previous observations under laser based tPBM. Consistent to our hypothesis, increased EEG alpha oscillations were seen in temporal, and parieto-occipital regions under tPBM stimulation. Delta oscillations were also observed to be increased in the temporal and motor regions.

3.2 MATERIAL AND METHODS

3.2.1 Subjects

Twenty-two (seven male and fifteen female, 26±5 years old) healthy volunteers were recruited. All subjects had a normal or corrected-to-normal vision and are neurologically and psychologically healthy. Subjects were excluded if they were younger than 18 years of age, currently pregnant (during the recruitment), had a presence of neurological disease, diabetes, psychiatric illness, had any tattoos on the head and face, or had caffeine consumed within 3 hours before the experiment. PVT is believed to be sensitive to caffeine (73). The study protocol was compiled with all applicable federal guidelines and approved by the Institutional Review Board (IRB) of the University of Texas at Arlington. Informed consent forms were obtained from every subject who participated in the study. Subjects were compensated for their participation after their last visit.

3.2.2 Setup and Experimental Paradigm

Electroencephalography (EEG) readings were collected using a 64-channel scalp EEG system (Biosemi instrumentation) at a data acquisition rate of 512 Hz. Channel Cz (48) was used as the reference. LED stimulation was delivered using a continuous-wave (CW), Light-emitting Diode (Thor-LX2, Thor industries, Elkhart, Indiana) on the right prefrontal cortex (74). Table 1-2 lists the device details and the tPBM parameters used in this study. For sham subjects, the power of light stimulation was adjusted to 0.1mW. Participants were seated in an upright position while maintaining their upright head position. The subjects wore safety goggles for the protection of their eyes. Since the LEDs have non-sensible heat, with the application of goggles, the subjects were not able to "see" or "feel" the LED illumination. This kept the subjects blind to the type of the stimulation types they were receiving. Before the experiment started, participants were asked to calm themselves and pay attention to the game presented before them.

Device information	**Specifications**
Manufacturer	Thor LX2 Laser and Light-emitting Diode Therapy System
Model identifier	LX2m
Year produced	2008
Emitter type	LED
Beam delivery system	Handheld probe
Number of emitters	104

Table 2: Device information and specifications. Left column lists the device details and the right column indicates the specifications related to the details.

Irradiation parameters	Value
Wavelength (nm)	660, 810
Operation model	CW
Power density (mW/cm^2)	30
Beam shape	circular
Aperture diameter (mm)	230
Total power (W)	2
Delivery timer (min)	5

Table 3: Irradiation parameters. The irradiation parameters considered are listed in the left column with their corresponding values in the right column.

A protocol of Psychomotor Vigilance Task Game (PVT) task designed by Pulsar Informatics was employed (75). In the PVT task, participants were asked to stare at a blank box at the center of a computer monitor and press the spacebar on the computer keyboard as soon as they see a timer going on the screen. After the press, the timer will disappear from the computer monitor, and left with a blank box. The inter-stimulus interval time was around one second. The reaction time for each stimulus was recorded. During their first visit, participants were given a three-minute practice session to get familiarized with the protocol and the PVT game.

The subjects were randomly assigned into a tPBM (n=11) and a sham group (n=11). Each subject has no information about the tPBM-sham group assignment and were told to receive tPBM on their foreheads during the experiment. Figure 3-1 represents the experimental protocol diagram. The protocol consisted of four time periods (TP), time period 1 (TP1), time period 2

(TP2), time period 3 (TP3), and time period 4 (TP4). TP1 and TP2 are before tPBM was delivered, whereas TP3 and TP4 are during tPBM. Each of the time periods consisted of five minutes (two minutes of resting period, followed by three minutes of gaming period). EEG recordings were taken for a total of 20 minutes. The reaction time for each subject at each stimulus was recorded. The subjects were required to attend two sessions for four weeks. The washout period between each two visits/sessions was more than 48 hours. EEG recordings were taken during the first and last visits.

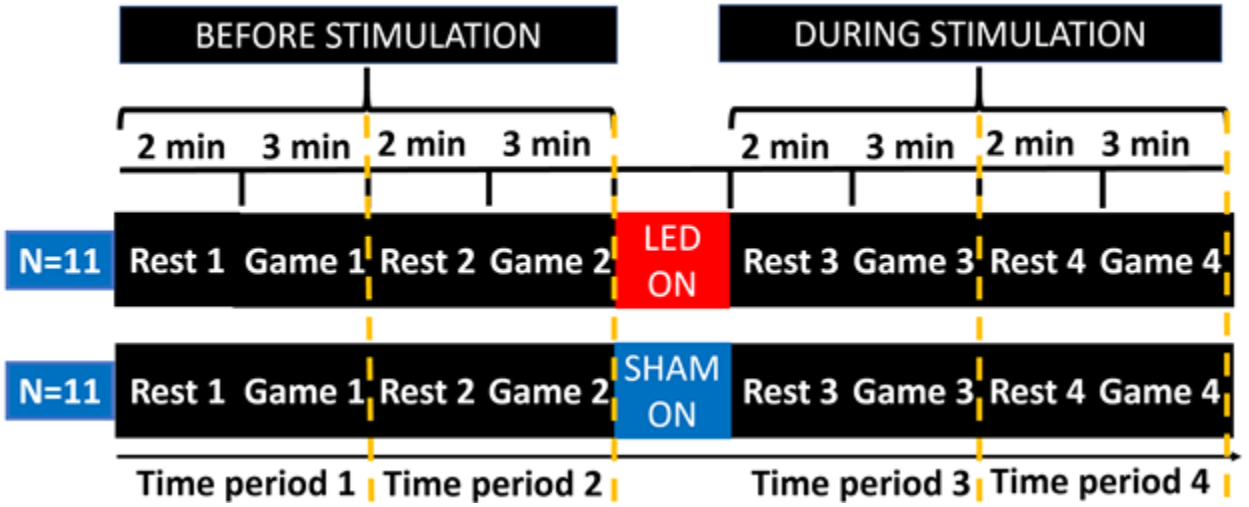

Figure 3-1: Schematic illustration of the Experiment Paradigm. During the first ten minutes, subjects were not under any stimulation. During the last ten minutes, LED or sham stimulation was delivered (during stimulation) on the right prefrontal cortex. One game and resting period together was considered as one time period (TP). Subjects underwent a resting period for 2 minutes, followed by 3 minutes of the game stimulus within every TP. This sequence was repeated four times during the whole experiment. Psychomotor Vigilance Task game was performed throughout four weeks to see the improvement in performance over time. A total of 22 subjects were randomly assigned to stimulation (tPBM) (n=11) and the sham group (n=11).

3.3 DATA ANALYSIS

3.3.1 EEG Data Processing

EEG time series were preprocessed using the EEGLAB toolbox on the MATLAB platform. Raw EEG data was initially bandpass filtered from 0.5 Hz to 70 Hz using a zero-phase butterworth filter in MATLAB. A power line noise of 60 Hz was removed using a notch filter. Data was re-referenced to the common means across the 64 electrodes before performing Independent Component Analysis (ICA) to remove artifacts of saccades, jaw clenches, heartbeats, and eye blinks. ICA was performed using the EEGLAB function “runica”. Components containing artifacts were visually inspected and removed from the data (21, 76). Next, the EEG signals were further segmented into 1 second epochs. An epoch was considered acceptable if the standard deviation of the epoch lies between the range of 0.1μV to 2 times the standard deviation of the channel. Moreover, a threshold of mean ±4 times the standard deviation of the electrode was applied to reject the outlier data points within each channel. Six of the subjects were removed from the study based on previously mentioned criteria (four tPBM and two sham subjects).

3.3.2 Power density analysis comparing resting and gaming periods

We temporally segmented the artifact-free data into resting and game periods as 2-minute and 3-minute windows, respectively. The power spectrum density (PSD) of each segment was calculated using the native MATLAB function “pwelch” (sampling frequency of 512 Hz, discrete fourier transform points of 4 seconds, 20 seconds hamming window, and 10 seconds overlap) for

each electrode and each subject. Pwelch resulted in a PSD of 0.25 Hz resolution, ranging from 0 Hz to 256 Hz. The detailed procedure is shown in Figure 3-2.

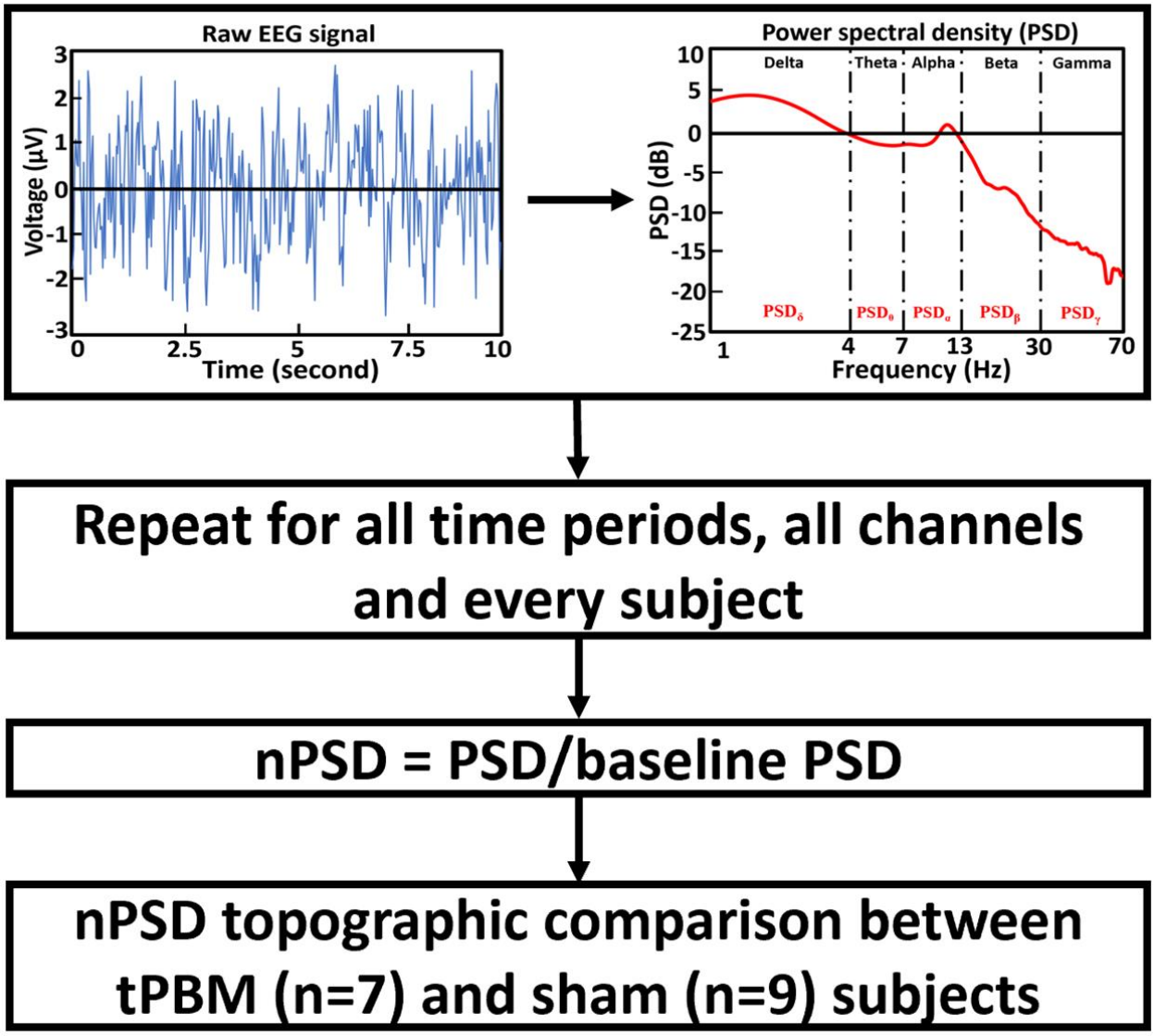

Figure 3-2: Procedure to calculate the nPSD in each frequency band for all the channels. The PSD is calculated for the raw EEG data for each channel, every subject, and time period. The normalized PSD (nPSD) is calculated by dividing the PSD of the time period by the PSD of the

baseline. The nPSD is then averaged across all subjects for each channel and time period, which is further utilized to generate brain activation topographies.

The power density values were then spectral averaged in five frequency bands of interest, delta (0.5 - 4 Hz), thets (4 - 7 Hz), alpha (7 - 13 Hz), beta (13 - 30 Hz), and gamma band (30 - 70 Hz), followed by normalization with respect to the first rest period (Rest 1). This produced the group-level normalized power spectral density (nPSD) at each EEG electrode for each frequency band, which were further utilized to generate topographies induced by tPBM or sham stimulation. Finally, the normalized PSDs ($\overline{nPSD}$) was calculated by further averaging the nPSD values across all EEG electrodes, in each section, and for each subject. This parameter was calculated and compared for each frequency band to statistically identify tPBM effects during specific time periods and on PVT behavior.

One-way ANOVA test was performed for all the subjects in all the frequency bands (n=16) during rest1, game1, rest2, and game2 conditions in R studio (77). This test was performed to determine the consistency of the $\overline{nPSD}$ in the resting and gaming conditions when the subjects are not under any type of stimulation. During stimulation, the subjects were divided into two groups: tPBM (n=7) and sham group (n=9) based on the type of stimulation which they received. During stimulation, the subjects underwent two resting and two gaming periods. One-way ANOVA test was performed for all the frequency bands on $\overline{nPSD}$ rest 3, game 3, rest 4, and game 4 to test the consistency of gaming and resting periods for tPBM and sham subjects, respectively.

The nPSD values during time period 3 (TP3) and time period 4 (TP4) were further calculated for all the subjects by averaging the nPSD values for resting and gaming periods in their respective

TP's. The nPSD values were initially averaged across all the channels for each subject separately. Then the global averaged nPSD values were then averaged across subjects within each subject group and compared between sham and tPBM treated groups. This was performed to observe the effect of tPBM over sham stimulation over EEG power.

3.3.3 Brain activation topographies for during stimulation period

We generated the power activation in topographical format. To generate these topographies, sham and tPBM subjects' band powers extracted from the power spectrum data, across all the sub-frequencies and bands were considered. First, the power spectrum was averaged across all the sub-frequencies within each band. Then we normalized the power density values by dividing over the values in the first resting period for each subject to obtain the normalized power density (nPSD), followed by average over subjects for each individual channel and each frequency band. The cross-subject averaged nPSD was used to generate activation topographical maps (Figure 3-4). Topographies of nPSD differences were generated for each TP and frequency band during stimulation using the EEGLAB toolbox from the MATLAB platform.

The nPSD values were compared between tPBM and sham subjects in all the frequency bands using a permutation test. The correction was performed using cluster-based permutation testing (78). Initially, two sample t-tests were performed on each channel to identify the channels with significant difference ($p<0.05$). Then, the sum of the t-values over two or more adjacent neighboring electrodes was calculated. The summed t-value was then compared with a null distribution. The null distribution used for comparison was obtained by randomly permuting 1000 values. This analysis was performed using the "ft_freqstatistics" function available in the

Fieldtrip toolbox in MATLAB (79). This test would allow us to examine whether LED stimulation would create a significant difference in brain response when compared with sham stimulation.

3.4 RESULTS

3.4.1 Enhanced delta and alpha band power under LED stimulation

The $\overline{nPSD}$ values during resting and game periods before tPBM were compared. A One-way ANOVA test was conducted between the $\overline{nPSD}$ values of rest 1, rest 2, game 1, and game 2 conditions among all the 16 subjects from both groups in all the frequency bands. The outcome shows the consistency in delta (p=0.99), theta (p=0.97), alpha (p=0.88), beta (p=0.92), and gamma frequency bands (p=0.89) between the resting and gaming period before stimulation.

Furthermore, we tested the consistency of $\overline{nPSD}$ values in each group during stimulation in two separately one-way ANOVAs. To do so, we averaged the resting and game $\overline{nPSD}$ values during TP3 and TP4. The TP3 $\overline{nPSD}$ values were calculated by averaging the rest 3 and game 3 $\overline{nPSD}$ values. Similarly, for TP4 the rest 4 and game 4 $\overline{nPSD}$ values were averaged. As a result, consistency was observed in the $\overline{nPSD}$ values between rest 3, rest 4, game 3, and game 4 periods for tPBM subjects (n=7) in delta (p=0.94), theta (p=0.86), alpha (p=0.86), beta (p=0.66), and gamma (p=0.31) bands as well as for sham subjects (n=9) in delta (p=0.74), theta (p=0.97), alpha (p=0.29), beta (p=0.75), and gamma (p=0.29) bands. Detailed statistical tests comparisons and p values are reported in Table 3.

Comparisons	Test	Frequency band (p value)				
		Delta	Theta	Alpha	Beta	Gamma
Rest 1, Game 1, Rest 2, Game 2	1-Way ANOVA	0.99	0.97	0.88	0.92	0.89
Led Rest 3, Led Rest 4, Led Game 3, Led Game 4	1-Way ANOVA	0.94	0.86	0.86	0.66	0.31
Sham Rest 3, Sham Rest 4, Sham Game 3, Sham Game 4	1-Way ANOVA	0.74	0.97	0.29	0.75	0.29

Table 4: Summarization of statistical tests. Column 1 depicts the comparison groups, column 2 represents the test conducted, and column 3 presents the results for different frequency bands. We observed consistency ($p>0.05$) in data during rest 1, rest 2, game 1, and game 2 for all the frequency bands. $\overline{nPSD}$ values in rest 3, game 3, rest 4, and game 4 ($p>0.05$) shows consistency in all the frequency bands for both sham and LED groups.

The nPSD values during time period 3 (TP3) and time period 4 (TP4) were further considered for all the subjects. The nPSD values were initially averaged between gaming and resting periods within each TP's. Then the nPSD values were averaged across all the channels for each subject separately. The global averaged nPSD values were further averaged across subjects within each subject group and compared between sham and tPBM treated groups as shown in

Figure 3-3. An increase in nPSD was observed in the alpha band for both TP's. Also, a decrease in the nPSD was observed in the gamma band.

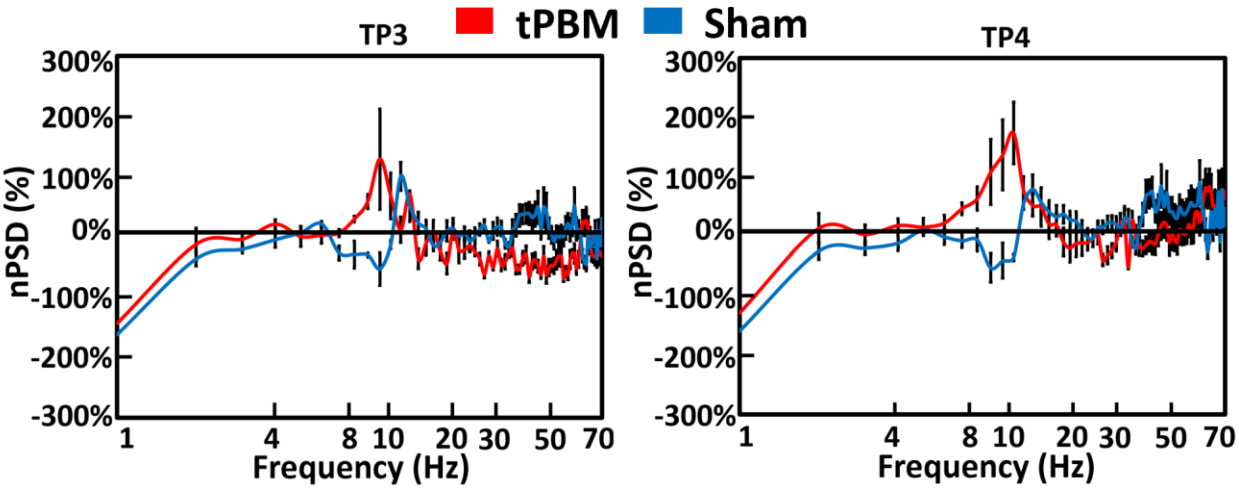

Figure 3-3: Normalized Power spectrum Density (nPSD) of all channels averaged. (a) nPSD during Time period 3 (TP3). (b) nPSD during Time period 4 (TP4). X-axis represents the percentage change in nPSD, and the y-axis denotes the frequency(Hz). An increase in nPSD was observed in the alpha and decrease in the gamma band for TP3. Similarly, increase in delta, alpha band and decrease in gamma band was observed for TP4.

3.4.2 Brain activation topographical maps evoked by LED stimulation

Brain activation topographical maps generated for TP3 and TP4 are shown in Figure 3-4. The power was averaged across subjects, time, and sub-frequencies for tPBM and sham subjects to obtain the nPSD for each channel and each frequency band. The nPSD was used to generate activation topographical maps using the EEGLAB extension from the MATLAB platform. The topographic map indicates activated cortical areas during stimulation. We observed a significant increase in cortical activation in the temporal and medial regions for the delta band. Alpha band

showed a significant increase in left temporal, left frontal and parieto-occipital regions during TP4 under LED. An increase of 30% was observed in nPSD in these regions.

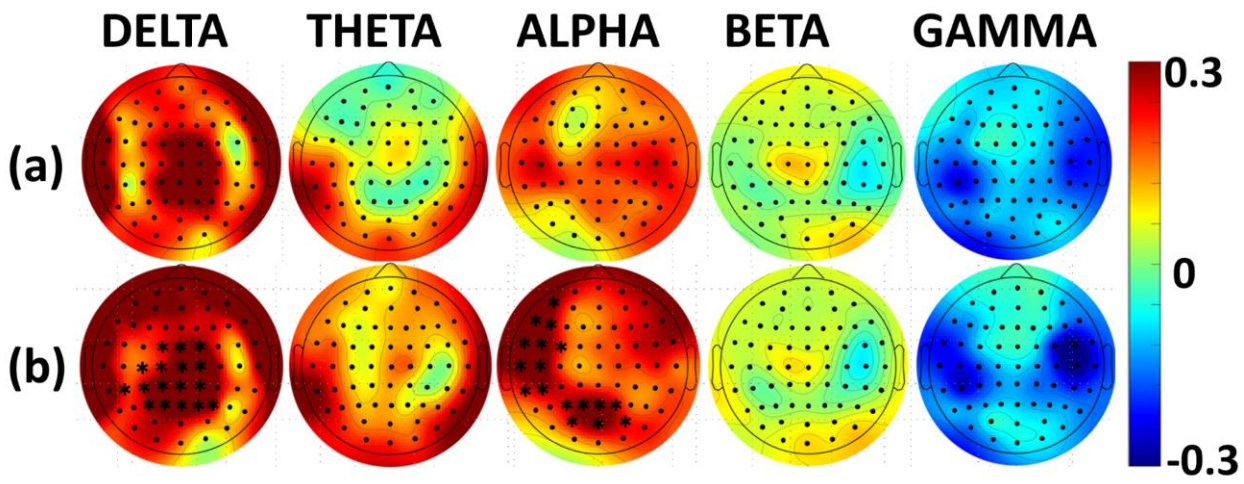

Figure 3-4: Topographic maps of nPSD showing the comparison between LED treated (n=7) and sham treated (n=9) groups during TP3 and TP4. The columns indicate delta, theta, alpha, beta, and gamma bands respectively. The first row demonstrates nPSD during TP3, and the second row shows the nPSD during TP4. Colorbar indicates the change in the nPSD. The "*" marks the p value < 0.05. During the TP4, 30% increase in cortical activation was observed during LED stimulation in the temporal and motor regions in the delta band. In the alpha band, 30% increase was also observed in left frontal, left temporal and parieto-occipital regions.

3.5 DISCUSSION

The ease-of-use of LED, along with advantages of being cheap, having low dose, and being harmless makes it a preferable choice of conducting tPBM. This is the first study, to our knowledge, that demonstrates the effects of LED stimulation on the prolonged improvement of attention performance and acute boost of electrophysiology functions on healthy subjects. We

conducted 64-channel EEG measurements from 22 healthy human subjects while they performed the PVT task. Improvement in vigilance/attention was tracked (reaction time) over four weeks. We found LEDs have significant effects on global EEG power at the temporal lobe and motor region in the delta band, and left temporal, parieto-occipital lobes in the alpha band in the human brain.

3.5.1 Power improvement of Brain oscillations by LED stimulation

In this study we observe LED increases EEG nPSD in alpha band at motor, pre-motor, and parietal lobes and in delta band in temporal lobe and motor region. Cognitive enhancement is associated with alpha-band power increase in frontal and parietal regions (80). Also, we observed an increase of EEG nPSD in parietal regions, which is consistent with previous studies (80-82). Consistent with these studies, we observe an increase in alpha band power during LED stimulation.

An increment is observed from Figure 3-4 in the frontal cortex nPSD for the EEG alpha band. The prefrontal cortex plays a role in sustained attention and gets activated in response to tasks requiring vigilance/attention (27). The frontal region controls the executing function. Executive functioning plays a role related to improving reaction time during the task (83). The salience network is said to be present in the prefrontal cortex (84). The salience network is responsible for the detection of distinct target inputs involved during PVT (84-86). Salience network is also responsible for alerting, top-down short-term attention processing (87). This network helps in maintaining vigilance in response to external stimuli. These observations may indicate that LED improves the attention-related networks present in the frontal region.

We observed a significant increment in pre-supplementary motor and motor areas nPSD under LED (Figure 3-4). Culham and colleagues demonstrated that the precentral region, supplementary motor, and right inferior parietal lobe have stronger responses when neurological attentional demands increase (88). In our study, fast responses from subjects could suggest that an internally higher attentional state was generated. Atefah's experimentation gave evidence of improved motor performance in finger tapping under LED stimulation (26). Faster reaction time is associated with increased cortical regions activity in achieving better motor performance (89). Motor sequences are controlled and coordinated by the premotor and precentral region (90). The supplementary motor area plays a role during simple repetitive motor responses (here for pressing the button for multiple trials) (91). An increment observed in motor regions nPSD under LED with better task performance may be due to high attentional state attainment.

An increased nPSD value in the parietal lobe was also observed under LED stimulation in delta and alpha bands. (Figure 3-4). The parietal lobe is said to top-down modulate the attention. Thus, allowing faster reactions towards the stimulus (88, 92, 93). Inferior parietal and frontal lobe are the commonly observed areas during sustained attention (94). Few studies have shown lateral frontal area and inferior parietal lobe together support executive control and attention maintenance (71, 87, 95). The left inferior parietal lobe has been shown to be activated in subjects showing faster reaction time (88, 92). The parietal cortex has been believed to be involved during spatial attention tasks, working memory, and decision-making (96, 97). In this study, an increased power of the inferior parietal lobe could explain the faster reaction time for LED treated subjects over time.

Most of the above mentioned studies used lasers for stimulation (16, 25, 72), whereas we observed similar areas activated using LED over time. LED stimulation has several advantages over laser stimulation, including low dose, less harmful, and cheap. In the future, to improve cognition, LEDs can become a viable alternative to laser stimulation.

3.5.2 Limitation and Future Work

This study had certain limitations. First, we analyzed the effects of the first 10 minutes of LED stimulation. However, More studies on the effects of prolonged stimulation during a single visit are required to determine the adequate stimulation time to get optimum improvement. The second limitation is the lower statistical probability due to the small sample size. Further studies with a larger sample size are needed to verify these results with better statistical probability. Another limitation of our study was the wavelength of light used for tPBM. We applied a combination of infrared (810 nm) and visible light (660 nm) frequencies. Further studies are required to determine the effect of different wavelengths and persistency in the LED stimulation effect.

3.6 CONCLUSION

Our observations provide substantial evidence that LED stimulation for ten minutes significantly affects brain activity. We showed for the first time that delta and alpha band power significantly increases during LED stimulation while performing tasks similar to laser stimulation. We also found LEDs have significant effects on EEG power at the temporal lobe and motor region in the delta band, and left temporal, parieto-occipital lobes in the alpha band in the human brain.

Future studies on the effect of LED on EEG band power due to prolonged stimulation are needed. The effect of LED on EEG power over weeks is required to study the effectiveness of increase in brain activation.

Chapter 4

Longitudinal effects on human reaction time and EEG oscillation sources induced by 4-week, right-forehead, LED tPBM:

4.1 INTRODUCTION

In this study, we designed a PVT task to evaluate the prolonged improvement of human cognitive performance over four weeks under active and sham LED-tPBM. Moreover, we recorded and quantified the acute enhancement of power in scalp EEG signal, during the first session of tPBM or sham. We have two major hypotheses. First, LED stimulation on the right prefrontal cortex of healthy subjects will improve attention over time by stimulating attention networks. Second that prolonged LED based tPBM over four weeks can induce an increase of the EEG power, similar to previous observations under laser based tPBM. Consistent to our hypothesis, improvement in reaction time under LED stimulation over four weeks was observed. Furthermore, an increase in EEG theta, beta, and gamma oscillations were seen globally after four weeks under tPBM stimulation.

Singular value decomposition (SVD) algorithm is commonly used to decompose one complex matrix into several orthogonal components or matrices (98, 99). SVD has been proven very useful in various areas of statistics, engineering, and science (100, 101). It has wide applications in solving linear inverse problems such as image processing and signal processing (102-106). Applications of utilizing the SVD algorithm to decompose multi-channel EEG signals have been reported in various previous studies. Hadded et al. applied SVD to resolve EEG

independent networks (107). Kamel et al. identified epileptic seizures using SVD on EEG signals (108). The fused component using EEG and fMRI data was reported by Jonmohamadil et al. with the help of SVD (109). Pirondini et al. in 2020 reported resting state EEG components using the SVD algorithm (110). Sandberg et al. in 2005 detected mismatch negativity in neonates using the EEG voltage fluctuations using the SVD algorithm (111). To the best of our knowledge, no study has utilized SVD as an analytical tool to quantify LED-based tPBM induced stimulation effects on the EEG brain networks.

Thus, in this study, we hypothesized that group SVD (gr-SVD) along with exact low resolution brain electromagnetic tomography (eLORETA) would enable to identify (a) LED-based tPBM induced human EEG networks on the 3D source space and 2D sensor domain, and (b) human brain's response to the LED-based tPBM on the right forehead on healthy humans while performing PVT task. To test our hypothesis, we designed a PVT task based study over four weeks, to evaluate the changes in the human brain cognitive brain network under active and sham LED-based tPBM. We were able to recognize 12 most-weighted, 2D principal components (PCs) using the gr-SVD approach (112, 113). These 12 PCs were considered as dominant EEG brain networks based on minimal temporal correlation among them. Further, using eLORETA on these gr-SVD-derived 2D topographies, we further generated three-dimensional (3D) cortical source locations for each network (114-116). The LED-based tPBM and sham induced power changes in each EEG frequency band (delta, theta, alpha, beta, and gamma) were quantified on the temporal dynamics of each brain network. We identified various LED-modulated EEG brain networks in theta, beta, and gamma bands by conducting pair-wise non-parametric statistical permutation

comparisons of power change between LED and sham conditions. These brain networks were consistent with MRI-based brain networks and also are related to human cognition and vigilance.

4.2 MATERIAL AND METHODS

4.2.1 Subjects

Twenty-two (seven male and fifteen female, 26±5 years old) healthy volunteers were recruited. The details of the inclusion exclusion criteria are given in details in Section 3.2.1

4.2.2 Setup and Experimental Paradigm

The detailed information on the setup and the experimental protocol used in this study is given in the Section 3.2.2.

4.3 DATA ANALYSIS

4.3.1 Data preprocessing

Six of the subjects during week 1 (four tPBM and two sham subjects) and six subjects during week 4 (three tPBM and three sham subjects) were removed from the study based on previously mentioned criteria in chapter 3.

4.3.2 Behavioral Data Analysis

According to Figure 3-1, in each visit, the subject will play four sessions of PVT games. Each session of the PVT game included 25-30 stimuli. The mean performance in each PVT game was obtained by averaging the reaction times across all the stimuli. Then, the mean reaction times of

the two PVT games during stimulation (i.e., Game3 and Game 4) were further averaged to be one single value (reaction time for this visit). This was repeated for all the subjects in both tPBM and sham groups during each visit. The average reaction time across subjects was calculated for tPBM and sham groups, respectively. The improvement along four weeks of visits was observed for each group to evaluate the effects of LED/sham on vigilance to address our first hypothesis.

4.3.3 Power Density calculation

The procedure mentioned in Chapter 3 was followed to obtain the nPSD and $\overline{nPSD}$ values for all the subjects during week 1 and week 4.

One-way ANOVA test was performed for all the frequency bands on $\overline{nPSD}$ rest 3, game 3, rest 4, and game 4 to test the consistency of gaming and resting periods for tPBM and sham subjects, respectively during both the weeks. The nPSD values were averaged between resting and gaming period during TP3 and TP4 for both week 1 and week 4, sham and tPBM treated subjects. These TP based nPSD values were then globally averaged across all the channels. The global averaged nPSD values were further subject averaged within each subject group for both the time periods. The global averaged, subject averaged nPSD values were then compared between week 1 and week 4 for both the tPBM and sham treated group, for both the TP's to evaluate the effect of four weeks of LED stimulation.

4.3.4 Brain activation topographies for during stimulation period

The nPSD values were further compared between week 4 and week 1. The cross-subject averaged nPSD was obtained for all the frequency bands during week 4 for both the groups (tPBM and

sham groups), following the similar procedure described above. The increment in the nPSD over the time was calculated by subtracting the subject averaged nPSD of first week from the subject averaged nPSD of the fourth week for each of the frequency bands, and groups. Topographies of nPSD differences between the tPBM and sham treated groups were generated for each TP and frequency band during stimulation using the EEGLAB toolbox.

The nPSD values were compared between tPBM and sham subjects in all the frequency bands using a permutation test for (a) week 1 (b) week 4 and week 1 comparison. The correction was performed using cluster-based permutation testing (78). Initially, two sample t-tests were performed on each channel to identify the channels with significant difference ($p<0.05$). Then, the sum of the t-values over two or more adjacent neighboring electrodes was calculated. The summed t-value was then compared with a null distribution. The null distribution used for comparison was obtained by randomly permuting 1000 values. This analysis was performed using the "ft_freqstatistics" function available in the Fieldtrip toolbox in MATLAB (79). This test would allow us to examine whether LED stimulation would create a significant difference in brain response when compared with sham stimulation, and to study the effects of four weeks of LED stimulation on the brain response.

4.3.5 Potential sources affected by LED-based tPBM using e-LORETA

Group SVD calculations (Step 2-4)

The group SVD can be considered as similar to the spatial group ICA that has been widely used in the field of fMRI (117-119). The pre-processed EEG data was initially standardized/ Z transformed

to minimize the subjects' biological variation. The temporal mean was subtracted from each subject's EEG time series for each of the channel, followed by further dividing by its temporal standard deviation. This standardization was performed to avoid the individual subject biasness in the SVD calculations who might have a larger oscillation power. After standardization, the artifact-free EEG time series data from all the 32 subjects (week 1: 16 subjects, week 4: 16 subjects) were concatenated into a single matrix, which included the data collected from both sham and LED groups for the first and fourth week. There are interconnections between slow and fast EEG rhythms in mediating the brain networks (120). Hence, the whole frequency band of EEG (i.e., delta, theta, alpha, beta, and gamma) is considered together rather than separating them into individual frequency bands while performing gr-SVD. Next Group SVD (gr-SVD) was performed on the concatenated matrices to identify the common Principal Components (PC) across four weeks and all the LED and sham subject groups using the native MATLAB function 'svd'. The gr-SVD was performed using 'economy-size decomposition' style to remove the extra rows and columns of zeros in time dynamics vector (U) and singular values vector (S). The mathematical equation of 'svd' function is shown in Eq. 1:

$$C = U \times S \times V^T \tag{1}$$

Where C is the transposed matrix of A (i.e. C = AT). Where, A is the concatenated EEG matrix, U denotes the time dynamics vector for all the 64 channels without a unit; V (64X64 size) denotes the components of 2D relative electrical potential (rEP) topographies with no unit (due to the Z transformation on each subject's EEG data); and S is a diagonal matrix containing the 64 singular values of C, which indicates the weight of each component in C. As a result, we obtained 64 gr-

SVD components of the major PCs, their respective weights over the original signal, and their corresponding 1D time series.

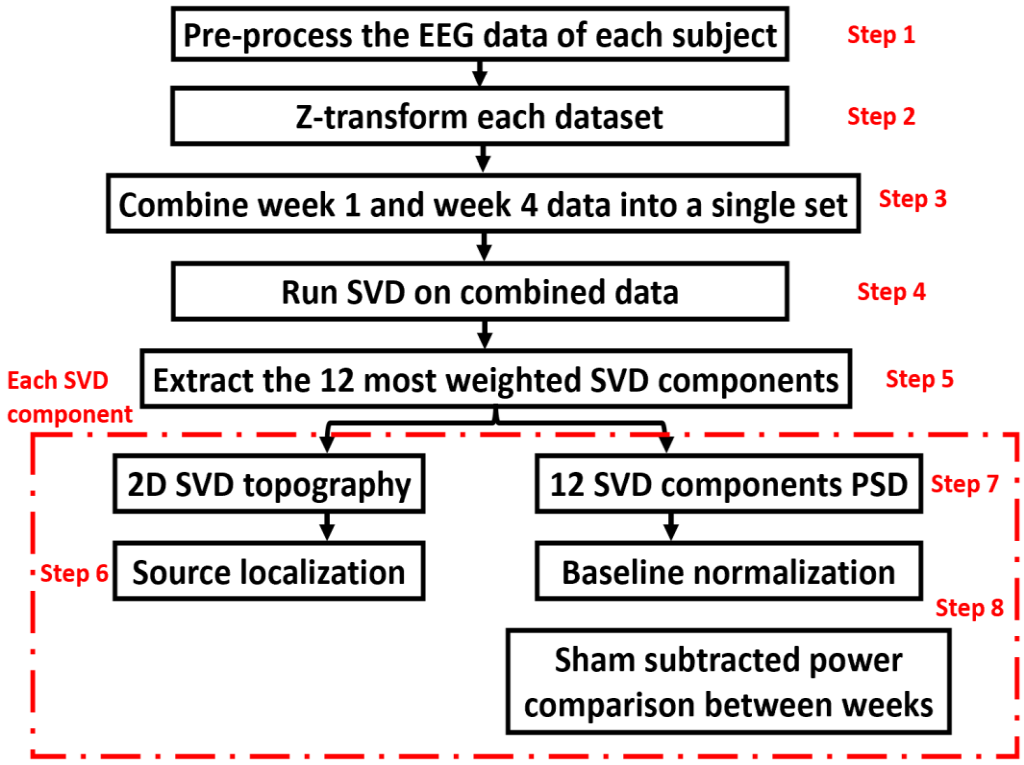

Figure 4-1: Flowchart of the eight steps involved in the EEG data processing. All steps were performed in the MATLAB except step six which was performed using the eLORETA software.

Extraction of the 12 gr-SVD components (Step 5)

In the previous step (step 4), the 12 most weighted gr-SVD components were identified. These components were extracted and further analyzed. The 3D cortical source localizations were projected using eLORETA for the 12 2D topographies. The detailed steps for source localization using eLORETA are given in step 6. The 1D time series (Variable U) was further segmented into different TP's, for each week (week 1 and week 4), for each participant and for each stimulation

type (LED, and Sham). Further, the power spectral density calculations were performed on the segmented data of each participant. Detailed steps are given in step 7.

Source localization by eLORETA (Step 6)

eLORETA is a free access software package (http://www.uzh.ch/keyinst/loreta.htm), which converts the 2D scalp distribution of electrical potential into 3D cortical distribution of current density. To localize the electric activity in the human cortex, eLORETA uses a total of 6239 voxels at 5-mm spatial resolution. eLORETA offers a weighted least-square based solution with zero localization error(121). In this study, eLORETA was utilized to localize 3D cortical sources (cortical space) of the 2D electric potential distribution (sensor space) of 12 SVD components. The Montreal Neurological Institute (MNI) coordinate system of the 64-electrode international 10-10 system was employed, and the default value of 1 was utilized as regularization parameter for the generation of transformation matrix. This procedure produced 3D cortical maps and 2D (sagittal, coronal, and axial) views were generated for each of the SVD components as shown in Figure 4-9.

Power spectral density of SVD time courses (Step 7)

For each subject, each TP and during each week, power spectral analysis was conducted on the time course of each SVD component using the native MATLAB function “pwelch” (20 seconds moving window, 10 seconds of overlap). This resulted in one power spectral density (PSD) curve with a resolution of 0.125 ranging from 0 – 256 Hz, for each SVD component, each subject, each week, and for each TP (TP1, TP2, Tp3, and TP4). The steps to quantify the power changes induced by LED stimulation are explained in Step 8.

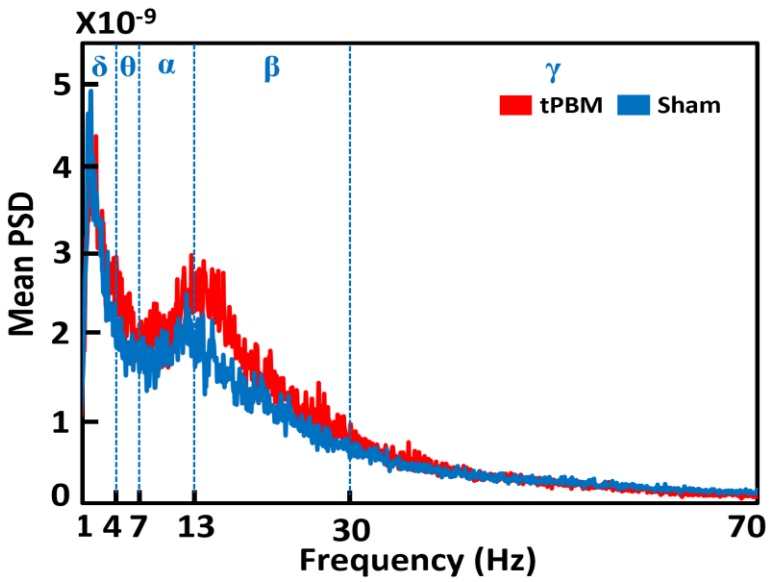

Figure 4-2: Group-averaged PSD during TP4, for component two (SVD #2). The red and blue lines represent the tPBM and sham treated groups, respectively. Blue vertical dashed lines mark the five EEG frequency bands, namely, delta (δ: 1-4 Hz), theta (θ: 4-7 Hz), alpha (α: 7-13 Hz), beta (β: 13-30 Hz), and gamma (γ: 30-70 Hz).

Computation of power changes induced by LED stimulation (Step 8)

To compute the absolute power change induced by the LED stimulation, we obtained the spectral averaged power by multiplying the average PSD value over the corresponding spectral band with the corresponding bandwidth for each subject over the five spectral bands (Delta: 0.5-4 Hz, Theta: 4-7 Hz, Alpha: 7-13 Hz, Beta: 13-30 Hz, and Gamma: 30-70 Hz) for each subject and each week. Since there was no significant difference between the time periods before stimulation, this operation was repeated for all the time periods under stimulation (i.e., TP3, and TP4). Next, each TP frequency-specific power was baseline normalized by dividing its own frequency-specific baseline power. Baseline normalization was performed for all the 12 SVD components, for all the

subjects, for both LED and sham conditions, in all five frequency bands, for all the four time periods, and for both weeks. The sham and LED treated normalized power spectral density (nPSD) was averaged across the subjects within their respective groups. Further, we subtracted the sham treated group averaged power from the LED treated group averaged power for both the weeks. In this way, the absolute percent changes (Δnp) in the power induced by LED were calculated for all the TP's during both week 1 and week 4, per SVD component, per subject, and per frequency band.

The consistency in the nPSD curves was determined between all the subjects for TP1, and TP2 (before stimulation) for week 1 and week 4, respectively using the one-way ANVOA test. The nPSD data were spectrally averaged within each frequency band for each subject under before stimulation conditions (i.e., TP1, TP2). The broadband data was then further averaged across the frequencies to obtain the spectral averaged power for each subject, each frequency band during TP1, TP2. Finally, one-sample, non-parametric tests(122, 123) were conducted between the Δnp during TP3 and TP4, versus zero for each SVD component, each frequency band, and during all the TP's under stimulation. The test was carried out using the native MATLAB function "ranksum". This test is equivalent to two-sample, pair-wise, non-parametric permutation comparisons between LED and sham. This test allowed us to compare the Δnp of all the SVD components between the LED and sham group.

4.4 RESULTS

4.4.1 Prolonged LED stimulation significantly improves behavioral measures

The averaged reaction time across subjects for both sham and tPBM groups under-stimulation across days was plotted (Figure 4-3). Data was fitted with different models (linear, exponential, and logarithmic models) to observe the trend over the time for tPBM and sham subjects. Among different models, the linear model showed the optimized fitting effects and highest R2. Therefore, the following analyses were all based on the linear fitting model. The significant improvement over four weeks was observed for tPBM subjects. The linear fitting showed a significant decrease in reaction time for tPBM subjects (p value of 0.002) as observed from Figure 4-3. Sham subjects' reaction time did not show any significant difference across time (p value of 0.07). This result suggests that LED stimulation for 10 minutes, twice each week for four weeks, improves vigilance in healthy subjects verifying our first hypothesis. Figure 4-3 shows an improvement in the reaction time for tPBM treated subjects when compared with the sham subjects.

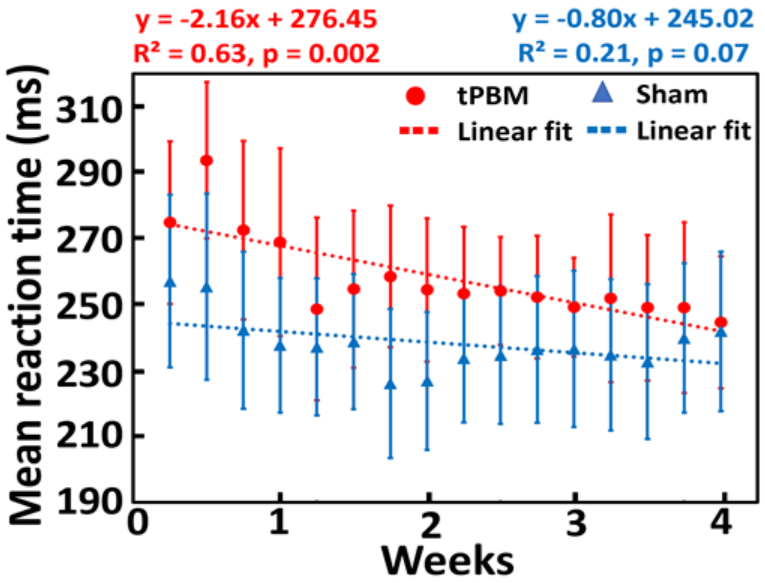

Figure 4-3: Effect of LED stimulation on the reaction time for sham (blue) and tPBM (red) subjects. The plot shows the mean reaction time across subjects over every stimulus and two games during stimulation across a period of four weeks. The dotted lines denote the improvement across time (blue dotted: Sham subjects data fitted line, Red dotted: tPBM subjects data fitted line). The p value of regression for tPBM shows a significant decrease over four weeks. Sham subjects did not show any significant change over time (sham subjects fitted line p value: 0.07, tPBM subjects fitted line p value: 0.0002).

4.4.2 Consistency between gaming and resting periods

The $\overline{nPSD}$ values during resting and game periods before tPBM were compared for both week 1 and week 4. Consistency between gaming and resting period before stimulation was also observed during week 4 in delta (p=0.31), theta (p=0.44), alpha (p=0.39), beta (p=0.05), and gamma (p=0.08) frequency bands.

Furthermore, we tested the consistency of $\overline{nPSD}$ values in each group during stimulation in two separately one-way ANOVAs for both the weeks. To do so, we averaged the resting and game $\overline{nPSD}$ values during TP3 and TP4. The TP3 $\overline{nPSD}$ values were calculated by averaging the rest 3 and game 3 $\overline{nPSD}$ values. Similarly, for TP4 the rest 4 and game 4 $\overline{nPSD}$ values were averaged. As a result, during week 1 consistency was observed in the $\overline{nPSD}$ values between rest 3, rest 4, game 3, and game 4 periods for tPBM subjects (n=7) in delta (p=0.94), theta (p=0.86), alpha (p=0.86), beta (p=0.66), and gamma (p=0.31) bands as well as for sham subjects (n=9) in delta (p=0.74), theta (p=0.97), alpha (p=0.29), beta (p=0.75), and gamma (p=0.29) bands. Similarly, during week 4 consistency was observed in the $\overline{nPSD}$ values between rest 3, rest 4, game 3, and

game 4 for sham subjects (n=8) in delta (p=0.6), theta (p=0.54), alpha (p=0.73), beta (p=0.48), and gamma (p=0.42) bands as well as for tPBM subjects (n=8) in delta (p=0.86), theta (p=0.41), alpha (p=0.72), beta (p=0.49), and gamma (p=0.43) frequency bands. Detailed statistical tests comparisons and p values are reported in supplementary Table 4.

Comparisons	**Test**	**Frequency band (p values)**				
		Delta	Theta	Alpha	Beta	Gamma
Rest 1, Game 1, Rest 2, Game 2	1-Way ANOVA	0.31	0.44	0.39	0.05	0.08
Led Rest 3, Led Rest 4, Led Game 3, Led Game 4	1-Way ANOVA	0.86	0.41	0.72	0.49	0.43
Sham Rest 3, Sham Rest 4, Sham Game 3, Sham Game 4	1-Way ANOVA	0.6	0.54	0.73	0.48	0.42

Table 5: Summarization of statistical tests for week 4. Column 1 depicts the comparison groups, column 2 presents the test conducted, and column 3 represents the results for different frequency bands. We observed consistency (p>0.05) in data during rest 1, rest 2, game 1, and game 2 for all the frequency bands. $\overline{nPSD}$ values in rest 3, game 3, rest 4, and game 4 (p>0.05) shows consistency in all the frequency bands for both sham and LED groups.

The global averaged, subject averaged nPSD values were then further compared between week 1 and week 4 for both sham and tPBM treated groups. An increase in nPSD was observed in all the frequency bands after four weeks of LED-based tPBM stimulation during TP4 (Figure 4-

4). Sham subjects showed an increase in delta band (0.5-4 Hz) and alpha band (7-13 Hz). Changes in the nPSD values across four weeks during TP3 are shown in Figure 4-5. No significant changes were observed for both LED-based tPBM and sham treated groups.

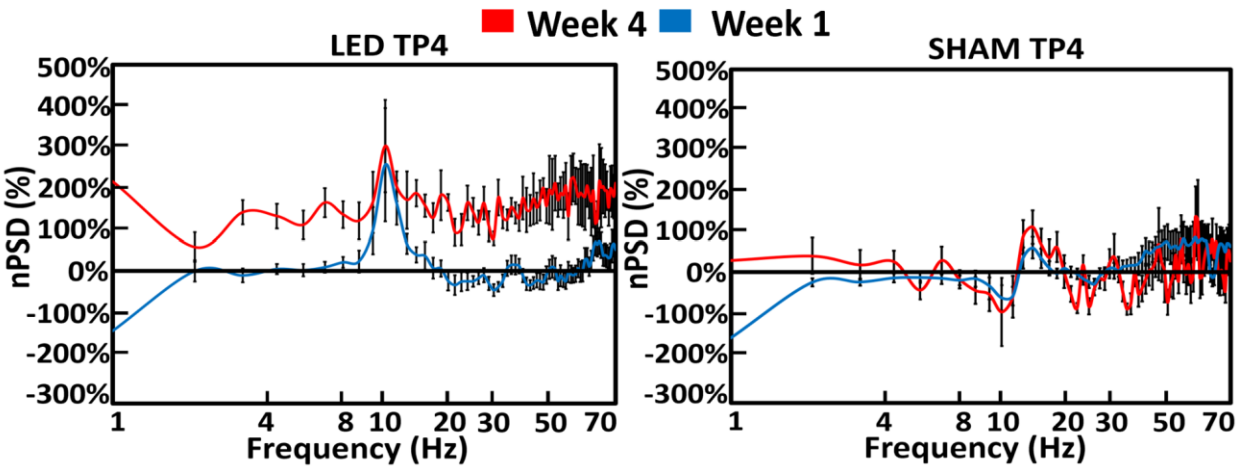

Figure 4-4: Normalized Power spectrum Density (nPSD) all channels averaged for Time period 4 (TP4). (a) nPSD for LED treated group. (b) nPSD for sham treated group. X-axis represents the percentage change in nPSD and the y-axis denotes the frequency(Hz). Blue curve indicates week 1, and red curve shows week 4 percentage change in nPSD. An increase in nPSD was observed in all the bands for LED subjects.

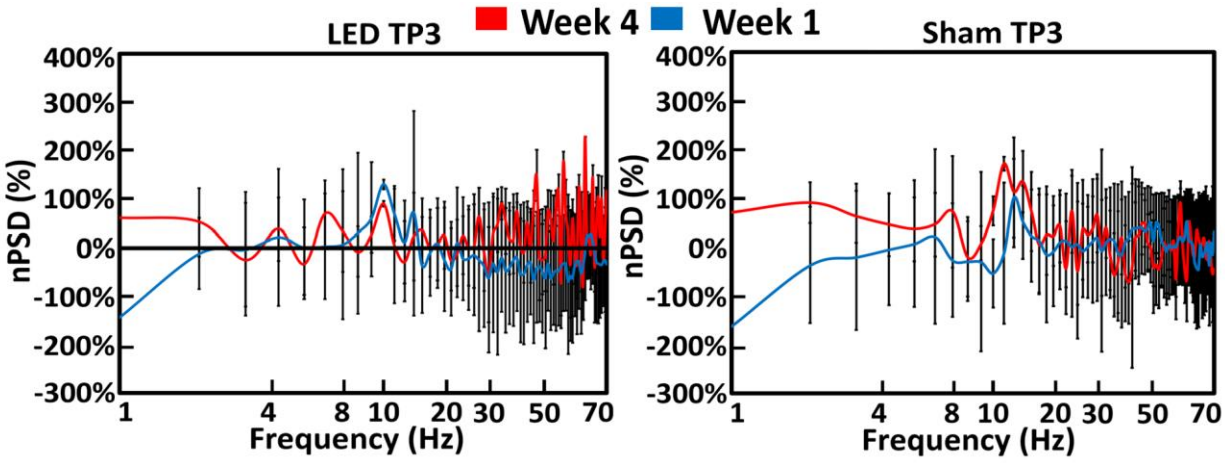

Figure 4-5: Normalized Power spectrum Density (nPSD) averaged across all channels for Time period 3 (TP3). (a) nPSD for LED treated group. (b) Sham treated subjects' nPSD. Y-axis represents the percentage change in nPSD, and the x-axis denotes the frequency(Hz). Red curves indicate week 4, whereas blue curve show week 1 nPSD percentage change. An increase in nPSD was observed in delta, and beta bands for LED subjects.

4.4.3 Brain activation topographical maps evoked by LED stimulation

Brain activation topographical maps induced after 4 weeks of stimulation generated for TP3 and TP4 are shown in Figure 4-6. The nPSD was obtained for each channel and each frequency band for both tPBM and sham during week 1 and week 4. The change in nPSD over four weeks was calculated by subtracting the first week nPSD from fourth week nPSD for all the frequency bands. The nPSD change was used to generate topographical maps using EEGLAB extension from MATLAB platform. The topographic maps indicate activated cortical areas after four weeks of tPBM stimulation. Gamma band showed a significant increase in left and right temporal lobes during TP3. We observed a significant increase in cortical activation globally for theta, beta, and gamma frequency bands during TP4. Delta band showed a significant increase in the right temporal and medial lobes, and the alpha band showed an increase in the right temporal and left occipital regions during TP4.

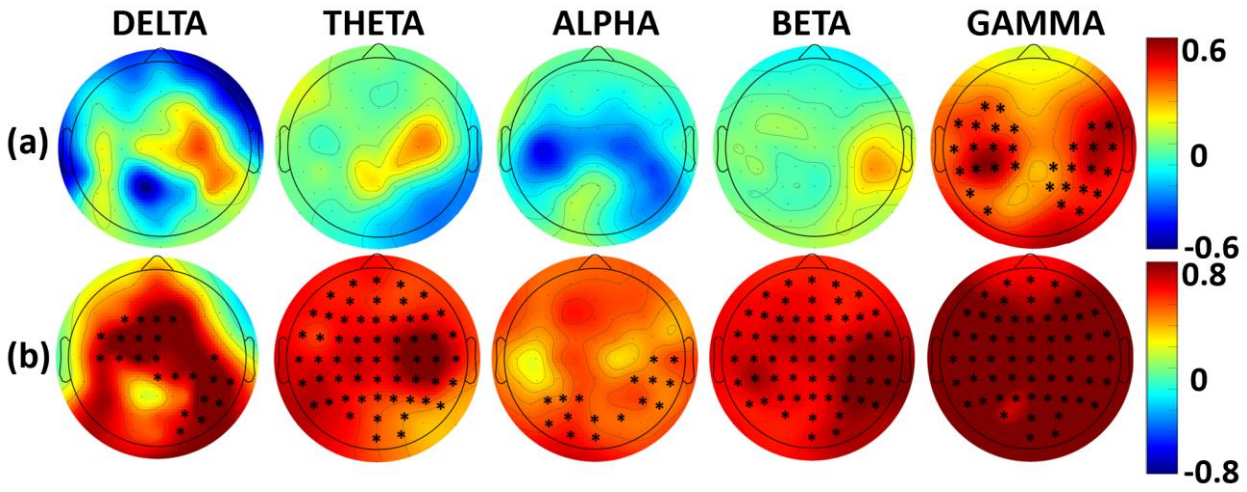

Figure 4-6: Topographic maps of nPSD depicting the comparison between week 4 and week 1 data during TP3 and TP4. The columns represent delta, theta, alpha, beta, and gamma frequency bands respectively. TP3, and TP4 nPSD changes across four weeks are demonstrated in the first and second row respectively. Colorbar indicates the change in the nPSD. The "*" marks the p value < 0.05. During the TP3, 60% increase in cortical activation was observed after 4 weeks of LED stimulation in the left and right temporal regions in gamma band. During the TP4, 80% increase was also observed globally in theta, beta, and gamma bands. Delta band showed a significant increase in the right temporal and medial lobes. An 80% increase was also observed in right temporal and left occipital regions for alpha band during TP4.

4.4.4 Extraction of 12 Most-weighted components from gr-SVD

This section presents the results developed from Step 5 in the data processing. The diagonal values of S variable are plotted in Figure 4-7 , which demonstrates the ranking of all the 64 SVD components based on their weights in the EEG signal after gr-SVD. As seen from Figure 4-7, an exponential decay in the weights is observed across the components. The components with less

than 90% decay when compared with the first/most-weighted component are chosen for further analysis. Thus, 12 dominant components were selected using this criterion (marked in red color in Figure 4-7). These 12 components contribute 73% of the entire EEG signal (i.e., the area under the curve of all the dominant components/ all the 64 components). 2D topographies for each of the SVD components are shown in the next section.

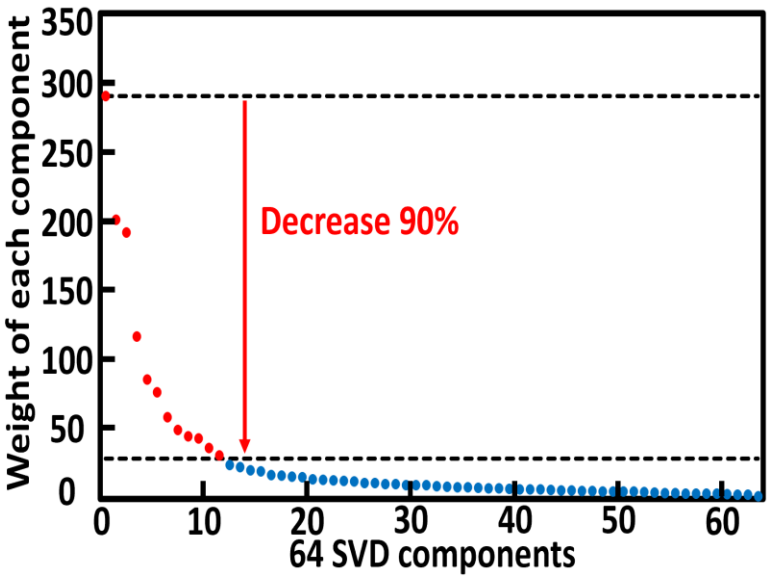

Figure 4-7: Weights of all the 64 SVD components obtained after gr-SVD. The y-axis indicates the weight of each component, while the x-axis denotes the rank of each component. The weight of each component shows an exponential decay pattern across the components. The 12 components weighting more than 90% of the most-weighted component, are marked by red dots and selected for further analysis.

4.4.5 Independent brain networks derived from gr-SVD

The 2D topographies of relative electrical potential (rEP) at sensor space for the 12 extracted SVD components are shown in Figure 4-8(a) (results generated from step 6). Unique and independent neural networks were observed among the topographies associated with each SVD component.

Furthermore, Pearson Correlation Coefficient (PCC) was performed between each pair of the 20-minute SVD networks for each subject, to quantify temporal correlations among all 12 gr-SVD components. Figure 4-8(b) depicts the group-averaged PCC values for every pair of the 12 SVD components. The color bar represents the PCC between each pair; the vertical and horizontal axis depicts the 12 SVD components. Since all the self-correlations are meaningless, all the pairs of SVD components were marked as N/A (i.e., not applicable). All the PCCs among the SVD components were less than 0.45, indicating orthogonal and independent activities. This provides evidence that all the gr-SVD components were temporally independent. Thus, these 12 PCs were considered as the EEG brain networks following the definitions of large-scale brain networks(120, 124, 125).

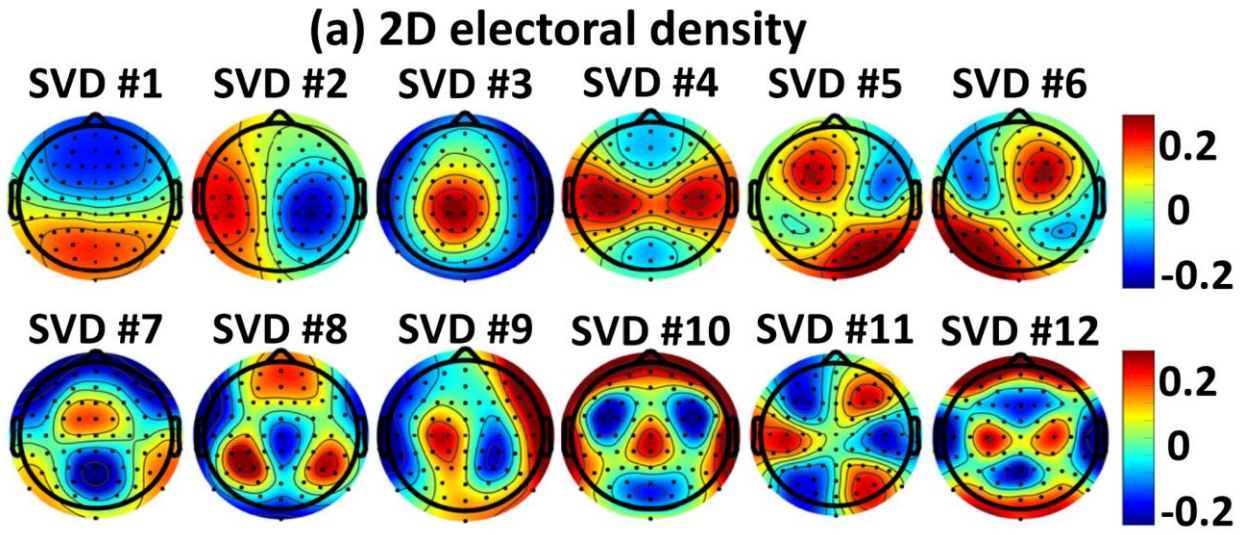

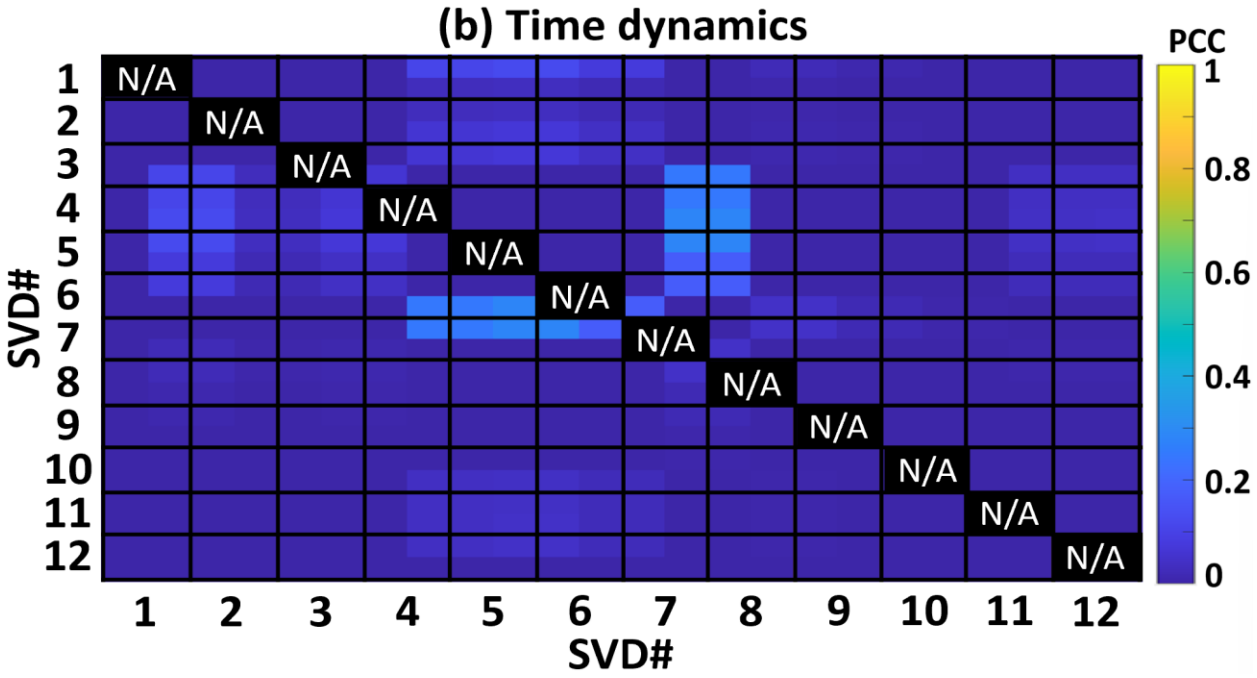

Figure 4-8: (a) 2D relative electrical potential (rEP) distributions; (b) the temporal dynamics' Pearson Correlation Coefficient (PCC) between each SVD component. The 12 SVD components have spatially distinct distributions along with a PCC of less than 0.4, suggesting independencies in brain networks. The self-correlation for each component is meaningless and hence marked with N/A (not applicable).

4.4.6 Mapping Brain activity of EEG networks common to both weeks in source space

To further compute the 3D models of the cortical/subcortical current density of each identified EEG brain network (SVD components), eLORETA was utilized as shown in Figure 4-9 (results generated from step 6). The 2D topographies of the EEG brain networks are shown in the left column of Figure 4-9. The color bar for each topography shows the rEP of the 'dipole' across the scalp (no unit). The axial, sagittal, and coronial views of the current density of neural activity are shown in the middle three columns. The 3D rendered brain templates' top and side views of the

left and right hemispheres are shown in the rightmost column. The medial sagittal views of the brain are shown for all the networks to expose anatomical locations of the subcortical sources. A threshold of >75% of the maximum neural activity indicating the binarized associated cortical locations is shown with yellow color in each 3D brain model. In other words, if the neural activity of the voxel lies within the top 25 percentile across the 6239 voxels, then the voxel was rendered with a yellow color. The anatomical and structural locations of cortical regions and loves were generated with the help of eLORETA for all the 12 EEG networks identified through gr-SVD.

With the help of eLORETA, we identified the key brain regions and cortical lobes that had the highest neural activity (i.e., cortical electrical density) for each SVD component, as listed in Table. 5. For example, SVD #12 represents a network corresponding to the precentral gyrus and inferior parietal lobe, while SVD #1 and #3 reveal a network corresponding to the cingulate gyrus and precuneus.

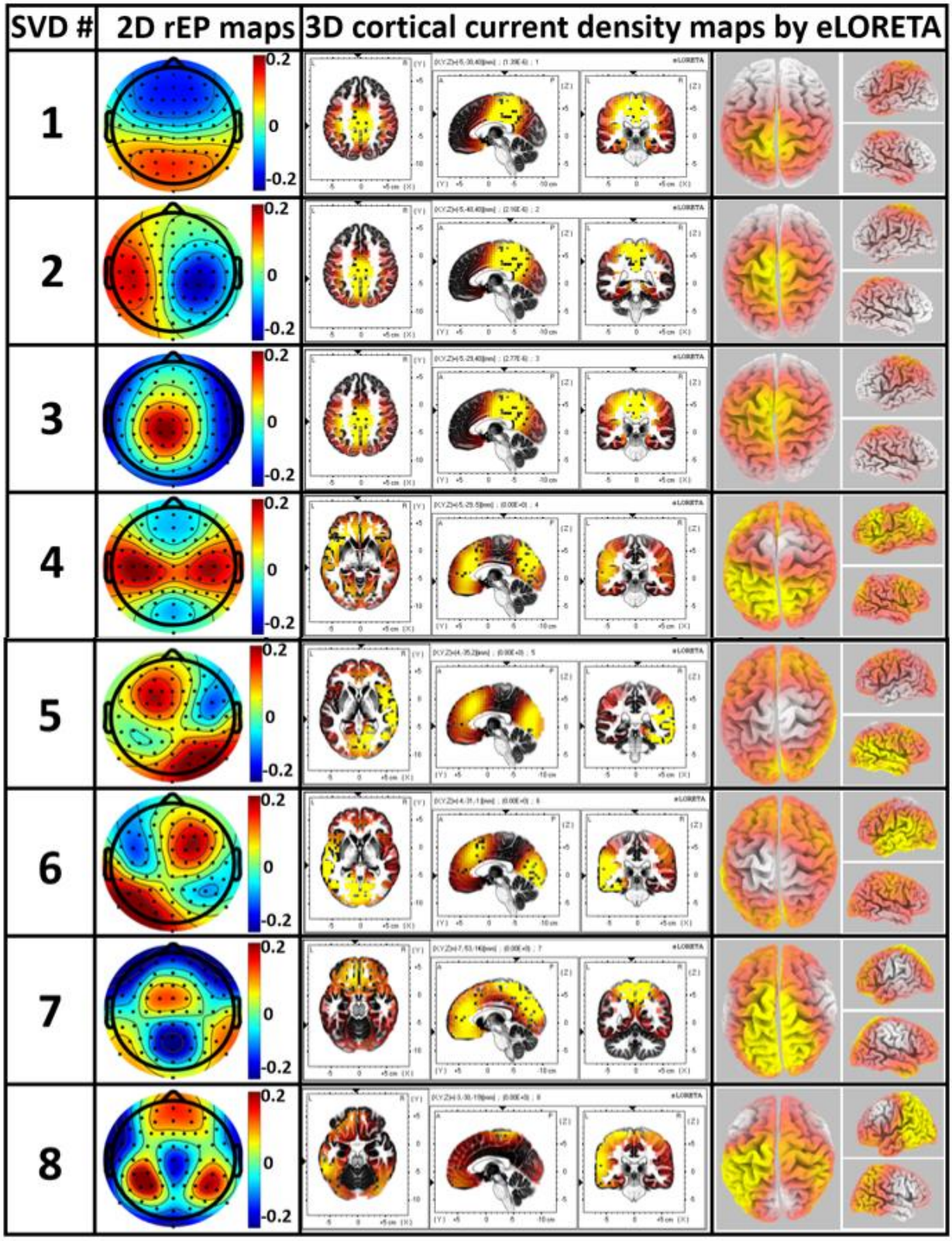
SVD #
2D rEP maps
3D cortical current density maps by eLORETA
1
2
3
4
5
6
7
8
0.2
0
-0.2

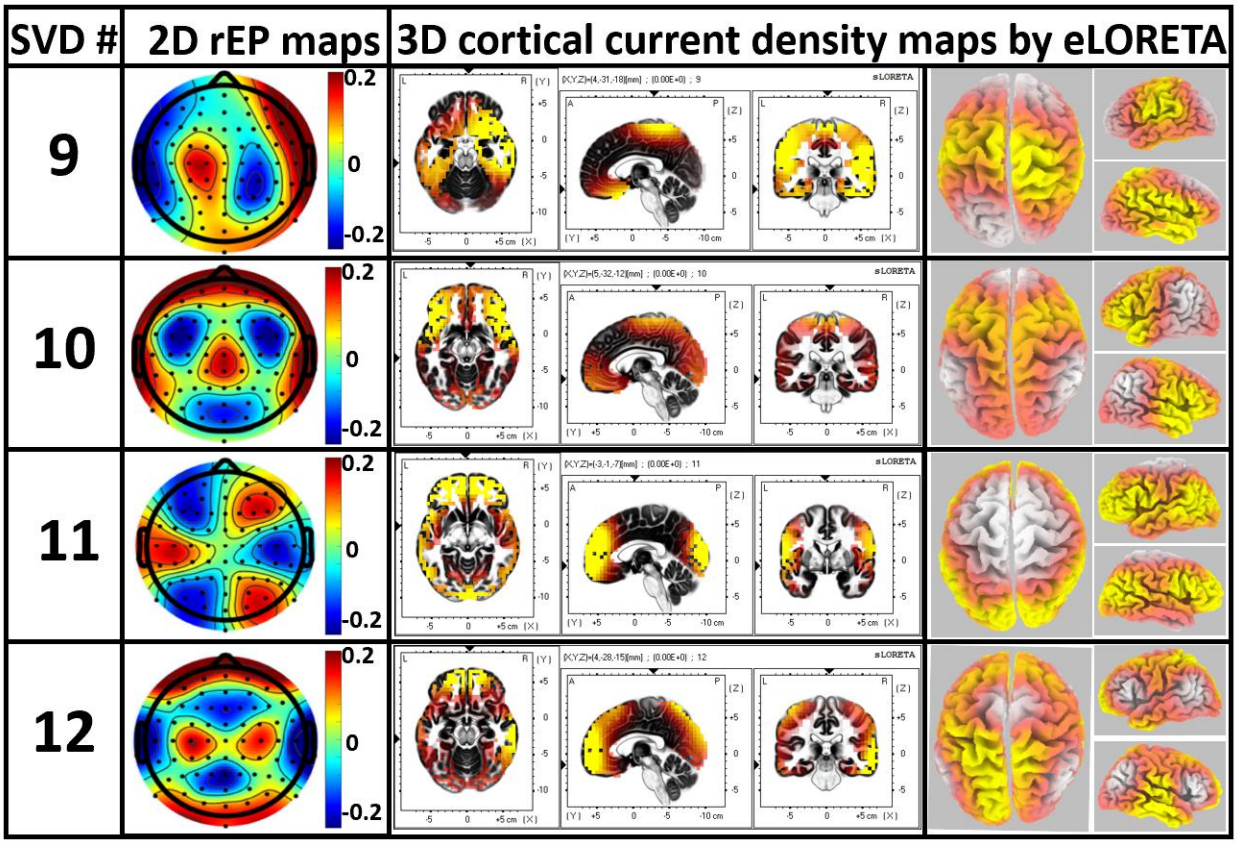

Figure 4-9: 3D source localization of cortical current density and 2D rEP maps of 12 identified SVD components. Left most column shows the 2D rEP map, middle column indicates the axial, sagittal, and coronial views for each rEP maps, and right most column depicts the top and side view of the left and right hemisphere for 3D rendered brain templates. The yellow color in each brain model indicates the binarized cortical current density for a threshold of >75% of the maximum neuronal activity in respective brain models.

4.4.7 Power change by LED stimulation during week 1 and week 4

The nPSD values were initially averaged across 0.5-70 Hz for TP1 and TP2. The consistency between the spectral averaged nPSD values was tested during TP1 and TP2 using one-way

ANOVA in all the frequency bands, both the weeks. The outcome shows consistency between TP1 and TP2 in all the frequency bands for both the weeks. The results are shown in Table A4-1.

SVD	Associated cerebral lobes	Associated brain regions
# 1	limbic lobe, parietal lobe	cingulate gyrus, precuneus
# 2	limbic lobe, parietal lobe	cingulate gyrus
# 3	limbic lobe, parietal lobe	cingulate gyrus, precuneus
# 4	Left: frontal, parietal lobe	Left: inferior frontal gyrus, inferior parietal lobule
# 5	Left: frontal, parietal, occipital lobe	Left: inferior frontal gyrus, inferior parietal lobule, precuneus
# 6	Right: frontal, parietal, occipital lobe	Right: inferior frontal gyrus, inferior parietal lobule, precuneus
# 7	medical frontal lobe, limbic lobe	medial frontal gyrus, anterior cingulate, cingulate gyrus
# 8	Frontal lobe, temporal lobe	Cingulate gyrus, lateral visual lobule
# 9	frontal lobe, parietal lobe	precentral gyrus, postcentral gyrus, inferior parietal lobule
# 10	Frontal lobe, limbic lobe	Cingulate gyrus
# 11	Right: occipital lobe	Right: middle occipital gyrus, cuneus
# 12	Frontal lobe, parietal lobe	Precentral gyrus, inferior parietal lobe

Table 6: Main associated cortical lobes and regions for the 12 networks from eLORETA.

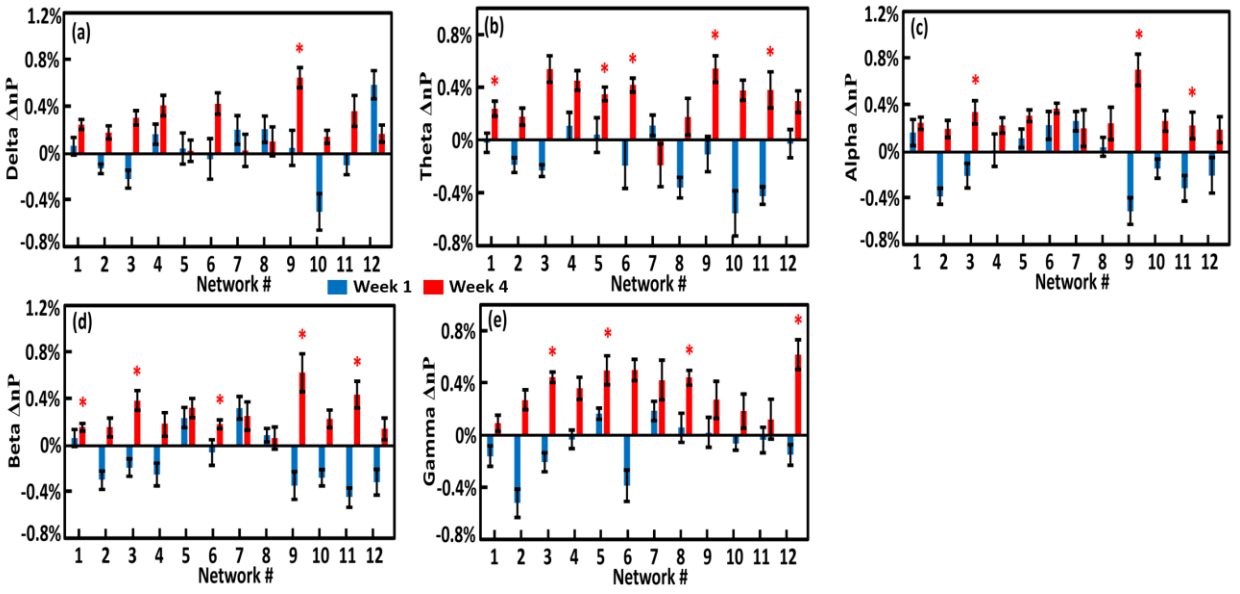

Figure 4-10: Group-level Δnp (i.e. baseline-normalized, sham subtracted EEG powers) for each brain network in (a) Delta, (b) Theta, (c) Alpha, (d) Beta, and (e) Gamma bands for TP3 during

week 4 (red) and week 1 (blue). The standard error of the mean is represented by the error bars. The significant differences of Δnp between LED and sham using one-sample non-parametric test between Δnp versus zero were performed at the significance level of $p<0.05$ and were indicated by '*'.

The results for power change by LED stimulation were developed from Step 8 in data processing. For both week 1 and week 4, Δnp was calculated within each frequency band by subtracting the baseline-normalized sham group averaged power from the baseline-normalized LED group averaged power for all the 12 brain networks. This procedure was followed for both time periods under the "during stimulation" condition (TP3 and TP4). Figure 4-10 and Figure 4-11 shows the group-level Δnp in all the frequency bands for TP3 and TP4 respectively. After inspecting each SVD network and the brain regions given in Table 5, we suggest that LED tends to increase theta, beta and gamma band oscillations at cingulate gyrus, precuneus, frontal, parietal and occipital lobes.

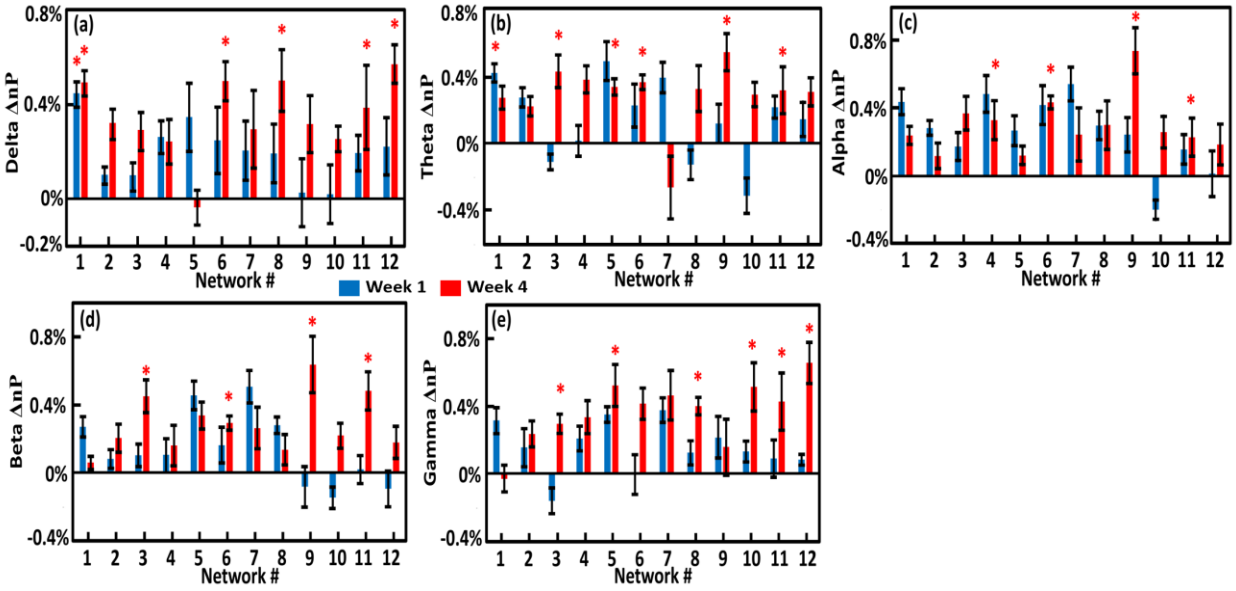

Figure 4-11: Group-level Δnp (i.e. baseline-normalized, sham subtracted EEG powers) for each brain network in (a) Delta, (b) Theta, (c) Alpha, (d) Beta, and (e) Gamma bands for TP4 during week 1 (blue) and week 4 (red). Error bars represents the standard error of the mean. The '*' mark indicates significant in Δnp between LED and sham using one-sample non-parametric tests between Δnp versus zero were performed at the significance level of $p<0.05$.

4.5 DISCUSSION

This is the first study, to our knowledge, that demonstrates the effects of LED stimulation on the prolonged improvement of attention performance and prolonged boost of electrophysiology functions on healthy subjects. We conducted 64-channel EEG measurements from 22 healthy human subjects while they performed the PVT task. Improvement in vigilance/attention was tracked (reaction time) over four weeks. We found a significant decrease in the reaction time of tPBM treated subjects over time. In addition, we found LEDs have significant effects on global EEG power at the temporal lobe and motor region in the delta band, and left temporal, parieto-occipital lobes in the alpha band in the human brain.

4.5.1 Effect of LED stimulation on gradual behavioral changes

LED effects on reaction time are reported in Figure 4-3. Reaction time significantly decreased over four weeks for subjects receiving active LED stimulation, which is consistent with previous studies (70). However, reaction time did not change significantly for sham subjects. To our knowledge, this is the first study that shows the improvement in reaction time due to LED stimulation over time in healthy subjects. These observations could be interpreted as LED

stimulation increasing the activity in the electron transport chain of mitochondria, particularly in transmembrane protein complex IV (CCO) (126). The major photo acceptor within, 600-900 nm wavelength range of red/NIR light is CCO (70). This increase in the activity of CCO provides more neuronal metabolic energy (ATP) available to perform the tasks. An increase in ATP would increase hemodynamic activation (cellular respiration and oxygenation) (70). Thus, with continuous tPBM over 4 weeks, LED stimulation improved attention by providing more energy in the form of ATP. This was reflected by the shortened reaction time over time of tPBM treated subjects.

4.5.2 Longitudinal Power improvement in Brain oscillations by LED stimulation

In this study, we observed that four weeks of LED stimulation increased global EEG nPSD in theta, beta, and gamma bands (Figure 4-6). Attention and efficient processing of the task is often associated with theta (127, 128), beta (128), and gamma bands (129-132). Consistent with these studies, we observed an increase in theta, beta, and gamma band power after four weeks of LED stimulation.

A global increment in nPSD is observed from Figure 4-6 for the EEG theta band. Theta band is often associated with the onset of drowsiness (133). Moreover, theta band is also associated with efficient processing of cognitive tasks and attention (127, 128, 134). It has been suggested that the prefrontal cortex exerts top-down control via inter-areal communication in the theta frequency range (87, 135, 136). An increase in theta activity in the frontal areas shows its involvement in the working memory tasks (137-139). Previous studies have revealed that increase in theta and gamma power represents the neural correlation of working memory

processing (140-142). These observations may indicate that LEDs improves efficiency in processing of the cognitive tasks.

Moreover, a global increase in nPSD was observed for the beta band after four weeks of LED stimulation (Figure 4-6). Beta band is associated with cognitive functions such as working memory (143-146), executive control of action (147-149), state of alert (128), and preventing distraction (150, 151). Some studies have suggested that beta oscillations convey moment-to-moment top-down modulatory signals to lower sensory cortices, maintaining the existing mental states (152, 153). Wrobel et. al. showed that beta band activity reflects arousal of the visual system during visual attention task (154). Beta oscillatory responses have been considered to be related to motor and somatosensory functions (155). Arousal of the visual system due to increased visual attention has also been thought to increase beta activity (154). All these observations indicate that LED stimulation improves the cognitive processing induced by the visual attention task.

Gamma band nPSD was observed to increase globally from Figure 4-6. Gamma frequency oscillations have been extensively studied in cognitive processes engaged in attention, memory, and perception (142, 156-160). Also, gamma oscillations have been correlated with memory loading, formation, and maintenance (161-163). During synchronized activity of neurons encoding sensory features of external stimuli in cat visual cortex, gamma oscillations are responsible for binding coherent object representations in the brain (164). Gamma oscillations have been proposed to play a role in mechanisms of synaptic plasticity and memory formations (159, 160, 165), and have been shown to be modulated by cognitive processes engaged in spatial working memory in monkeys (144), and recognition memory task in humans (166). Hence, these

oscillations have been thought to play a role in synchronizing neural processing during cognitive processes within the timeframe of the gamma oscillations cycle, setting a temporal window or a 'clock' (159). So even though their role in information processing in the brain is unclear, increase in the gamma oscillations after LED stimulation are likely to reflect neural processing supporting cognition.

4.5.3 Large scale neural activities presented by gr-SVD-derived EEG brain networks

4.5.3.1 Similarity of gr-SVD-derived EEG brain networks to fMRI defined networks

The application of gSVD with eLORETA enabled us to isolate and identify 12 intrinsic EEG brain networks. Figure 4-8 shows the 12 SVD dominant networks, which take 73% of the total contribution in the recorded EEG signal. This is consistent with the neural physiology that communication among neurons and functional activity in the human brain takes about 60-80% of total energy (125). We recognized spatial co-localizations between the SVD-identified EEG networks and fMRI-recognized networks (109, 167-171), by inspecting the active cortical localizations of each EEG network shown in Figure 4-9 and Table 5. Although, EEG records electrophysiological oscillations at much higher frequencies with lower spatial resolution than fMRI, SVD-derived EEG brain networks may reflect the same neural activity recognized using fMRI-defined brain networks. For example, EEG network #7 is related to the anatomical sites involving the executive control network (ECN). The gr-SVD derived EEG networks #1-3 represent the posterior default mode network (pDMN) of fMRI. Whereas #4 and #5 networks share the anatomical locations with the left and right fronto-parietal networks (L- and R-FPN).

4.5.3.2 Advantages of using gr-SVD to monitor the vigilance-sensitive networks

The first 7 most-weighted gr-SVD derived EEG networks took about 61% (area under the curve for the first 7 points in Figure 4-7) of the total EEG signal contribution. These networks represent the fMRI-recognized, cognitive-sensitive networks such as DMN, FPN, and ECN. These observations indicated the potential advantage of using gr-SVD along with eLORETA to monitor EEG network-based fast neuronal activity in these cognition-related networks.

Networks #1, 2, 3 and 8 were found to be associated with the DMN network. The DMN is considered as the most important and dominant network in the human brain (172-174). Our results found are consistent with this statement. Specifically, these networks associated with the DMN network accounted for almost 43.6% and 60% of all the EEG signals (64 components) and 12 most weighted/ dominant brain networks. Thus, gr-SVD along with eLORETA offer a potentially feasible means to extract the dominant DMN fluctuations of the human brain from EEG recordings. Recent studies have reported the importance of DMN network in many cognitive tasks, such as memory consolidation (175), memory encoding (174), and attention (176). DMN network has also been found to be associated with mental health and psychological conditions of the human brain (177-179). Thus, the ability of gr-SVD along with eLORETA to detect the DMN network by EEG will expand EEG's applications as a potential neural monitoring tool along with providing high temporal resolution.

FPN (left and right) and ECN brain networks were also identified by the gr-SVD algorithm, ranked as #4-7. These networks contributed about 27.5% among the 12 dominant networks. FPN is a commonly observed network during sustained attentional tasks (94). The FPN network has

been known to play an important role in cognition (171, 180, 181), attention, memory consolidation and memory encoding (182-185). Similarly, the ECN network plays a crucial role in humans executive control functions during sustained attentional tasks such as cognitive inhibition, inhibitory control, working memory, reasoning, memory, problem solving, and planning (182, 186, 187). The ability of SVD algorithm along with eLORETA to detect these memory related networks would expand the applications of EEG for high-temporal resolution monitoring of cognitive functions in the human brain.

4.5.3.3 Enhancement of Theta power by LED in selected brain networks

As observed from Figure 4-10(b) and Figure 4-11(b), after self-baseline normalization, LED-based tPBM increases EEG theta power in several brain networks, when compared with sham conditions. Significant effects of LED-based stimulation on theta power were observed at SVD network #3 (pDMN), #6 (right FPN), #9 (FPN), #11 (occipital) throughout the 4 weeks of stimulation period. Previous studies have reported that theta band activity is related to attention and efficient processing of cognitive tasks (127, 188-190). Theta power increase has also been linked to orienting (189), memory (134, 191), and effective processing mechanisms (192, 193). However, these studies were presented over a large cortical area of the human brain. There was a lack of association of neuromodulation effect of LED-based tPBM with brain networks associated with vigilance to localize the special cortical regions.

The implementation of gr-SVD for temporal-spatial decomposition of EEG signal (98), is analogous to the principle component analysis (194). Thus, we can consider the gr-SVD derived components from the EEG as dominant networks of the EEG signal. The gr-SVD implementation

generated 64 orthogonal dominant networks. Table 5 revealed that enhancement in theta power originated from the cingulate gyrus, precuneus, right inferior frontal and parietal lobule, precentral gyrus, postcentral gyrus, and occipital gyrus. All these brain regions are associated with human cognitive functions. The anterior cingulate and medial frontal gyrus are active in decision making (195); the parietal lobule is involved for the information manipulation during working memory (196); the cingulate gyrus is related with memory processing (197); the inferior frontal and parietal lobule plays a major role in decision making (198, 199); the occipital lobe is required for perception (196); and the precuneus is related to processing memory tasks (200). Hence, we speculate that the LED-based tPBM induced augmentation of vigilance, maybe a result from the increment of theta power in these cognition related EEG cortical networks.

4.5.3.4 Enhancement of Beta power by LED in selected gr-SVD derived EEG brain networks

Increase in EEG beta power was also observed after LED-based tPBM was observed from Figure 4-10(d) and Figure 4-11(d) after removing the sham effects in several EEG brain networks. Similar to theta band, an increase was observed at gr-SVD derived networks #3 (pDMN), #6 (right FPN), #9 (FPN), #11 (occipital).

Beta band activity increase was reported in alert state, having their eyes open, or anxious (128). Beta activity is predominant in frontal and central regions (188) under alert state. It was shown that enhancement of the beta band occurs when subjects expect a visual stimulus (201). It was also shown that EEG beta band locking was linked with subjects successfully perceiving the visual stimuli (202). These studies could indicate towards increase in beta band activity in this

study could mean subjects successfully perceiving the visual stimuli and an increase in alertness/vigilance after four weeks of LED-based tPBM.

According to Table 5, Figure 4-10(d), and Figure 4-11(d), the major cortical regions with modulated beta oscillations are the cingulate gyrus, precuneus, right inferior frontal and parietal lobule, precentral gyrus, postcentral gyrus, and occipital gyrus. An increase in activity of beta oscillations has been reported in the right parietal hemisphere after LED stimulation ((203)). The increase of beta power in parietal regions for faster reaction time has been related to attention processing in many fMRI studies ((204-206)). In this study, enhancement in parietal lobule could be related to enhancement of parietal attention network. It is also possible that beta band enhancement in fronto-parietal regions could reflect top-down attentional control ((207)). These results are in agreement with previous MEG study showing that beta oscillations serve as a mechanism for spreading attentional arousal among higher cortical areas ((208)). Thus, the increase in beta band activity in all these cortical areas can potentially explain the improvement in vigilance.

4.5.3.5 Enhancement of Gamma power by LED in selected brain networks

In addition to the effect on theta, beta band, a significant increase in gamma power was also observed from Figure 4-10(e) and Figure 4-11(e). A significant increase was observed in #3 (DMN), #5 (FPN), # 8 (DMN), #10 (occipital), #11 (occipital), and #12 (FPN) gr-SVD derived brain networks.

Gamma band oscillations are associated with cognitive functions such as, attention, perception, and memory (142, 157, 158). Gamma band oscillations have also been thought to play a role in mechanisms of synaptic plasticity and memory formation (159, 160, 165). Gamma oscillations have also been shown to be modulated in spatial working memory in monkeys (146) by cognitive processing engaged in recognizing memory tasks in humans (166). The increase in LED-based gamma oscillations in this study could indicate improved cognitive processing.

According to Table 5 and Figure 4-11(e), the major cortical areas with modulated gamma oscillations included the cingulate gyrus, inferior frontal and parietal lobules, precuneus, lateral visual lobule, and precentral gyrus. LED-based tPBM modulates the gamma power in the occipital gyrus, which plays a role in tactile information (209) processing as well as for cognitive processing for depression (210). Thus, the increase in gamma power in the above mentioned cortical locations can potentially explain the improvement in vigilance and cognitive functions (19, 211).

4.5.4 Limitation and future work

This study had certain limitations. First, we analyzed the effects of the first 10 minutes of LED stimulation. However, more studies on the effects of prolonged stimulation during a single visit are required to determine the adequate stimulation time to get optimum improvement. The second limitation is the in this study the source localization was performed using a 64 channel EEG system, which might not have provided high spatial resolution for an accurate localization of the cortical sources. Further studies are required using high density EEG measurements with 256 electrodes, which may improve the spatial resolution of the source localization using eLORETA.

Second, the lower sample size could have led to lower statistical probability. More studies with a larger sample size are required to verify the results.

4.6 CONCLUSION

Our observations provide substantial evidence that LED stimulation for ten minutes significantly affects brain activity. We showed for the first time that acute increase in delta and alpha band power during LED stimulation while performing tasks similar to laser stimulation. We also showed that theta, beta, and gamma band power significantly increased globally after four weeks of LED stimulation. Another novel finding was that reaction time for LED treated subjects improved significantly over four weeks (Prolonged improvement in vigilance). Future more we implemented a novel methodology of gr-SVD, followed by eLORETA source localization to analyze the human EEG signal under the LED-based stimulation while performing a vigilance based task. This resulted in the identification of 12 independent and orthogonal EEG brain networks in both source space as well as in sensor space. We showed for the first time that theta, beta, and gamma band powers are significantly neuromodulated under LED stimulation in various gr-SVD derived brain networks. Moreover, many well-defined fMRI-derived brain networks were identified and found to be neuromodulated such as, the default mode network, executive control network, and fronto-parietal network. These results clearly reveal the mechanisms behind LED-based tPBM and its effect on cognitive/vigilance outcomes.

Chapter 5- CONCLUSION AND FUTURE SCOPE

5.1 CONCLUSION

The primary objective of this work was to develop algorithms to analyze biological signals. Specifically, my dissertation work focused on two major topics: (1) EGG response to GI maturity in preterm, term neonates under different feeding interventions; and (2) Mapping of electrophysiological responses in healthy human brain in response to tPBM using LED-based stimulation. In all, the outcome of this work was to develop algorithms and biological signal processing to identify the biomarkers for GI maturity in neonates and LED-based tPBM electrophysiological changes in healthy human brain.

Specifically, in the first study, as presented in chapter 2, EGG was used to characterize different parameters of gastric myoelectric activity in neonates of different GA under before, during and post feeding conditions, which is currently absent in the current EGG studies. The gastric myoelectric activity in preterm neonates had no alterations in EGG PSD in response to any feeding period. The mean PSD values were found to significantly increase in normogastria (2-4 cpm), and tachygastria (4-9 cpm) with increase of gestational age. The percentage of time spent in normogastria also increased with increase in GA regardless of sub-feeding period. The findings in this study provides promising potential biomarkers for assessment of feeding readiness in preterm neonates.

The second study presented in this dissertation, in chapter 3, studied the electro-physiological changes induced by ten minutes of LED-based stimulation on healthy human brain. EEG was used to measure the electro-physiological changes induced by LED-based stimulation

under task-based condition in healthy human brain throughout the experimental paradigm, which is currently absent in current neuroimaging studies. Delta and Alpha band power significantly increased during LED stimulation while performing PVT task similar to laser stimulation. EEG power at the temporal lobe and motor regions were found to increase in delta band, and left-temporal, parietal-occipital lobes in the alpha band in the healthy human brain. These results imply that LED-based stimulation for ten minutes modulates electro-physiological changes in the delta, and alpha frequency bands.

After thorough investigation of acute electro-physiological changes, the final study, presented in chapter 4, investigated the prolonged effect of LED-based stimulation on EEG power, reaction time and brain networks. This study revealed that the reaction time significantly decreases over four weeks suggesting improvement in vigilance. The Power in Theta (4-7 Hz), Beta (13-30 Hz), and Gamma (30-70 Hz) frequency bands significantly increases after four weeks under LED-based stimulation. Furthermore, power increment was also found in default mode network, executive control network, fronto-parietal network, and visual network. These results may help understand the underlying mechanisms of LED-based tPBM modulated brain networks while performing vigilance tasks.

5.2 FUTURE SCOPE

In the future, this work could be improved upon several limitations.

First, in chapter 2, the sample size for the term babies was too small, preventing reliable statistical conclusions. Further studies are required to verify the outcomes of this study with higher sample size of term babies. The EGG is sensitive to motion artifacts, thus additional motion artifact identification, removal and denoising algorithms to acquire a higher quality of

EGG data are few future directions before EGG can serve as a standard tool to measure GI maturity in preterm neonates.

Second, in chapter 3 and 4, the lower sample size led to lower statistical probability. Further studies with larger sample size are required to verify the results. Another limitation in LED-based study is that a combination of infrared (810 nm) and visible light (660 nm) frequencies was used for stimulation, further studies on effects of different wavelengths are required. The source localization was performed using a 64-channel EEG system, which might have limited the spatial resolution for an accurate localization of the cortical sources. Further studies using high density EEG with 256 electrodes, may improve spatial resolution of the source localization using eLORETA.

References:

1. D. J. Raiten et al., "Working group reports: evaluation of the evidence to support practice guidelines for nutritional care of preterm infants-the Pre-B Project," *Am J Clin Nutr.* 1938-3207 (Electronic)), 103(102):648S-178S (2016).
2. J. Neu, and L. Zhang, "Feeding intolerance in very-low-birthweight infants: what is it and what can we do about it?," *Acta Paediatr Suppl.* 0803-5326 (Print)), 94(449):493-499 (2005).
3. T. A. Moore, and R. H. Pickler, "Feeding intolerance, inflammation, and neurobehaviors in preterm infants," *J Neonatal Nurs.* 1355-1841 (Print)), 23(23):134-141 (2017).
4. J. D. Chen, R. W. Schirmer Bd Fau - McCallum, and R. W. McCallum, "Serosal and cutaneous recordings of gastric myoelectrical activity in patients with gastroparesis," *Am J Physiol* 0002-9513 (Print)), 266(261 Pt 261):G290-G298 (1994).
5. B. Pfaffenbach et al., "Gastric dysrhythmias and delayed gastric emptying in patients with functional dyspepsia," *Dig Dis Sci.* 0163-2116 (Print)), 42(10):2094-2099 (1997).
6. S. Cucchiara et al., "Gastric electrical dysrhythmias and delayed gastric emptying in gastroesophageal reflux disease," *Am J Gastroenterol* 92(97):1103-1108 (1997).
7. A. Siegl et al., "Postprandial tachygastria is frequent in infants with gastroesophageal reflux," *Pediatr Surg Int.* 0179-0358 (Print)), 13(18):569-571 (1998).
8. J. Bustorff-Silva, "Electrogastrography for evaluating neurologically impaired children with recurrent vomiting," *J Pediatr Gastroenterol Nutr.* 27(23):373-374 (1998).
9. A. M. Ravelli, and P. J. Milla, "Vomiting and gastroesophageal motor activity in children with disorders of the central nervous system," *J Pediatr Gastroenterol Nutr.* 0277-2116 (Print)), 26(21):56-63 (1998).
10. J. D. Chen et al., "Abnormal gastric myoelectrical activity and delayed gastric emptying in patients with symptoms suggestive of gastroparesis," *Dig Dis Sci.* 41(48):1538-1545 (1996).
11. A. R. Precioso, F. A. C. Pereira Gr Fau - Vaz, and F. A. Vaz, "Gastric myoelectrical activity in neonates of different gestational ages by means of electrogastrography," *Rev Hosp Clin Fac Med Sao Paulo* 0041-8781 (Print)), 58(52):81-90 (2003).
12. J. D. Chen, and R. W. McCallum, "Clinical applications of electrogastrography," *Am J Gastroenterol* 88(89):1324-1336 (1993).
13. R. D. Rothstein, J. C. Alavi A Fau - Reynolds, and J. C. Reynolds, "Electrogastrography in patients with gastroparesis and effect of long-term cisapride," *Dig Dis Sci.* 0163-2116 (Print)), 38(38):1518-1524 (1993).
14. J. Y. Park et al., "Illumination influences working memory: an EEG study," *Neuroscience* **247**(386-394 (2013).
15. J. T. Eells et al., "Mitochondrial signal transduction in accelerated wound and retinal healing by near-infrared light therapy," 1567-7249 (Print)).
16. E. Vargas et al., "Beneficial neurocognitive effects of transcranial laser in older adults," *Lasers in Medical Science* **32**(5), 1153-1162 (2017).
17. X. Wang et al., "Transcranial Laser Stimulation Increases Power of Brain Oscillations and Information Flow Measured by EEG," in OSA Technical Digest, *Biophotonics Congress: Biomedical Optics Congress 2018 (Microscopy/Translational/Brain/OTS)* JTh3A.56 (2018).
18. X. Wang et al., "Up-regulation of cerebral cytochrome-c-oxidase and hemodynamics by transcranial infrared laser stimulation: A broadband near-infrared spectroscopy study," 1559-7016 (Electronic)).
19. D. W. Barrett, and F. Gonzalez-Lima, "Transcranial infrared laser stimulation produces beneficial cognitive and emotional effects in humans," 1873-7544 (Electronic)).

20. N. J. Blanco, C. L. Saucedo, and F. Gonzalez-Lima, "Transcranial infrared laser stimulation improves rule-based, but not information-integration, category learning in humans," 1095-9564 (Electronic)).
21. X. Wang et al., "Transcranial photobiomodulation with 1064-nm laser modulates brain electroencephalogram rhythms," *Neurophotonics* **6**(2), 025013 (2019).
22. N. A. Busch et al., "Size matters: effects of stimulus size, duration and eccentricity on the visual gamma-band response," 1388-2457 (Print)).
23. S. Johannes et al., "Luminance and spatial attention effects on early visual processing," 0926-6410 (Print)).
24. K. Momose, "Determination of the Chromatic Contrast Responses using Wavelet Analysis of Visual Evoked Potentials," *2005 IEEE Engineering in Medicine and Biology 27th Annual Conference* 6993-6995 (2005).
25. M. H. Berman et al., "Photobiomodulation with Near Infrared Light Helmet in a Pilot, Placebo Controlled Clinical Trial in Dementia Patients Testing Memory and Cognition. LID - 176 [pii] LID - 10.21767/2171-6625.1000176 [doi]," 2171-6625 (Print)).
26. A. Fekri et al., "Short-term Effects of Transcranial Near-Infrared Photobiomodulation on Motor Performance in Healthy Human Subjects: An Experimental SingleBlind Randomized Clinical Trial," *J Lasers Med Sci* **10**(4), 317-323 (2019).
27. M. A. Naeser et al., "Improved cognitive function after transcranial, light-emitting diode treatments in chronic, traumatic brain injury: two case reports," 1557-8550 (Electronic)).
28. A. E. Saltmarche et al., "Significant Improvement in Cognition in Mild to Moderately Severe Dementia Cases Treated with Transcranial Plus Intranasal Photobiomodulation: Case Series Report," 1557-8550 (Electronic)).
29. C. JD, "Spectral analysis of electrogastrogram and its clinical significance.," *World J Gastroenterol* 2(Suppl1): 9-11 (1996).
30. A. Lange, P. Huang L Fau - Funch-Jensen, and P. Funch-Jensen, "Electrogastrography in neonates," *Neurogastroenterol Motil* 1350-1925 (Print)), 17(14):512-517 (2005).
31. E. B. Ortigoza et al., "Electrogastrography, Near-infrared Spectroscopy, and Acoustics to Measure Gastrointestinal Development in Preterm Babies," *J Pediatr Gastroenterol Nutr.* 1536-4801 (Electronic)), 66(66):e146-e152 (2018).
32. J. D. Chen et al., "Detection of gastric slow wave propagation from the cutaneous electrogastrogram," *Am J Physiol* 0002-9513 (Print)), 277(272):G424-G430 (1999).
33. A. Kasicka-Jonderko et al., "Comparison of multichannel electrogastrograms obtained with the use of three different electrode types," *J Smooth Muscle Res.* 0916-8737 (Print)), 42(42-43):89-101 (2006).
34. Z. Rossi et al., "Electrogastrography," *Eur Rev Med Pharmacol Sci.* 1128-3602 (Print)), 9(5 Suppl 1):29-35 (2005).
35. J. Xu et al., "FC-NIRS: A Functional Connectivity Analysis Tool for Near-Infrared Spectroscopy Data," *BioMed Research International* **2015**(248724 (2015).
36. H. Niu, and Y. He, "Resting-state functional brain connectivity: lessons from functional near-infrared spectroscopy," *Neuroscientist* 1089-4098 (Electronic)), 20(22):173-188 (2014).
37. S. Jevrejeva, J. C. Moore, and A. Grinsted, "Influence of the Arctic Oscillation and El Niño-Southern Oscillation (ENSO) on ice conditions in the Baltic Sea: The wavelet approach," *Journal of Geophysical Research: Atmospheres* **108**(D21), (2003).
38. G. Riezzo et al., "Comparison of gastric electrical activity and gastric emptying in healthy and dyspeptic children," *Dig Dis Sci.* 0163-2116 (Print)), 45(43):517-524 (2000).

39. G. Riezzo et al., "Gastric electrical activity in normal neonates during the first year of life: effect of feeding with breast milk and formula," *J Gastroenterol Hepatol* 0944-1174 (Print)), 38(39):836-843 (2003).
40. J. Liang et al., "Development of gastric slow waves in preterm infants measured by electrogastrography," *Am J Physiol* 0002-9513 (Print)), 274(273):G503-G508 (1998).
41. J. Zhang et al., "Development of gastric slow waves and effects of feeding in pre-term and full-term infants," *Neurogastroenterol Motil.* 1350-1925 (Print)), 18(14):284-291 (2006).
42. S. Cucchiara et al., "Gestational maturation of electrical activity of the stomach," *Dig Dis Sci.* 44(10):2008-2013 (1999).
43. M. Patterson, D. A. Rintala R Fau - Lloyd, and D. A. Lloyd, "A longitudinal study of electrogastrography in normal neonates," *J Pediatr Surg* 0022-3468 (Print)), 35(31):59-61 (2000).
44. F. Y. Chang, "Electrogastrography: basic knowledge, recording, processing and its clinical applications," *J Gastroenterol Hepatol* 20(24):502-516 (2005).
45. H. P. Parkman et al., "Electrogastrography: a document prepared by the gastric section of the American Motility Society Clinical GI Motility Testing Task Force," *Neurogastroenterol Motil* 1350-1925 (Print)), 15(12):89-102 (2003).
46. N. M. Devanarayana, H. J. de Silva Dg Fau - de Silva, and H. J. de Silva, "Gastric myoelectrical and motor abnormalities in children and adolescents with functional recurrent abdominal pain," *J Gastroenterol Hepatol* 1440-1746 (Electronic)), 23(11):1672-1677 (2008).
47. Z. Lin et al., "Postprandial response of gastric slow waves: correlation of serosal recordings with the electrogastrogram," *Dig Dis Sci.* 0163-2116 (Print)), 45(44):645-651 (2000).
48. R. W. Summers, "Electrogastrography, Principles and Applications," *Gastrointestinal Endoscopy* **42**(4), 384-385 (1995).
49. C. P. Sanmiguel, K. L. Mintchev Mp Fau - Bowes, and K. L. Bowes, "Electrogastrography: a noninvasive technique to evaluate gastric electrical activity," *Can J Gastroenterol* 0835-7900 (Print)), 12(16):423-430 (1998).
50. M. I. Oppenheim, and D. F. Sittig, "An innovative dicrotic notch detection algorithm which combines rule-based logic with digital signal processing techniques," *Comput Biomed Res* 0010-4809 (Print)), 28(22):154-170 (1995).
51. G. Riezzo, F. Russo F Fau - Indrio, and F. Indrio, "Electrogastrography in adults and children: the strength, pitfalls, and clinical significance of the cutaneous recording of the gastric electrical activity," *Biomed Res Int.* 2314-6141 (Electronic)), 2013:282757 (2013).
52. G. Strang, "Wavelets and Dilation Equations: A Brief Introduction," *SIAM Rev.* **31**(614-627 (1989).
53. O. Herrera Alcántara, and M. González Mendoza, "Optimization of Parameterized Compactly Supported Orthogonal Wavelets for Data Compression," I. Batyrshin, and G. Sidorov, Eds., *Advances in Soft Computing* 510-521 (2011).
54. A. Al Kafee, and A. Akan, "Analysis of gastric myoelectrical activity from the electrogastrogram signals based on wavelet transform and line length feature," *Proc Inst Mech Eng H* **232**(4), 403-411 (2018).
55. G. W. Reynolds et al., "Continuous wavelet analysis of postprandial EGGs suggests sustained gastric slow waves may be slow to develop in infants with colic," *Neurogastroenterol Motil* **29**(3), (2017).
56. D. Komorowski, and S. Pietraszek, "The Use of Continuous Wavelet Transform Based on the Fast Fourier Transform in the Analysis of Multi-channel Electrogastrography Recordings," *J Med Syst* **40**(1), 10 (2016).
57. M. Tokmakci, "Analysis of the electrogastrogram using discrete wavelet transform and statistical methods to detect gastric dysrhythmia," *J Med Syst* **31**(4), 295-302 (2007).

58. I. V. Tchervensky et al., "Centre-specific multichannel electrogastrographic testing utilizing wavelet-based decomposition," *Physiol Meas* **27**(7), 569-584 (2006).
59. S. Kara, F. Dirgenali, and S. Okkesim, "Detection of gastric dysrhythmia using WT and ANN in diabetic gastroparesis patients," *Comput Biol Med* **36**(3), 276-290 (2006).
60. F. Dirgenali, S. Kara, and S. Okkesim, "Estimation of wavelet and short-time Fourier transform sonograms of normal and diabetic subjects' electrogastrogram," *Comput Biol Med* **36**(12), 1289-1302 (2006).
61. R. J. de Sobral Cintra et al., "Optimal wavelets for electrogastrography," *Conf Proc IEEE Eng Med Biol Soc* **2006**(329-332 (2004).
62. J. D. Chen et al., "Gastric myoelectrical activity in healthy children and children with functional dyspepsia," *Dig Dis Sci.* 0163-2116 (Print)), 43(11):2384-2391 (1998).
63. H. B. Cotler et al., "The Use of Low Level Laser Therapy (LLLT) For Musculoskeletal Pain," *MOJ Orthop Rheumatol* **2**(5), 00068 (2015).
64. H. T. Whelan et al., "Effect of NASA light-emitting diode irradiation on wound healing," 1044-5471 (Print)).
65. C. E. Tedford et al., "Quantitative analysis of transcranial and intraparenchymal light penetration in human cadaver brain tissue," 1096-9101 (Electronic)).
66. J. A. Wan S Fau - Parrish et al., "Transmittance of nonionizing radiation in human tissues," 0031-8655 (Print)).
67. J. R. Jagdeo et al., "Transcranial red and near infrared light transmission in a cadaveric model," 1932-6203 (Electronic)).
68. A. E. Young et al., "Behaviour of near-infrared light in the adult human head: implications for clinical near-infrared spectroscopy," 0007-0912 (Print)).
69. S. G. Hipskind et al., "Pulsed Transcranial Red/Near-Infrared Light Therapy Using Light-Emitting Diodes Improves Cerebral Blood Flow and Cognitive Function in Veterans with Chronic Traumatic Brain Injury: A Case Series. LID - 10.1089/pho.2018.4489 [doi]," 1557-8550 (Electronic)).
70. A. Jahan et al., "Transcranial near-infrared photobiomodulation could modulate brain electrophysiological features and attentional performance in healthy young adults," *Lasers in Medical Science* **34**(6), 1193-1200 (2019).
71. M. A.-O. DiFrancesco et al., "Network-based Responses to the Psychomotor Vigilance Task during Lapses in Adolescents after Short and Extended Sleep," 2045-2322 (Electronic)).
72. J. Hwang, D. M. Castelli, and F. Gonzalez-Lima, "Cognitive enhancement by transcranial laser stimulation and acute aerobic exercise," *Lasers in Medical Science* **31**(6), 1151-1160 (2016).
73. H. P. Van Dongen et al., "The cumulative cost of additional wakefulness: dose-response effects on neurobehavioral functions and sleep physiology from chronic sleep restriction and total sleep deprivation," 0161-8105 (Print)).
74. T. Industries, "Contact Information."
75. P. informatics, "Pulsar informatics."
76. A. Hyvärinen, and E. Oja, "Simple neuron models for independent component analysis," 0129-0657 (Print)).
77. R Core Team, "R: A language and environment for statistical computing. R Foundation for Statistical Computing, Vienna, Austria.," (2019).
78. T. Popov, R. Oostenveld, and J. M. Schoffelen, "FieldTrip Made Easy: An Analysis Protocol for Group Analysis of the Auditory Steady State Brain Response in Time, Frequency, and Space," 1662-4548 (Print)).
79. R. Oostenveld et al., "FieldTrip: Open source software for advanced analysis of MEG, EEG, and invasive electrophysiological data," 1687-5273 (Electronic)).

80. E. Başar, "A review of gamma oscillations in healthy subjects and in cognitive impairment," *International Journal of Psychophysiology* **90**(2), 99-117 (2013).
81. M. Tanaka et al., "Effect of mental fatigue on the central nervous system: an electroencephalography study," 1744-9081 (Electronic)).
82. S. Palva, and J. M. Palva, "Functional roles of alpha-band phase synchronization in local and large-scale cortical networks," 1664-1078 (Electronic)).
83. S. Tekin, and J. L. Cummings, "Frontal-subcortical neuronal circuits and clinical neuropsychiatry: an update," 0022-3999 (Print)).
84. J. D. Power et al., "Functional network organization of the human brain," 1097-4199 (Electronic)).
85. A. Kucyi, K. D. Hodaie M Fau - Davis, and K. D. Davis, "Lateralization in intrinsic functional connectivity of the temporoparietal junction with salience- and attention-related brain networks," 1522-1598 (Electronic)).
86. V. Menon, and L. Q. Uddin, "Saliency, switching, attention and control: a network model of insula function," 1863-2661 (Electronic)).
87. J. B. Hopfinger, G. R. Buonocore Mh Fau - Mangun, and G. R. Mangun, "The neural mechanisms of top-down attentional control," 1097-6256 (Print)).
88. J. C. Culham, N. G. Cavanagh P Fau - Kanwisher, and N. G. Kanwisher, "Attention response functions: characterizing brain areas using fMRI activation during parametric variations of attentional load," 0896-6273 (Print)).
89. X. Lu, and J. Ashe, "Anticipatory activity in primary motor cortex codes memorized movement sequences," 0896-6273 (Print)).
90. U. Halsband et al., "The role of premotor cortex and the supplementary motor area in the temporal control of movement in man," 0006-8950 (Print)).
91. M. P. Caligiuri et al., "A functional magnetic resonance imaging study of cortical asymmetry in bipolar disorder," 1398-5647 (Print)).
92. W. Sturm, and K. Willmes, "On the functional neuroanatomy of intrinsic and phasic alertness," 1053-8119 (Print)).
93. H. Yamasaki, K. S. LaBar, and G. McCarthy, "Dissociable prefrontal brain systems for attention and emotion," *Proceedings of the National Academy of Sciences* **99**(17), 11447 (2002).
94. S. P. Drummond et al., "The neural basis of the psychomotor vigilance task," 0161-8105 (Print)).
95. R. Langner, and S. B. Eickhoff, "Sustaining attention to simple tasks: a meta-analytic review of the neural mechanisms of vigilant attention," 1939-1455 (Electronic)).
96. J. Parvizi, and A. D. Wagner, "Memory, Numbers, and Action Decision in Human Posterior Parietal Cortex," *Neuron* **97**(1), 7-10 (2018).
97. J. Qi et al., "Altered insula-prefrontal functional connectivity correlates to decreased vigilant attention after total sleep deprivation," *Sleep Medicine* **84**(187-194 (2021).
98. P. Bender et al., *Using the singular value decomposition to extract 2D correlation functions from scattering patterns* (2019).
99. G. W. Stewart, "On the Early History of the Singular Value Decomposition," *SIAM Review* **35**(4), 551-566 (1993).
100. A. G. Akritas, and G. I. Malaschonok, "Applications of singular-value decomposition (SVD)," *Mathematics and Computers in Simulation* **67**(1), 15-31 (2004).
101. H. Xu, "An SVD-like matrix decomposition and its applications," *Linear Algebra and its Applications* **368**(1-24 (2003).
102. S. R. Chowdhury, and J. Dutta, "Higher-order singular value decomposition-based lung parcellation for breathing motion management," *Journal of Medical Imaging* **6**(2), 024004 (2019).

103. A. Ginebreda, L. Sabater-Liesa, and D. Barceló, "Quantification of ecological complexity and resilience from multivariate biological metrics datasets using singular value decomposition entropy," *MethodsX* **6**(1668-1676 (2019).
104. V. A.-O. Guillemot et al., "A constrained singular value decomposition method that integrates sparsity and orthogonality," 1932-6203 (Electronic)).
105. P. K. Sadasivan, and D. N. Dutt, "SVD based technique for noise reduction in electroencephalographic signals," *Signal Processing* **55**(2), 179-189 (1996).
106. E. Biglieri, and K. Yao, "Some properties of singular value decomposition and their applications to digital signal processing," *Signal Processing* **18**(3), 277-289 (1989).
107. L. Haddad Ae Fau - Najafizadeh, and L. Najafizadeh, "Global EEG segmentation using singular value decomposition," 2694-0604 (Electronic)).
108. A. Shahid, N. Kamel, and A. S. Malik, "Singular values as a detector of epileptic seizures in EEG signals," *2014 5th International Conference on Intelligent and Advanced Systems (ICIAS)* 1-5 (2014).
109. Y. Jonmohamadi et al., "Constrained temporal parallel decomposition for EEG-fMRI fusion," 1741-2552 (Electronic)).
110. E. Pirondini et al., "Resting-state EEG topographies: Reliable and sensitive signatures of unilateral spatial neglect," 2213-1582 (Electronic)).
111. J. Sandberg, M. Hansson M Fau - Lindgren, and M. Lindgren, "Detecting MMN in Infants EEG with Singular Value Decomposition," 1557-170X (Print)).
112. R. N. Harner, "Singular value decomposition--a general linear model for analysis of multivariate structure in the electroencephalogram," 0896-0267 (Print)).
113. Y. Bai M Fau - Huang et al., "Fast backward singular value decomposition (SVD) algorithm for magnetocardiographic signal reconstruction from pulsed atomic magnetometer data," 1094-4087 (Electronic)).
114. S. Ikeda et al., "Automated Source Estimation of Scalp EEG Epileptic Activity Using eLORETA Kurtosis Analysis," *Neuropsychobiology* **77**(1-9 (2019).
115. C. Imperatori et al., "Modification of EEG functional connectivity and EEG power spectra in overweight and obese patients with food addiction: An eLORETA study," 1931-7565 (Electronic)).
116. M. A. Jatoi et al., "EEG based brain source localization comparison of sLORETA and eLORETA," 1879-5447 (Electronic)).
117. S. Li et al., "Analysis of group ICA-based connectivity measures from fMRI: application to Alzheimer's disease," 1932-6203 (Electronic)).
118. V. D. Calhoun, T. Liu J Fau - Adali, and T. Adali, "A review of group ICA for fMRI data and ICA for joint inference of imaging, genetic, and ERP data," 1095-9572 (Electronic)).
119. C. Liu, J. JaJa, and L. Pessoa, "LEICA: Laplacian eigenmaps for group ICA decomposition of fMRI data," 1095-9572 (Electronic)).
120. D. Mantini et al., "Electrophysiological signatures of resting state networks in the human brain," 0027-8424 (Print)).
121. R. D. Pascual-Marqui et al., "Assessing interactions in the brain with exact low-resolution electromagnetic tomography," 1364-503X (Print)).
122. G. M. Clements et al., "Spontaneous Alpha and Theta Oscillations Are Related to Complementary Aspects of Cognitive Control in Younger and Older Adults," 1662-5161 (Print)).
123. Mathworks, "https://www.mathworks.com/matlabcentral/fileexchange/63276-permutation-test," (2021).
124. E. Tagliazucchi et al., "Dynamic BOLD functional connectivity in humans and its electrophysiological correlates," 1662-5161 (Electronic)).

125. M. E. Raichle, and A. Z. Snyder, "A default mode of brain function: a brief history of an evolving idea," 1053-8119 (Print)).
126. R. Zomorrodi et al., "Pulsed Near Infrared Transcranial and Intranasal Photobiomodulation Significantly Modulates Neural Oscillations: a pilot exploratory study," 2045-2322 (Electronic)).
127. L. I. Aftanas, and S. A. Golocheikine, "Human anterior and frontal midline theta and lower alpha reflect emotionally positive state and internalized attention: high-resolution EEG investigation of meditation," 0304-3940 (Print)).
128. R. Stern, Ray, W., & Quigley, K. (2000-12-21). *Psychophysiological Recording. : Oxford University Press.* (2022).
129. C. Zheng et al., "Spatial Sequence Coding Differs during Slow and Fast Gamma Rhythms in the Hippocampus," 1097-4199 (Electronic)).
130. L. L. Colgin, "Do slow and fast gamma rhythms correspond to distinct functional states in the hippocampal network?," 1872-6240 (Electronic)).
131. L. L. Colgin, "Theta-gamma coupling in the entorhinal-hippocampal system," 1873-6882 (Electronic)).
132. L. L. Colgin, "Rhythms of the hippocampal network," 1471-0048 (Electronic)).
133. M. Libenson, *Practical Approach to Electroencephalography*, Saunders, Philadelphia, PA, USA (2010).
134. W. Klimesch, "EEG alpha and theta oscillations reflect cognitive and memory performance: a review and analysis," *Brain Research Reviews* **29**(2), 169-195 (1999).
135. M. M. Botvinick, "Conflict monitoring and decision making: Reconciling two perspectives on anterior cingulate function," *Cognitive, Affective, & Behavioral Neuroscience* **7**(4), 356-366 (2007).
136. R. F. Helfrich, and R. T. Knight, "Oscillatory Dynamics of Prefrontal Cognitive Control," 1879-307X (Electronic)).
137. A. Fernández et al., "Working memory load modulates oscillatory activity and the distribution of fast frequencies across frontal theta phase during working memory maintenance," 1095-9564 (Electronic)).
138. W. E. DeCoteau et al., "Oscillations of local field potentials in the rat dorsal striatum during spontaneous and instructed behaviors," 0022-3077 (Print)).
139. S. Liebe et al., "Theta coupling between V4 and prefrontal cortex predicts visual short-term memory performance," 1546-1726 (Electronic)).
140. P. Sauseng, and W. Klimesch, "What does phase information of oscillatory brain activity tell us about cognitive processes?," 0149-7634 (Print)).
141. L. T. Hsieh, and C. Ranganath, "Frontal midline theta oscillations during working memory maintenance and episodic encoding and retrieval," 1095-9572 (Electronic)).
142. W. Singer, "Synchronization of cortical activity and its putative role in information processing and learning," 0066-4278 (Print)).
143. E. K. Miller, M. Lundqvist, and A. M. Bastos, "Working Memory 2.0," 1097-4199 (Electronic)).
144. M. Lundqvist et al., "Gamma and beta bursts during working memory readout suggest roles in its volitional control," *Nature Communications* **9**(1), 394 (2018).
145. M. Lundqvist, A. Herman P Fau - Lansner, and A. Lansner, "Theta and gamma power increases and alpha/beta power decreases with memory load in an attractor network model," 1530-8898 (Electronic)).
146. M. Lundqvist et al., "Gamma and Beta Bursts Underlie Working Memory," 1097-4199 (Electronic)).
147. N. Swann et al., "Intracranial EEG reveals a time- and frequency-specific role for the right inferior frontal gyrus and primary motor cortex in stopping initiated responses," 1529-2401 (Electronic)).

148. M. H. Ruiz et al., "EEG oscillatory patterns are associated with error prediction during music performance and are altered in musician's dystonia," 1095-9572 (Electronic)).
149. J. R. Wessel et al., "Chronometric electrical stimulation of right inferior frontal cortex increases motor braking," *J Neurosci* **33**(50), 19611-19619 (2013).
150. S. Hanslmayr, J. Matuschek, and M. C. Fellner, "Entrainment of prefrontal beta oscillations induces an endogenous echo and impairs memory formation," 1879-0445 (Electronic)).
151. B. A. Zavala, A. I. Jang, and K. A. Zaghloul, "Human subthalamic nucleus activity during non-motor decision making," *Elife* **6**(e31007 (2017).
152. A. K. Engel, and P. Fries, "Beta-band oscillation‟ signalling the status quo?," *Current Opinion in Neurobiology* **20**(156-165 (2010).
153. S. L. Bressler, and C. G. Richter, "Interareal oscillatory synchronization in top-down neocortical processing," 1873-6882 (Electronic)).
154. A. Wróbel, "Beta activity: a carrier for visual attention," 0065-1400 (Print)).
155. G. Pfurtscheller, A. Stancák, and C. Neuper, "Post-movement beta synchronization. A correlate of an idling motor area?," *Electroencephalography and Clinical Neurophysiology* **98**(4), 281-293 (1996).
156. J. R. Hughes, "RESPONSES FROM THE VISUAL CORTEX OF UNANESTHETIZED MONKEYS," 0074-7742 (Print)).
157. C. Tallon-Baudry, and O. Bertrand, "Oscillatory gamma activity in humans and its role in object representation," 1879-307X (Electronic)).
158. O. Jensen, J.-P. Kaiser J Fau - Lachaux, and J. P. Lachaux, "Human gamma-frequency oscillations associated with attention and memory," 0166-2236 (Print)).
159. P. Fries, "Neuronal gamma-band synchronization as a fundamental process in cortical computation," 1545-4126 (Electronic)).
160. E. Düzel, N. Penny Wd Fau - Burgess, and N. Burgess, "Brain oscillations and memory," 1873-6882 (Electronic)).
161. M. W. Howard et al., "Gamma oscillations correlate with working memory load in humans," 1047-3211 (Print)).
162. P. B. Sederberg et al., "Hippocampal and neocortical gamma oscillations predict memory formation in humans," 1047-3211 (Print)).
163. F. Roux et al., "Gamma-band activity in human prefrontal cortex codes for the number of relevant items maintained in working memory," 1529-2401 (Electronic)).
164. W. Singer, and C. M. Gray, "Visual feature integration and the temporal correlation hypothesis," 0147-006X (Print)).
165. G. Buzsáki, and X. J. Wang, "Mechanisms of gamma oscillations," 1545-4126 (Electronic)).
166. M. T. Kucewicz et al., "High frequency oscillations are associated with cognitive processing in human recognition memory," 1460-2156 (Electronic)).
167. Y. Aoki et al., "Detection of EEG-resting state independent networks by eLORETA-ICA method," 1662-5161 (Print)).
168. I. M. Veer et al., "Whole brain resting-state analysis reveals decreased functional connectivity in major depression. LID - 41 [pii] LID - 10.3389/fnsys.2010.00041 [doi]," 1662-5137 (Electronic)).
169. H. H. Shen, "Core Concept: Resting-state connectivity," 1091-6490 (Electronic)).
170. C. Piano et al., "Sleep-related modifications of EEG connectivity in the sensory-motor networks in Huntington Disease: An eLORETA study and review of the literature," 1872-8952 (Electronic)).
171. K. Jann et al., "Topographic electrophysiological signatures of FMRI Resting State Networks," 1932-6203 (Electronic)).
172. A. Mohan et al., "The Significance of the Default Mode Network (DMN) in Neurological and Neuropsychiatric Disorders: A Review," 1551-4056 (Electronic)).

173. C. Murphy et al., "Distant from input: Evidence of regions within the default mode network supporting perceptually-decoupled and conceptually-guided cognition," 1095-9572 (Electronic)).
174. M. A.-O. Sormaz et al., "Default mode network can support the level of detail in experience during active task states," 1091-6490 (Electronic)).
175. E. Lefebvre, and A. A.-O. D'Angiulli, "Imagery-Mediated Verbal Learning Depends on Vividness-Familiarity Interactions: The Possible Role of Dualistic Resting State Network Activity Interference. LID - 10.3390/brainsci9060143 [doi] LID - 143," 2076-3425 (Print)).
176. M. Dastjerdi et al., "Differential electrophysiological response during rest, self-referential, and non-self-referential tasks in human posteromedial cortex," 1091-6490 (Electronic)).
177. R. L. Buckner, D. L. Andrews-Hanna Jr Fau - Schacter, and D. L. Schacter, "The brain's default network: anatomy, function, and relevance to disease," 0077-8923 (Print)).
178. T. J. Akiki et al., "Default mode network abnormalities in posttraumatic stress disorder: A novel network-restricted topology approach," 1095-9572 (Electronic)).
179. J. Fang et al., "Transcutaneous Vagus Nerve Stimulation Modulates Default Mode Network in Major Depressive Disorder," 1873-2402 (Electronic)).
180. S. Marek, and N. U. F. Dosenbach, "The frontoparietal network: function, electrophysiology, and importance of individual precision mapping," 1958-5969 (Electronic)).
181. M. S. Vendetti, and S. A. Bunge, "Evolutionary and developmental changes in the lateral frontoparietal network: a little goes a long way for higher-level cognition," 1097-4199 (Electronic)).
182. R. C. Chan et al., "Assessment of executive functions: review of instruments and identification of critical issues," 0887-6177 (Print)).
183. A. Collins, and E. Koechlin, "Reasoning, learning, and creativity: frontal lobe function and human decision-making," 1545-7885 (Electronic)).
184. M. Kawasaki, Y. Kitajo K Fau - Yamaguchi, and Y. Yamaguchi, "Dynamic links between theta executive functions and alpha storage buffers in auditory and visual working memory," 1460-9568 (Electronic)).
185. J. D. Nielsen et al., "Working Memory Modulation of Frontoparietal Network Connectivity in First-Episode Schizophrenia," 1460-2199 (Electronic)).
186. A. Diamond, "Executive functions," 1545-2085 (Electronic)).
187. J. B. Hopfinger, and S. D. Slotnick, "Attentional Control and Executive Function," 1758-8936 (Electronic)).
188. Y. A.-O. X. Shan et al., "Effect of Near-Infrared Pulsed Light on the Human Brain Using Electroencephalography," 1741-427X (Print)).
189. T. Dietl et al., "Orienting response and frontal midline theta activity: a somatosensory spectral perturbation study," 1388-2457 (Print)).
190. E. Başar, O. Schürmann M Fau - Sakowitz, and O. Sakowitz, "The selectively distributed theta system: functions," 0167-8760 (Print)).
191. W. Klimesch et al., "Theta synchronization and alpha desynchronization in a memory task," 0048-5772 (Print)).
192. L. I. Aftanas et al., "Non-linear dynamical coupling between different brain areas during evoked emotions: an EEG investigation," 0301-0511 (Print)).
193. L. I. Aftanas et al., "Affective picture processing: event-related synchronization within individually defined human theta band is modulated by valence dimension," 0304-3940 (Print)).
194. T. D. Lagerlund, N. E. Sharbrough Fw Fau - Busacker, and N. E. Busacker, "Spatial filtering of multichannel electroencephalographic recordings through principal component analysis by singular value decomposition," 0736-0258 (Print)).

195. F. L. Stevens, K. H. Hurley Ra Fau - Taber, and K. H. Taber, "Anterior cingulate cortex: unique role in cognition and emotion," 1545-7222 (Electronic)).
196. K. Grill-Spector, N. Kourtzi Z Fau - Kanwisher, and N. Kanwisher, "The lateral occipital complex and its role in object recognition," 0042-6989 (Print)).
197. R. Leech, and D. J. Sharp, "The role of the posterior cingulate cortex in cognition and disease," 1460-2156 (Electronic)).
198. J. R. Binder, and R. H. Desai, "The neurobiology of semantic memory," 1879-307X (Electronic)).
199. M. Tops, and M. A. Boksem, "A potential role of the inferior frontal gyrus and anterior insula in cognitive control, brain rhythms, and event-related potentials," 1664-1078 (Electronic)).
200. M. Wallentin et al., "Parallel memory systems for talking about location and age in precuneus, caudate and Broca's region," 1053-8119 (Print)).
201. L. F. Basile et al., "Interindividual variability in EEG correlates of attention and limits of functional mapping," 0167-8760 (Print)).
202. S. Hanslmayr et al., "Prestimulus oscillations predict visual perception performance between and within subjects," 1053-8119 (Print)).
203. J. H. Wu et al., "Effect of low-level laser stimulation on EEG," 1741-4288 (Electronic)).
204. R. Cabeza, and L. Nyberg, "Imaging cognition II: An empirical review of 275 PET and fMRI studies," 0898-929X (Print)).
205. J. W. Bisley, and M. E. Goldberg, "Neuronal activity in the lateral intraparietal area and spatial attention," 1095-9203 (Electronic)).
206. J. A. Posner Mi Fau - Walker et al., "Effects of parietal injury on covert orienting of attention," 0270-6474 (Print)).
207. J. Kamiński et al., "β band oscillations engagement in human alertness process," 1872-7697 (Electronic)).
208. J. Gross et al., "Modulation of long-range neural synchrony reflects temporal limitations of visual attention in humans," 0027-8424 (Print)).
209. L. A. Renier et al., "Preserved functional specialization for spatial processing in the middle occipital gyrus of the early blind," 1097-4199 (Electronic)).
210. C. Teng et al., "Abnormal resting state activity of left middle occipital gyrus and its functional connectivity in female patients with major depressive disorder," 1471-244X (Electronic)).
211. A. Chaudhari et al., "Transcranial photobiomodulation with light emitting diodes increases vigilance performance and EEG alpha power of the human brain," in OSA Technical Digest C. M. K. H. C. W. M. Q. K. S.-K. M. D. N. E. D. C. F. O. L. E. V. M. O. Boudoux, and E. Buckley, Eds., *Biophotonics Congress 2021* JW1A.20 (2021).

Appendix A: Appendix for chapter 2

In addition to the above mentioned analysis, I have also done further investigation in dominant power, power ratio, and WTC calculations between EGG and fNIRS data, which are provided in this section.

A.2.1 MATERIAL AND METHODS

A.2.1.1 Nirs Data Preprocessing

Raw NIRS data was initially detrended by subtracting the trend using a 3rd order polynomial fit. The spikes in the data were further removed from the detrended data. The data were then further divided into sub-feeding periods based on the feeding times.

A.2.1.2 Dominant Power Calculations

The EGG dominant frequency is defined as the frequency at which the power of an EGG signal has its peak value in the frequency range of 0.5 to 9 cpm. The dominant power is defined as the power at the dominant frequency (1).

The PSD obtained for each sub-feeding period for both feeding periods was averaged across feeding periods as described before. Dominant power was then calculated for each averaged sub-feeding period separately for all the neonates. Average dominant power was obtained during each sub-feeding period for each neonate group by averaging the dominant power across neonates within the group. Dominant power was then compared across all the postmenstrual groups within each sub-feeding period to determine the effect of postmenstrual

age on power. Two-sample t-tests were carried out between each group for every sub-feeding period.

A.2.1.2 Power Ratio Calculations

Power ratios are calculated because the absolute values of EGG power are influenced by skin conductance, the variable shape of the stomach, and distance between the electrodes and the wall of the stomach (2).

We further considered the dominant power obtained during each sub-feeding period to calculate the power ratio. The ratio of post and pre-feed (post/pre) was calculated for each neonate. Similarly, the ratio of the during and before-feed (during/pre) periods was calculated. The ratios were averaged across neonates within each group. Two-sample t-tests were carried out for both ratios to determine changes in gastric contractions between each group.

A.2.1.3 Time-Frequency Analysis Between EEG and NIRS

The coupling relationship between EGG and NIRSa, EGG and NIRSc, and NIRSa and NIRSc was calculated using the time-frequency calculations. The EGG and NIRS data were initially preprocessed as mentioned before.

The pre-processed NIRS data were further divided into sub-feeding periods based on the feeding times. We then considered EGG (Figure A.2.1(a)) and NIRS (Figure A.2.1 (b)) signal for wavelet transform calculations. Next, we performed wavelet transform on NIRSa vs EGG, NIRSc vs EGG, and NIRSa vs NIRSc pairs for all the sub-feeding periods. One such example of WTC map is shown in Figure A.2.1 (c). Inphase, 90 degree, antiphase, and 270 degree coupling phase values

were extracted for all the comparisons. Then we calculated the percentage coupling for each sub-feeding period by dividing each of the phase values by all the phase values (Figure A.2.1 (d)). The percentage coupling values were then averaged across neonates and sub-feeding periods within each group. These neonate, sub-feeding averaged percentage coupling values were then compared between early, mid, and term neonates using two-sample t-tests at each sub-frequency.

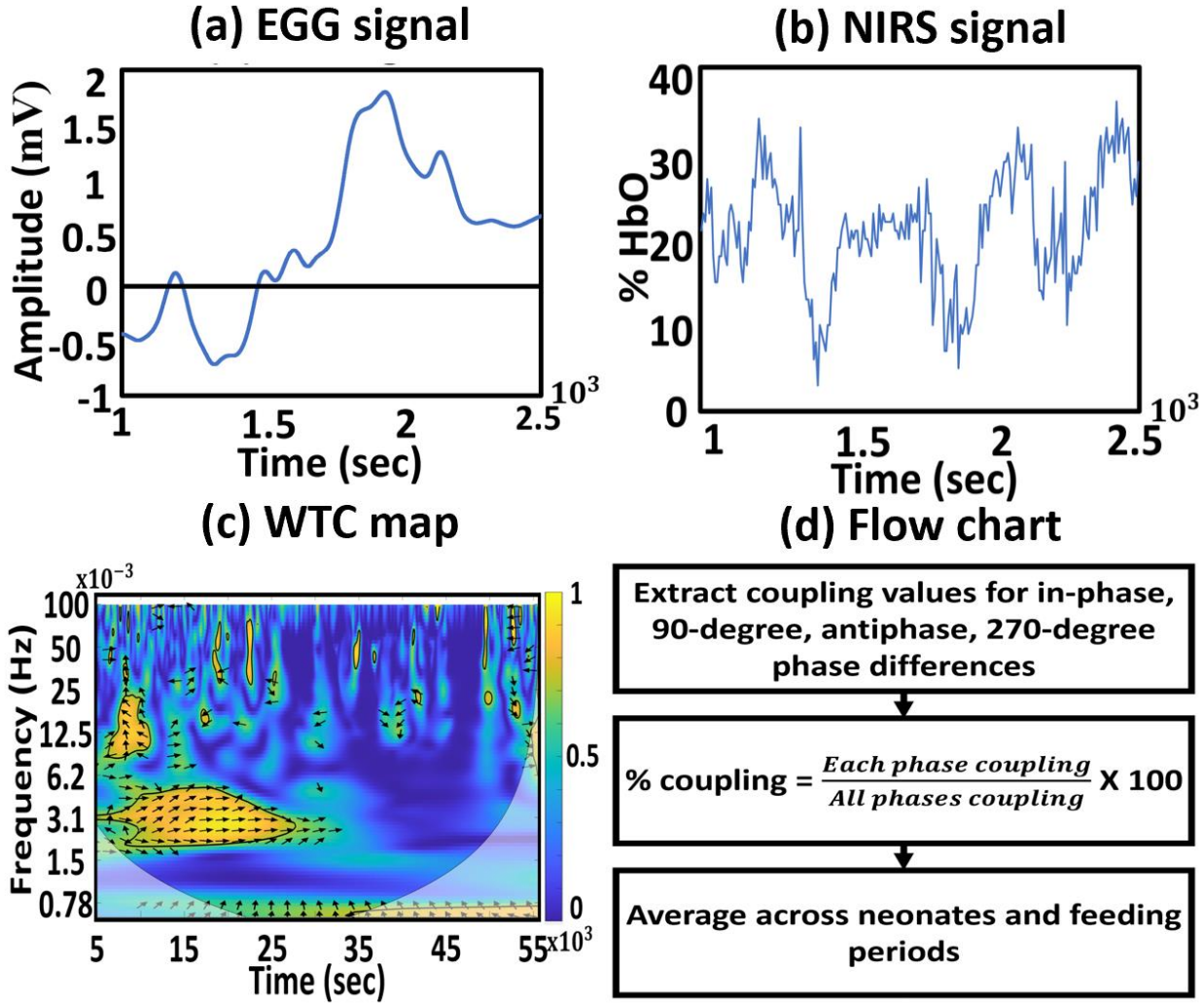

Figure A.2.1: Procedure to calculate the Wavelet coherence. (a) One neonate's preprocessed EGG signal. (b) One neonate's preprocessed NIRS signal. (c) WTC map for that neonate for whole

time of the sub-feeding period. (d) Procedure to calculate the % coupling. The coupling values were initially extracted for all the phase differences between NIRS and EGG. Then percentage coupling was calculated by dividing each phase coupling with all phases coupling. The percentage coupling was then averaged across neonates and all the feeding periods.

A.2.2 RESULTS

A.2.2.1 Term neonates dominant power increase during and post-feed:

Dominant power comparison between postmenstrual groups for each sub-feeding period is shown in Figure A.2.2. The PSD was used to calculate the dominant power for each sub-feeding period across all neonate groups. Statistical tests showed that for the pre-feed period the term neonates had significantly lower dominant power than early ($p=0.045$) and mid-neonates ($p=0.048$), while in the during-feed period, neonates had significantly higher dominant power when compared with early ($p=0.041$) and mid-neonates ($p=0.03$). Also, for post-feed period, term ($p=0.015$) and mid-neonates ($p=0.006$) had significantly higher dominant power compared to early neonates.

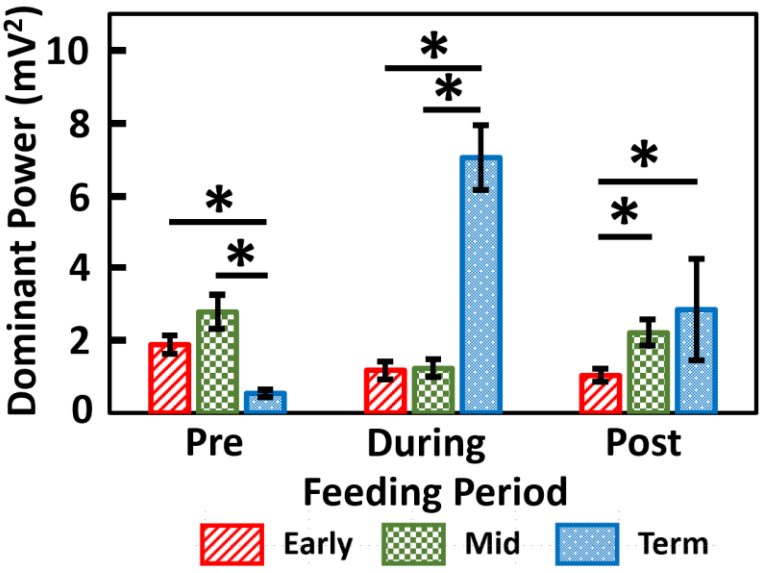

Figure A.2.2: Dominant power comparison between postmenstrual groups for all the sub-feeding periods. X-axis represents the sub-feeding period. Y-axis denotes the dominant power. '*' marks significance of $p<0.05$ (with compounded type 1 error). Error bar: Standard mean error of the dominant power across neonates. Term neonates showed significantly higher dominant power in during and post-feed periods. Pre-feed dominant power for term neonates was observed to be significantly lower than mid and early neonates.

A.2.2.2 Term neonates shows normal gastric emptying:

Post and during-feed power comparisons with pre-feed are shown in Figure A.2.3. The dominant power ratio of post and pre-feed (post/pre-feed) was calculated for all neonates. Similarly, a ratio of during and pre-feed (during/pre-feed) was obtained. The ratios were then averaged across neonates within each premenstrual group. Significant increase in post/pre-feed and during/pre-feed power ratio was observed in term neonates when compared with early (post/pre: $p = 0.0116$; during/pre: $p=0.03$) and mid-neonates (post/pre: $p=0.0041$, during/pre: $p=0.005$).

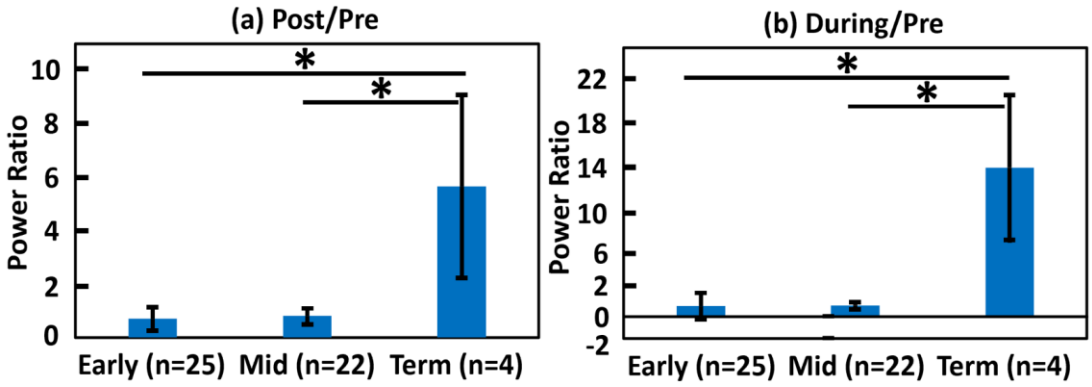

Figure A.2.3: Power ratio comparison between different postmenstrual groups. (a) The power ratio of post-feed and before-feed. (b) during-feed and before-feed power ratio. X-axis represents the postmenstrual group, and Y-axis depicts the power ratio. Term neonates were observed to have significantly higher power ratio than early and mid neonates.

A.2.2.3 Time-frequency analysis between EGG and NIRS data:

The percent coupling comparisons between EGG vs NIRSa, EGG vs NIRSc, NIRSa vs NIRSc for in-phase, 90 degree lead, anti-phase, and 270 degree lead are shown in Figure 8, Figure 9, Figure 10, and Figure 11 respectively. Wavelet analysis was performed between EGG vs NIRSa, EGG vs NIRSc, NIRSa vs NIRSc for all the sub-feeding periods and all the neonates' groups. The percentage coupling was calculated for inphase, 90 degree, antiphase, and 270 degree phase differences. Figure A.2.4, Figure A.2.5, Figure A.2.6, Figure A.2.7 shows inphase, 90 degree, antiphase, and 270 degree phase difference coupling percentage comparisons between early, mid, and term neonates for all the comparisons. Similarly, Significant differences were observed between mid vs term neonates and early vs term neonates in all the comparisons.

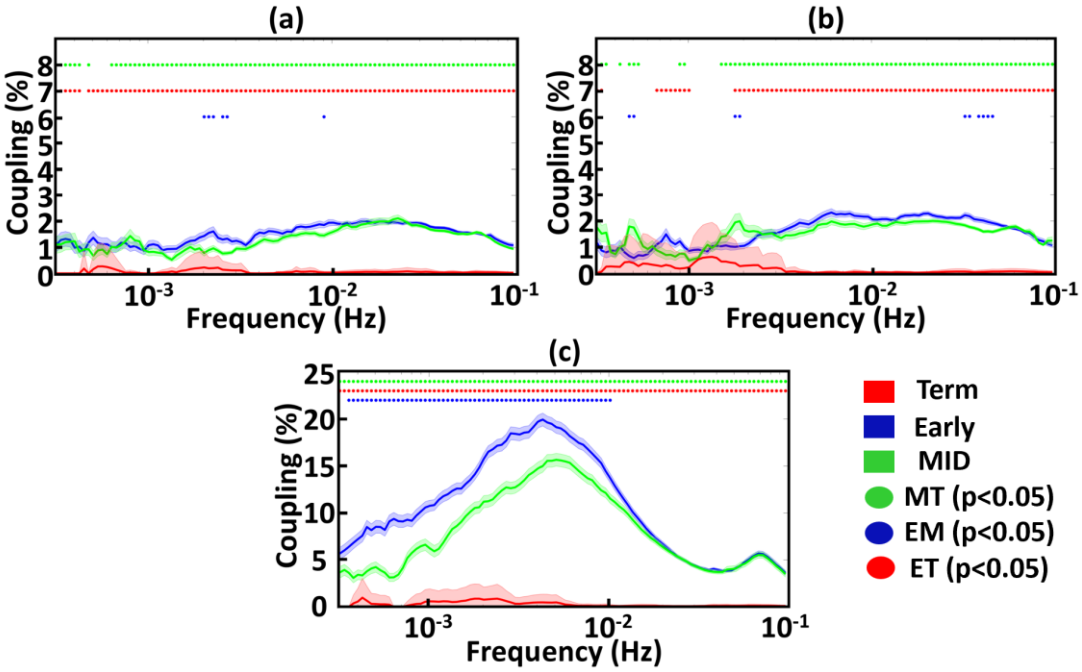

Figure A.2.4: Coupling percentage calculated for in-phase comparisons. (a) NIRSa-EGG coupling percentage comparison between term, mid, and early neonates. (b) Neonate group comparisons of coupling percentage for NIRSc-EGG. (c) NIRSa-NIRSc coupling percentage comparison between term, mid, and early neonates. X-axis denotes frequency (Hz) and Y-axis represents the percentage of coupling. Red, purple, and green curve show term, early and mid neonates respectively. Green dots represent significant changes between mid and term neonates. Purple dots show significant change between early and mid neonates. Significant changes between early and term neonates are shown using red dots. Significant changes were observed in all the comparisons between mid vs term neonates and early vs term neonates.

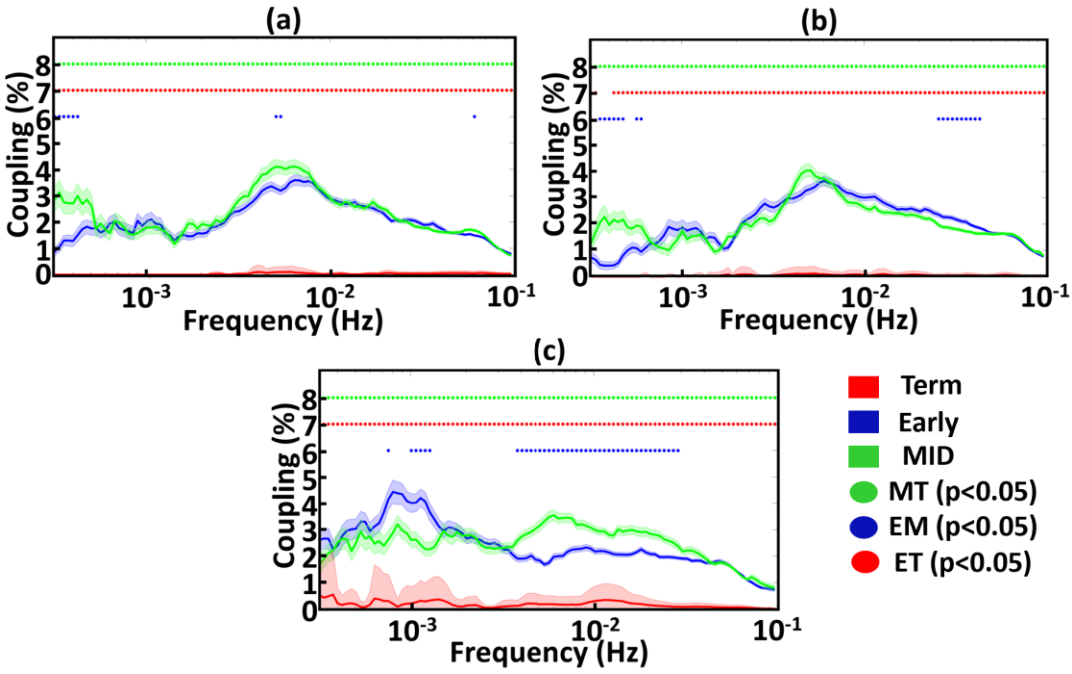

Figure A.2.5: Coupling percentage calculated for 90-degree phase comparisons. (a) Percentage coupling of NIRSa-EGG between term, mid, and early neonates. (b) Neonate group comparisons of coupling percentage for NIRSc-EGG. (c) NIRSa-NIRSc coupling percentage comparison between term, mid, and early neonates. Significant changes were observed in all the comparisons between mid vs term neonates and early vs term neonates.

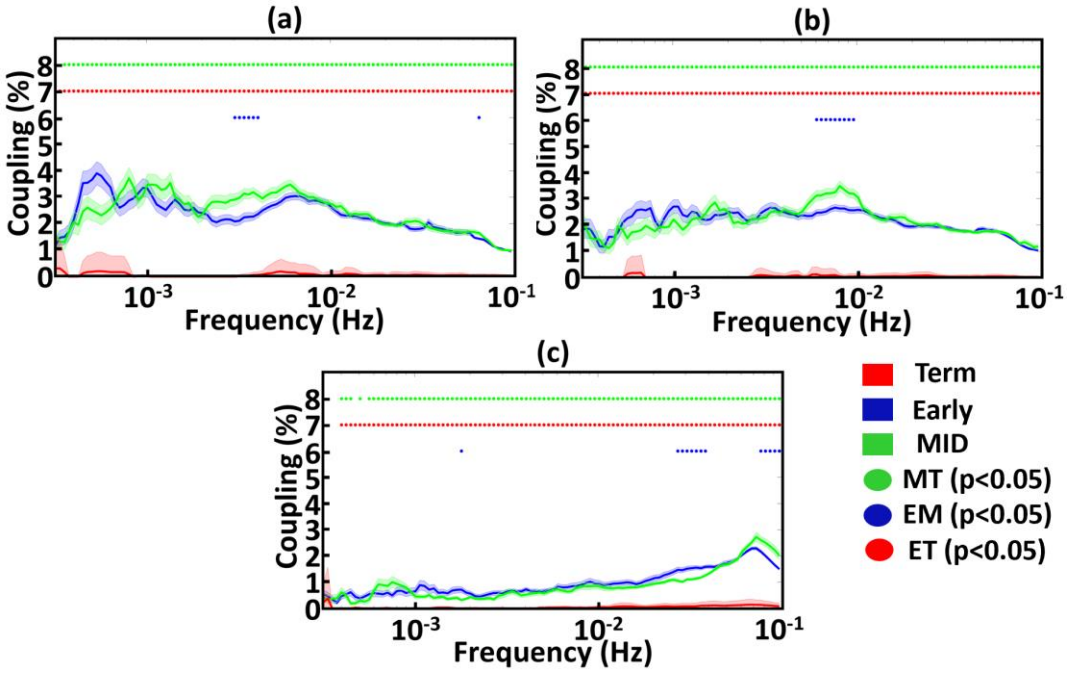

Figure A.2.6: Coupling percentage calculated for anti-phase comparisons. (a) NIRSa-EGG coupling percentage comparison between term, mid, and early neonates. (b) Neonate group comparisons of coupling percentage for NIRSc-EGG. (c) Percentage coupling comparisons for NIRSa-NIRSc between term, mid, and early neonates. Significant changes were observed in all the comparisons between mid vs term neonates and early vs term neonates.

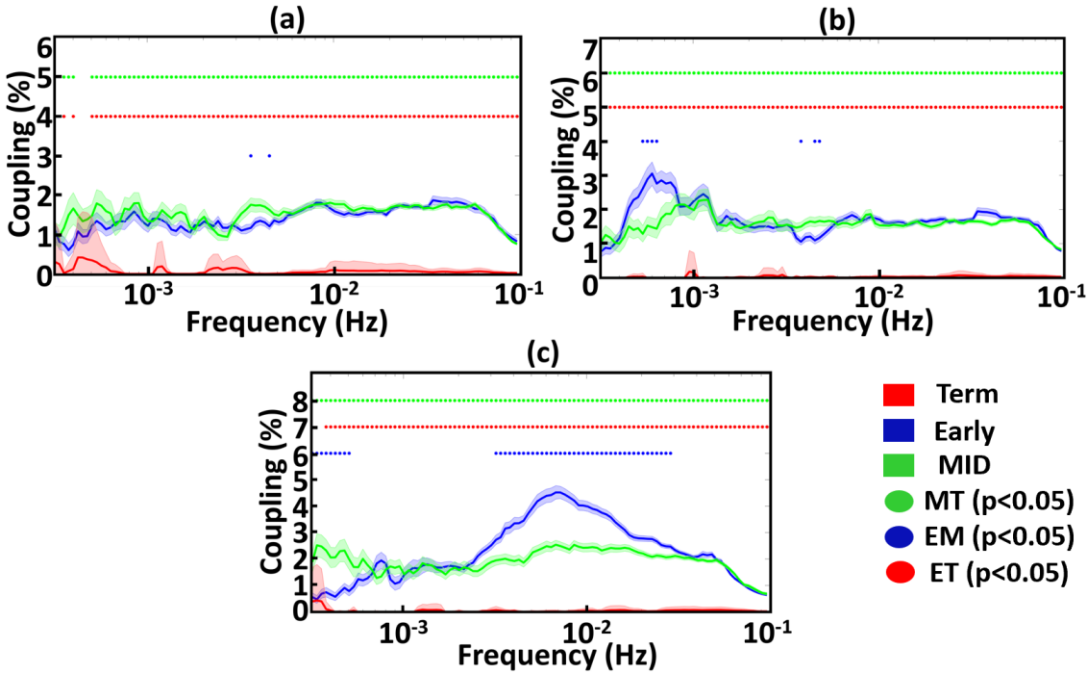

Figure A.2.7: Coupling percentage calculated for 270-degree phase comparisons. (a) Neonates group comparisons of coupling percentage for NIRSa-EGG. (b) Neonate group comparisons of coupling percentage for NIRSc-EGG. (c) NIRSa-NIRSc coupling percentage comparison between term, mid, and early neonates. Significant changes were observed in all the comparisons between mid vs term neonates and early vs term neonates.

References for Appendix A

1. A. R. Precioso, F. A. C. Pereira Gr Fau - Vaz, and F. A. Vaz, "Gastric myoelectrical activity in neonates of different gestational ages by means of electrogastrography," 0041-8781 (Print)).
2. G. Riezzo, F. Russo F Fau - Indrio, and F. Indrio, "Electrogastrography in adults and children: the strength, pitfalls, and clinical significance of the cutaneous recording of the gastric electrical activity," 2314-6141 (Electronic)).

Appendix B: Appendix for chapter 4:

	Week 1					Week 4				
SVD#	Delta	Theta	Alpha	Beta	Gamma	Delta	Theta	Alpha	Beta	Gamma
1	0.94	0.69	0.61	0.83	0.98	0.90	0.72	0.68	0.69	0.93
2	0.96	0.97	0.93	0.90	0.88	0.72	0.96	1.00	0.94	0.85
3	0.92	0.75	0.97	0.96	0.85	0.56	0.79	0.97	0.86	0.99
4	0.82	1.00	0.95	0.90	0.84	0.83	0.88	0.84	0.81	0.89
5	0.83	0.87	0.93	0.95	0.86	0.95	0.93	0.93	0.85	0.96
6	0.90	0.83	0.92	0.88	0.98	0.87	0.81	0.85	1.00	0.95
7	0.93	0.89	0.92	0.99	0.96	0.95	0.95	0.97	0.89	0.97
8	0.97	0.69	0.91	0.98	0.82	0.98	0.95	0.73	0.79	0.92
9	0.99	0.99	0.96	0.86	0.85	0.88	0.80	0.86	0.99	0.83
10	0.75	0.92	0.99	0.69	0.59	0.99	0.89	0.87	0.93	0.95
11	0.96	0.92	0.99	0.90	0.89	0.67	0.83	0.81	0.85	0.78
12	0.95	1.00	0.89	0.92	1.00	0.99	0.86	0.89	0.86	0.94

Table B.1: P values of one way ANVOA test for “before-stimulation” period. No significant difference was observed in any band, for every SVD component and during both the weeks.

Appendix C: MATLAB codes for the Dissertation Work

This section consists of the MATLAB codes that were used for processing each aim.

C.1 MEAN PSD CALCULATIONS FOR CHAPTER 2

```
clear all;  clc;
sub_no = strcat('POOH018');      sub_no2 = 18;
% load the excel containing the time of feeding
cd('C:\New folder');    timings_excel = importdata('FeedingTime.csv');
line_no = find(strcmpi(timings_excel.textdata(:,1),sub_no));
timing_data = timings_excel.data(line_no-1,:); clear timings_excel line_no
% to get all the files for that subject from the folder
direc = strcat('C:\New folder\result_data\POOH0',sub_no2);  cd(direc); clear sub_no2
k=1; k1=1;
conte = dir(fullfile(direc)); % gets the names of files in the folder
for iab=3:length(conte)-3 % ignore 1,2 names i.e. .;..
   if length(conte(iab).name)>16
      a = conte(iab).name;
      b = split(a,'.'); b1 = char(b(1,1)); clear b a
      c = isstrprop(b1,'digit'); c1 = b1(c);
      sub_read = str2num(c1);
      % load the EEG_nirs combined file
      name_load = strcat('EGG_nirs_data',c1,'.mat'); clear b1 c c1
      load(name_load);
      % change EGG_121_time to downsampled data
      EGG_time = linspace(EGG_121_time(1,1),EGG_121_time(end,1),size(EGG_121_data_final,2));
      EGG_121_time = EGG_time';    clear EGG_time
      fs_EGG = size(EGG_121_data_final,2)/EGG_121_time(end,1);
      % extract the feeding periods from the excel sheet
      % col 4-5 feed 1 start-end;  col 8-9 feed 2 start-end
```

```
sub_time(1,:) = timing_data(find(timing_data(:,1)==sub_read),:);
feed_time = [sub_time(1,4) sub_time(1,5) sub_time(1,8) sub_time(1,9)];
diff_f = feed_time(1,2)-feed_time(1,1);
% some conditions to make sure that data is in right format
if diff_f~=0
  if feed_time(1,1)~=0
    % extract time for feeding 1, pre, dur and post
    tt.EGG_dur1 = [max(find(EGG_121_time(:,1)<=feed_time(1,1)))
max(find(EGG_121_time(:,1)<=feed_time(1,2)))];
    tt.EGG_pre1 = [1 tt.EGG_dur1(1,1)];
    if isnan(feed_time(1,3))
      tt.EGG_post1 = [tt.EGG_dur1(1,2) max(find(EGG_121_time(:,1)<=(feed_time(1,2)+30*60)))];
% 30 min as post 1
      tt.EGG_dur2 = [NaN NaN];  tt.EGG_pre2 = [NaN NaN]; tt.EGG_post2 = [NaN NaN];
    else
      tt.EGG_dur2 = [max(find(EGG_121_time(:,1)<=feed_time(1,3)))
max(find(EGG_121_time(:,1)<=feed_time(1,4)))];
      EGG_mid = tt.EGG_dur2(1,1) - tt.EGG_dur1(1,2);
      tt.EGG_post1 = [tt.EGG_dur1(1,2) tt.EGG_dur1(1,2)+(EGG_mid/2)];
      tt.EGG_pre2 = [tt.EGG_dur2(1,1)-(EGG_mid/2) tt.EGG_dur2(1,1)]; clear EGG_mid
      tt.EGG_post2 = [tt.EGG_dur2(1,2) size(EGG_121_time,1)];
    end
    % extract data from the whole EEG data
    f_data.EGG_pre1 = EGG_121_data_final(1,tt.EGG_pre1(1,1):tt.EGG_pre1(1,2));
    f_data.EGG_dur1 = EGG_121_data_final(1,tt.EGG_dur1(1,1):tt.EGG_dur1(1,2));
    f_data.EGG_post1 = EGG_121_data_final(1,tt.EGG_post1(1,1):tt.EGG_post1(1,2));
    if length(f_data.EGG_pre1)>30 % check if pre feeding is > 30 min
      if length(f_data.EGG_dur1)>30 % check if dur feeding is > 30 min
        if length(f_data.EGG_post1)>30 % check if post feeding is > 30 min
          % run pwelch to get the PSD
          [EGG_pre1_psd(:,k) freq_EGG_psd(:,k)] =
pwelch(f_data.EGG_pre1,240*fs_EGG,0.5*240*fs_EGG,round(1000*fs_EGG),fs_EGG);
```

```
                EGG_dur1_psd(:,k) =
pwelch(f_data.EGG_dur1,4*hamming(fs_EGG)*60,0.5*fs_EGG*60,512*4);

                EGG_post1_psd(:,k) =
pwelch(f_data.EGG_post1,4*hamming(fs_EGG)*60,0.5*fs_EGG*60,512*4);

                k=k+1;

            end

        end

    end

    if ~isnan(tt.EGG_dur2(1,1))

        f_data.EGG_pre2 = EGG_121_data_final(1,tt.EGG_pre2(1,1):tt.EGG_pre2(1,2));

        f_data.EGG_dur2 = EGG_121_data_final(1,tt.EGG_dur2(1,1):tt.EGG_dur2(1,2));

        f_data.EGG_post2 = EGG_121_data_final(1,tt.EGG_post2(1,1):tt.EGG_post2(1,2));

        if length(f_data.EGG_pre2)>30 % check if pre feeding is > 30 min

            if length(f_data.EGG_dur2)>30 % check if dur feeding is > 30 min

                if length(f_data.EGG_post2)>30 % check if post feeding is > 30 min

                    % run pwelch to get the PSD

                    EGG_pre2_psd(:,k1) =
pwelch(f_data.EGG_pre2,4*hamming(fs_EGG)*60,0.5*fs_EGG*60,512*4);

                    EGG_dur2_psd(:,k1) =
pwelch(f_data.EGG_dur2,4*hamming(fs_EGG)*60,0.5*fs_EGG*60,512*4);

                    EGG_post2_psd(:,k1) =
pwelch(f_data.EGG_post2,4*hamming(fs_EGG)*60,0.5*fs_EGG*60,512*4);

                    k1=k1+1;

                end

            end

        end

        clear tt nirs_a_121 nirs_c_121 EGG_121_data_final f_data EGG_121_time fs_EGG name_load

    else

        clear EGG_121_data_final EGG_121_time feed_time fs_EGG fs_nirs name_load nirs_121_time
nirs_a_121 nirs_c_121

    end
```

```
    end
  end
end
cd(direc);     save('EGG_psd4.mat','-v7.3');
```

C.2 CODE FOR PSD COMPARISON BETWEEN EARLY, MID AND TERM SUBJECTS FOR CHAPTER 2

```
clear all;  clc; % here comparing early, mid and term
for load_da=1
  term = [2 3 4 5]; count_term=0;
  for i=1:length(term)
    cd(strcat('C:\New folder\result_data\POOH00',num2str(term(i))));
    load('EGG_psd4.mat');   count_term=count_term+size(EGG_pre1_psd,2);
    te.b1(:,i) = EGG_pre1_psd; te.d1(:,i) = EGG_dur1_psd; clear EGG_pre1_psd EGG_dur1_psd
    te.po1(:,i) = EGG_post1_psd; te.b2(:,i) = EGG_pre2_psd; clear EGG_post1_psd EGG_pre2_psd
    te.d2(:,i) = EGG_dur2_psd; te.po2(:,i) = EGG_post2_psd; clear EGG_dur2_psd EGG_post2_psd
    te.freq(:,i) = freq_EGG_psd; clear freq_EGG_psd
  end
  te.count_term = count_term; te.sub = term;  clear i direc count_term glob_count term
  early_ivh = [19, 20, 28, 31, 32, 34, 35, 36,39,46,59]; count_early_ivh=0;
  for i=1:length(early_ivh)
    cd(strcat('C:\New folder\result_data\POOH0',num2str(early_ivh(i))));
    load('EGG_psd4.mat');   count_early_ivh=count_early_ivh+size(EGG_dur1_psd,2);
    if(exist('EGG_pre1_psd')) ea_i.b1(:,i) = mean(EGG_pre1_psd,2); clear EGG_pre1_psd end
    if(exist('EGG_dur1_psd')) ea_i.d1(:,i) = mean(EGG_dur1_psd,2); clear EGG_dur1_psd end
    if(exist('EGG_post1_psd')) ea_i.po1(:,i) = mean(EGG_post1_psd,2); clear EGG_post1_psd end
    if(exist('EGG_pre2_psd')) ea_i.b2(:,i) = mean(EGG_pre2_psd,2); clear EGG_pre2_psd end
    if(exist('EGG_dur2_psd')) ea_i.d2(:,i) = mean(EGG_dur2_psd,2); clear EGG_dur2_psd end
    if(exist('EGG_post2_psd')) ea_i.po2(:,i) = mean(EGG_post2_psd,2); clear EGG_post2_psd end
    ea_i.freq(:,i) = mean(freq_EGG_psd,2); clear freq_EGG_psd
  end
```

```
ea_i.count_early_ivh=count_early_ivh; clear i direc count_early_ivh glob_count list
early_noivh = [15,16,18,21,22,23,24,26,33,38,47,58,65,66];count_early_noivh=0;
for i=1:length(early_noivh)
   cd(strcat('C:\New folder\result_data\POOH0',num2str(early_noivh(i))));
   load('EGG_psd4.mat');   count_early_noivh=count_early_noivh+size(EGG_dur1_psd,2);
   if(exist('EGG_pre1_psd')) ea_no.b1(:,i) = mean(EGG_pre1_psd,2); clear EGG_pre1_psd end
   if(exist('EGG_dur1_psd')) ea_no.d1(:,i) = mean(EGG_dur1_psd,2); clear EGG_dur1_psd end
   if(exist('EGG_post1_psd')) ea_no.po1(:,i) = mean(EGG_post1_psd,2); clear EGG_post1_psd end
   if(exist('EGG_pre2_psd')) ea_no.b2(:,i) = mean(EGG_pre2_psd,2); clear EGG_pre2_psd end
   if(exist('EGG_dur2_psd')) ea_no.d2(:,i) = mean(EGG_dur2_psd,2); clear EGG_dur2_psd end
   if(exist('EGG_post2_psd')) ea_no.po2(:,i) = mean(EGG_post2_psd,2); clear EGG_post2_psd end
   ea_no.freq(:,i) = mean(freq_EGG_psd,2); clear freq_EGG_psd
end
ea_no.count_early_noivh=count_early_noivh; clear i direc count_early_noivh glob_count list ans
ea.sub = [early_ivh early_noivh]; clear early_ivh early_noivh
mid_ivh = [17,37,41,54];count_mid_ivh=0;
for i=1:length(mid_ivh)
   cd(strcat('C:\New folder\result_data\POOH0',num2str(mid_ivh(i))));
   load('EGG_psd4.mat');   count_mid_ivh=count_mid_ivh+size(EGG_dur1_psd,2);
   if(exist('EGG_pre1_psd')) m_i.b1(:,i) = mean(EGG_pre1_psd,2); clear EGG_pre1_psd end
   if(exist('EGG_dur1_psd')) m_i.d1(:,i) = mean(EGG_dur1_psd,2); clear EGG_dur1_psd end
   if(exist('EGG_post1_psd')) m_i.po1(:,i) = mean(EGG_post1_psd,2); clear EGG_post1_psd end
   if(exist('EGG_pre2_psd')) m_i.b2(:,i) = mean(EGG_pre2_psd,2); clear EGG_pre2_psd end
   if(exist('EGG_dur2_psd')) m_i.d2(:,i) = mean(EGG_dur2_psd,2); clear EGG_dur2_psd end
   if(exist('EGG_post2_psd')) m_i.po2(:,i) = mean(EGG_post2_psd,2); clear EGG_post2_psd end
   m_i.freq(:,i) = mean(freq_EGG_psd,2); clear freq_EGG_psd
end
m_i.count_mid_ivh = count_mid_ivh; clear i direc count_mid_ivh glob_count list

mid_noivh = [25,27,29,30,42,43,44,45,49,50,51,53,55,56,57,62,64];count_mid_noivh=0;%61,
```

```
    for i=1:length(mid_noivh)
        cd(strcat('C:\New folder\result_data\POOH0',num2str(mid_noivh(i))));
        load('EGG_psd4.mat');
        if exist('EGG_dur1_psd')
            count_mid_noivh=count_mid_noivh+size(EGG_dur1_psd,2);
        else
            count_mid_noivh=count_mid_noivh+size(EGG_dur2_psd,2);
        end
        if(exist('EGG_pre1_psd')) m_no.b1(:,i) = mean(EGG_pre1_psd,2); clear EGG_pre1_psd end
        if(exist('EGG_dur1_psd')) m_no.d1(:,i) = mean(EGG_dur1_psd,2); clear EGG_dur1_psd end
        if(exist('EGG_post1_psd')) m_no.po1(:,i) = mean(EGG_post1_psd,2); clear EGG_post1_psd end
        if(exist('EGG_pre2_psd')) m_no.b2(:,i) = mean(EGG_pre2_psd,2); clear EGG_pre2_psd end
        if(exist('EGG_dur2_psd')) m_no.d2(:,i) = mean(EGG_dur2_psd,2); clear EGG_dur2_psd end
        if(exist('EGG_post2_psd')) m_no.po2(:,i) = mean(EGG_post2_psd,2); clear EGG_post2_psd end
        if(i<5) m_no.freq(:,i) = mean(freq_EGG_psd,2); clear freq_EGG_psd end
    end
    m_no.count_mid_noivh = count_mid_noivh; clear i direc count_mid_noivh glob_count list load_da
    m.sub = [mid_ivh mid_noivh]; clear mid_ivh mid_noivh
end

for abc=1
    % extract limits of frequencies of all bands
    % brady: 0.5-2 cpm, Normo: 2-4 cpm, Tachy: 4-9 cpm
    aa_big = [max(find(fre(:,2)<=0.5)) max(find(fre(:,2)<=2)) max(find(fre(:,2)<=4)) max(find(fre(:,2)<=9))];
    clear fre freq_EGG_psd lim
    % put noivh and ivh together
    ea.b1 = [ea_i.b1 ea_no.b1]; ea.d1 = [ea_i.d1 ea_no.d1]; ea.po1 = [ea_i.po1 ea_no.po1];
    ea.b2 = [ea_i.b2 ea_no.b2]; ea.d2 = [ea_i.d2 ea_no.d2]; ea.po2 = [ea_i.po2 ea_no.po2];
    m.b1 = [m_i.b1 m_no.b1]; m.d1 = [m_i.d1 m_no.d1]; m.po1 = [m_i.po1 m_no.po1];
```

```
m.b2 = [m_i.b2 m_no.b2]; m.d2 = [m_i.d2 m_no.d2]; m.po2 = [m_i.po2 m_no.po2]; clear ea_i ea_no
m_i m_no

% mean across both feeding periods

a = ea.b1; a(:,1:size(ea.b2,2),2) = ea.b2; ea.b = mean(a,3); clear a

a = ea.d1; a(:,1:size(ea.d2,2),2) = ea.d2; ea.d = mean(a,3); clear a

a = ea.po1; a(:,1:size(ea.po2,2),2) = ea.po2; ea.po = mean(a,3); clear a

a = m.b1; a(:,1:size(m.b2,2),2) = m.b2; m.b = mean(a,3); clear a

a = m.d1; a(:,1:size(m.d2,2),2) = m.d2; m.d = mean(a,3); clear a

a = m.po1; a(:,1:size(m.po2,2),2) = m.po2; m.po = mean(a,3); clear a

a = te.b1; a(:,1:size(te.b2,2),2) = te.b2; te.b = mean(a,3); clear a

a = te.d1; a(:,1:size(te.d2,2),2) = te.d2; te.d = mean(a,3); clear a

a = te.po1; a(:,1:size(te.po2,2),2) = te.po2; te.po = mean(a,3); clear a

% mean across sub frequencies in each band

ea_br(1,:) = mean(ea.b(aa_big(1,1):aa_big(1,2),:));    ea_br(2,1:size(ea.d,2)) =
mean(ea.d(aa_big(1,1):aa_big(1,2),:));

ea_br(3,1:size(ea.po,2)) = mean(ea.po(aa_big(1,1):aa_big(1,2),:));

ea_nr(1,:) = mean(ea.b(aa_big(1,2):aa_big(1,3),:));    ea_nr(2,1:size(ea.d,2)) =
mean(ea.d(aa_big(1,2):aa_big(1,3),:));

ea_nr(3,1:size(ea.po,2)) = mean(ea.po(aa_big(1,2):aa_big(1,3),:));

ea_tr(1,:) = mean(ea.b(aa_big(1,3):aa_big(1,4),:));    ea_tr(2,1:size(ea.d,2)) =
mean(ea.d(aa_big(1,3):aa_big(1,4),:));

ea_tr(3,1:size(ea.po,2)) = mean(ea.po(aa_big(1,3):aa_big(1,4),:));

m_br(1,:) = mean(m.b(aa_big(1,1):aa_big(1,2),:));      m_br(2,1:size(m.d,2)) =
mean(m.d(aa_big(1,1):aa_big(1,2),:));

m_br(3,1:size(m.po,2)) = mean(m.po(aa_big(1,1):aa_big(1,2),:));

m_nr(1,:) = mean(m.b(aa_big(1,2):aa_big(1,3),:));      m_nr(2,1:size(m.d,2)) =
mean(m.d(aa_big(1,2):aa_big(1,3),:));

m_nr(3,1:size(m.po,2)) = mean(m.po(aa_big(1,2):aa_big(1,3),:));

m_tr(1,:) = mean(m.b(aa_big(1,3):aa_big(1,4),:));      m_tr(2,1:size(m.d,2)) =
mean(m.d(aa_big(1,3):aa_big(1,4),:));

m_tr(3,1:size(m.po,2)) = mean(m.po(aa_big(1,3):aa_big(1,4),:));

te_br(1,:) = mean(te.b(aa_big(1,1):aa_big(1,2),:));    te_br(2,1:size(te.d,2)) =
mean(te.d(aa_big(1,1):aa_big(1,2),:));
```

```
   te_br(3,1:size(te.po,2)) = mean(te.po(aa_big(1,1):aa_big(1,2),:));

   te_nr(1,:) = mean(te.b(aa_big(1,2):aa_big(1,3),:));     te_nr(2,1:size(te.d,2)) =
mean(te.d(aa_big(1,2):aa_big(1,3),:));

   te_nr(3,1:size(te.po,2)) = mean(te.po(aa_big(1,2):aa_big(1,3),:));

   te_tr(1,:) = mean(te.b(aa_big(1,3):aa_big(1,4),:));     te_tr(2,1:size(te.d,2)) =
mean(te.d(aa_big(1,3):aa_big(1,4),:));

   te_tr(3,1:size(te.po,2)) = mean(te.po(aa_big(1,3):aa_big(1,4),:)); clear aa_big abc

end

for sta=1

   % 2 sample t-test for comparisons of early, mid and term

   [~,st.br_pre(1,1)] = ttest2(ea_br(1,:),m_br(1,:));  [~,st.br_pre(1,2)] = ttest2(m_br(1,:),te_br(1,:));

   [~,st.br_pre(1,3)] = ttest2(te_br(1,:),ea_br(1,:));

   [~,st.br_dur(1,1)] = ttest2(ea_br(2,1:size(ea.d,2)),m_br(2,1:size(m.d,2)));

   [~,st.br_dur(1,2)] = ttest2(m_br(2,1:size(m.d,2)),te_br(2,1:size(te.d,2)));

   [~,st.br_dur(1,3)] = ttest2(te_br(2,1:size(te.d,2)),ea_br(2,1:size(ea.d,2)));

   [~,st.br_po(1,1)] = ttest2(ea_br(3,1:size(ea.po,2)),m_br(3,1:size(m.po,2)));

   [~,st.br_po(1,2)] = ttest2(m_br(3,1:size(m.po,2)),te_br(3,1:size(te.po,2)));

   [~,st.br_po(1,3)] = ttest2(te_br(3,1:size(te.po,2)),ea_br(3,1:size(ea.po,2)));

   [~,st.nr_pre(1,1)] = ttest2(ea_nr(1,:),m_nr(1,:));  [~,st.nr_pre(1,2)] = ttest2(m_nr(1,:),te_nr(1,:));

   [~,st.nr_pre(1,3)] = ttest2(te_nr(1,:),ea_nr(1,:));

   [~,st.nr_dur(1,1)] = ttest2(ea_nr(2,1:size(ea.d,2)),m_nr(2,1:size(m.d,2)));

   [~,st.nr_dur(1,2)] = ttest2(m_nr(2,1:size(m.d,2)),te_nr(2,1:size(te.d,2)));

   [~,st.nr_dur(1,3)] = ttest2(te_nr(2,1:size(te.d,2)),ea_nr(2,1:size(ea.d,2)));

   [~,st.nr_po(1,1)] = ttest2(ea_nr(3,1:size(ea.po,2)),m_nr(3,1:size(m.po,2)));

   [~,st.nr_po(1,2)] = ttest2(m_nr(3,1:size(m.po,2)),te_nr(3,1:size(te.po,2)));

   [~,st.nr_po(1,3)] = ttest2(te_nr(3,1:size(te.po,2)),ea_nr(3,1:size(ea.po,2)));

   [~,st.tr_pre(1,1)] = ttest2(ea_tr(1,:),m_tr(1,:));  [~,st.tr_pre(1,2)] = ttest2(m_tr(1,:),te_tr(1,:));

   [~,st.tr_pre(1,3)] = ttest2(te_tr(1,:),ea_tr(1,:));

   [~,st.tr_dur(1,1)] = ttest2(ea_tr(2,1:size(ea.d,2)),m_tr(2,1:size(m.d,2)));

   [~,st.tr_dur(1,2)] = ttest2(m_tr(2,1:size(m.d,2)),te_tr(2,1:size(te.d,2)));

   [~,st.tr_dur(1,3)] = ttest2(te_tr(2,1:size(te.d,2)),ea_tr(2,1:size(ea.d,2)));
```

```
   [~,st.tr_po(1,1)] = ttest2(ea_tr(3,1:size(ea.po,2)),m_tr(3,1:size(m.po,2)));

   [~,st.tr_po(1,2)] = ttest2(m_tr(3,1:size(m.po,2)),te_tr(3,1:size(te.po,2)));

   [~,st.tr_po(1,3)] = ttest2(te_tr(3,1:size(te.po,2)),ea_tr(3,1:size(ea.po,2))); clear sta

end

for plot0=1

   title_name = {'Brady Gastria (0.5 - 2 cpm)','Normal Gastria (2 - 4 cpm)','Tachy Gastria (4 - 9 cpm)'};

   a = mean(ea_br,2);  a(:,2) = mean(m_br,2);  a(:,3) = mean(te_br,2);

   a_std = std(ea_br,[],2)./sqrt(25); a_std(:,2) = std(m_br,[],2)./sqrt(22); a_std(:,3) =
std(te_br,[],2)./sqrt(4);

   figure; set(gcf, 'Position', get(0, 'Screensize')); subplot(2,2,1);

   bar(a); hold on; legend('Early (n=25)','Mid (n=22)','Term
(n=4)');title(title_name(1),'FontSize',20,'FontWeight','bold');

   set(gca, 'XTickLabel', {'Before','During','Post'},'FontSize',15);

   ylabel('Mean PSD (mV^2/Hz)','FontSize',20,'FontWeight','bold');

   aa1 = [0.78:2.78];aa2 = [1.23:3.23]; aa3 = 1:3;

   er = errorbar(aa1,a(:,1),a_std(:,1),a_std(:,1),'LineWidth',2);er.Color = 'black';er.LineStyle = 'none';hold
on;

   er = errorbar(aa3,a(:,2),a_std(:,2),a_std(:,2),'LineWidth',2);er.Color = 'black';er.LineStyle = 'none';hold
on;

   er = errorbar(aa2,a(:,3),a_std(:,3),a_std(:,3),'LineWidth',2);er.Color = 'black';er.LineStyle = 'none';hold
off;
```

C.3 CODE FOR CWT CALCULATIONS FOR CHAPTER 2

```
clear all;      clc;

%% load data

sub_no = 'POOH003'; cd('C:\New folder');    timings_excel = importdata('FeedingTime.csv');

% extract time for that subject from the excel sheet

line_no = find(strcmpi(timings_excel.textdata(:,1),sub_no));

timing_data = timings_excel.data(line_no-1,:); clear timings_excel line_no

% extract the feeding time for that subject

feed_time = [timing_data(1,4) timing_data(1,5) timing_data(1,8) timing_data(1,9)]; clear timing_data
```

```
% load the EGG nirs compiled data

cd('C:\New folder\result_data\POOH003');        load('EGG_nirs_data1.mat');

% create the time vector for EGG time bcoz the dps are different

EGG_time = linspace(EGG_121_time(1,1),EGG_121_time(end,1),size(EGG_121_data_final,2));

EGG_121_time = EGG_time';

% calculate the sampling frequency for the EGG

fs_EGG = round(size(EGG_121_data_final,2)/EGG_121_time(end,1));

% seprate the time into pre, dur and post feeding periods

tt.EGG_dur1 = [max(find(EGG_121_time(:,1)<=feed_time(1,1)))
max(find(EGG_121_time(:,1)<=feed_time(1,2)))];

tt.EGG_pre1 = [1 tt.EGG_dur1(1,1)];

tt.EGG_dur2 = [max(find(EGG_121_time(:,1)<=feed_time(1,3)))
max(find(EGG_121_time(:,1)<=feed_time(1,4)))];

EGG_mid = tt.EGG_dur2(1,1) - tt.EGG_dur1(1,2);

tt.EGG_post1 = [tt.EGG_dur1(1,2) tt.EGG_dur1(1,2)+(EGG_mid/2)];

tt.EGG_pre2 = [tt.EGG_dur2(1,1)-(EGG_mid/2) tt.EGG_dur2(1,1)]; clear EGG_mid

tt.EGG_post2 = [tt.EGG_dur2(1,2) size(EGG_121_time,1)]; clear feed_time

% extract data for each feeding period

f_data.EGG_pre1 = EGG_121_data_final(1,tt.EGG_pre1(1,1):tt.EGG_pre1(1,2));

f_data.EGG_dur1 = EGG_121_data_final(1,tt.EGG_dur1(1,1):tt.EGG_dur1(1,2));

f_data.EGG_post1 = EGG_121_data_final(1,tt.EGG_post1(1,1):tt.EGG_post1(1,2));

f_data.EGG_pre2 = EGG_121_data_final(1,tt.EGG_pre2(1,1):tt.EGG_pre2(1,2));

f_data.EGG_dur2 = EGG_121_data_final(1,tt.EGG_dur2(1,1):tt.EGG_dur2(1,2));

f_data.EGG_post2 = EGG_121_data_final(1,tt.EGG_post2(1,1):tt.EGG_post2(1,2));

% time in min

tt2.pre1_time = EGG_121_time(tt.EGG_pre1(1,2),1)/60;

tt2.dur1_time = ((EGG_121_time(tt.EGG_dur1(1,2),1))-(EGG_121_time(tt.EGG_dur1(1,1),1)))/60;

tt2.post1_time = ((EGG_121_time(round(tt.EGG_post1(1,2)),1)) -
(EGG_121_time(tt.EGG_post1(1,1),1)))/60;
```

```
tt2.pre2_time = (EGG_121_time(tt.EGG_pre2(1,2),1)-EGG_121_time(round(tt.EGG_pre2(1,1)),1))/60;

tt2.dur2_time = (EGG_121_time(round(tt.EGG_dur2(1,2)),1)-
EGG_121_time(round(tt.EGG_dur2(1,1)),1))/60;

tt2.post2_time = (EGG_121_time(round(tt.EGG_post2(1,2)),1)-
EGG_121_time(round(tt.EGG_post2(1,1)),1))/60; clear tt EGG_121_time

%% cwt running -> for 0.5-15 cpm

for run_cwt=1

   % filter the data from 0.5 to 15 Hz using filtfilt filter

   fl=0.5/60; [b,a]=butter(2,fl/(fs_EGG/2) ,'high');  dataOut1=filtfilt(b,a,f_data.EGG_pre1); clear a b fl

   fl=15/60; [b,a]=butter(2,fl/(fs_EGG/2) ,'low');   dataOut=filtfilt(b,a,dataOut1); clear a b dataOut1 fl

   % run cwt on the data with input as filtered data and sampling

   % frequency

   [pre1.cwt,pre1.f,pre1.coi] = cwt(dataOut,fs_EGG);

   % find the limits for brady, normo, tachy gastria

   pre1.band_lim = [max(find(pre1.f>=9/60)) max(find(pre1.f>=4/60)) max(find(pre1.f>=2/60))
max(find(pre1.f>=0.5/60))];

   fl=0.5/60; [b,a]=butter(2,fl/(fs_EGG/2) ,'high');  dataOut1=filtfilt(b,a,f_data.EGG_dur1); clear a b fl

   fl=15/60; [b,a]=butter(2,fl/(fs_EGG/2) ,'low');   dataOut=filtfilt(b,a,dataOut1); clear a b dataOut1 fl

   [dur1.cwt,dur1.f,dur1.coi] = cwt(dataOut,fs_EGG); clear dataOut

   dur1.band_lim = [max(find(dur1.f>=9/60)) max(find(dur1.f>=4/60)) max(find(dur1.f>=2/60))
max(find(dur1.f>=0.5/60))];

   fl=0.5/60; [b,a]=butter(2,fl/(fs_EGG/2) ,'high');  dataOut1=filtfilt(b,a,f_data.EGG_post1); clear a b fl

   fl=15/60; [b,a]=butter(2,fl/(fs_EGG/2) ,'low');   dataOut=filtfilt(b,a,dataOut1); clear a b dataOut1 fl

   [post1.cwt,post1.f,post1.coi] = cwt(dataOut,fs_EGG); clear dataOut

   post1.band_lim = [max(find(post1.f>=9/60)) max(find(post1.f>=4/60)) max(find(post1.f>=2/60))
max(find(post1.f>=0.5/60))];

   fl=0.5/60; [b,a]=butter(2,fl/(fs_EGG/2) ,'high');  dataOut1=filtfilt(b,a,f_data.EGG_pre2); clear a b fl

   fl=15/60; [b,a]=butter(2,fl/(fs_EGG/2) ,'low');   dataOut=filtfilt(b,a,dataOut1); clear a b dataOut1 fl

   [pre2.cwt,pre2.f,pre2.coi] = cwt(dataOut,fs_EGG); clear dataOut

   pre2.band_lim = [max(find(pre2.f>=9/60)) max(find(pre2.f>=4/60)) max(find(pre2.f>=2/60))
max(find(pre2.f>=0.5/60))];
```

```
   fl=0.5/60; [b,a]=butter(2,fl/(fs_EGG/2) ,'high');  dataOut1=filtfilt(b,a,f_data.EGG_dur2); clear a b fl

   fl=15/60; [b,a]=butter(2,fl/(fs_EGG/2) ,'low');   dataOut=filtfilt(b,a,dataOut1); clear a b dataOut1 fl

   [dur2.cwt,dur2.f,dur2.coi] = cwt(dataOut,fs_EGG); clear dataOut

   dur2.band_lim = [max(find(dur2.f>=9/60)) max(find(dur2.f>=4/60)) max(find(dur2.f>=2/60))
max(find(dur2.f>=0.5/60))];

   fl=0.5/60; [b,a]=butter(2,fl/(fs_EGG/2) ,'high');  dataOut1=filtfilt(b,a,f_data.EGG_post2); clear a b fl

   fl=15/60; [b,a]=butter(2,fl/(fs_EGG/2) ,'low');   dataOut=filtfilt(b,a,dataOut1); clear a b dataOut1 fl

   [post2.cwt,post2.f,post2.coi] = cwt(dataOut,fs_EGG); clear dataOut

   post2.band_lim = [max(find(post2.f>=9/60)) max(find(post2.f>=4/60)) max(find(post2.f>=2/60))
max(find(post2.f>=0.5/60))]; clear fs_EGG run_cwt

end

%%

% find dominant power in each band and for each min

for aaa=1

   b = linspace(1,size(pre1.coi,1),tt2.pre1_time+1);

   for i=1:length(b)-1

      % the max value will be the dominant power for each frequency band

      % brady

      pre1.min_wise_cwt(1,i) =
abs(max(max(pre1.cwt(pre1.band_lim(1,1):pre1.band_lim(1,2),round(b(i)):round(b(i+1))))));

      % normo

      pre1.min_wise_cwt(2,i) =
abs(max(max(pre1.cwt(pre1.band_lim(1,2):pre1.band_lim(1,3),round(b(i)):round(b(i+1))))));

      % tachy

      pre1.min_wise_cwt(3,i) =
abs(max(max(pre1.cwt(pre1.band_lim(1,3):pre1.band_lim(1,4),round(b(i)):round(b(i+1))))));

   end

   b = linspace(1,size(dur1.coi,1),tt2.dur1_time+1);

   for i=1:length(b)-1
```

```
    dur1.min_wise_cwt(1,i) =
abs(max(max(dur1.cwt(dur1.band_lim(1,1):dur1.band_lim(1,2),round(b(i)):round(b(i+1))))));

    dur1.min_wise_cwt(2,i) =
abs(max(max(dur1.cwt(dur1.band_lim(1,2):dur1.band_lim(1,3),round(b(i)):round(b(i+1))))));

    dur1.min_wise_cwt(3,i) =
abs(max(max(dur1.cwt(dur1.band_lim(1,3):dur1.band_lim(1,4),round(b(i)):round(b(i+1))))));

  end

  b = linspace(1,size(post1.coi,1),tt2.post1_time+1);

  for i=1:length(b)-1

    post1.min_wise_cwt(1,i) =
abs(max(max(post1.cwt(post1.band_lim(1,1):post1.band_lim(1,2),round(b(i)):round(b(i+1))))));

    post1.min_wise_cwt(2,i) =
abs(max(max(post1.cwt(post1.band_lim(1,2):post1.band_lim(1,3),round(b(i)):round(b(i+1))))));

    post1.min_wise_cwt(3,i) =
abs(max(max(post1.cwt(post1.band_lim(1,3):post1.band_lim(1,4),round(b(i)):round(b(i+1))))));

  end

  b = linspace(1,size(pre2.coi,1),tt2.pre2_time+1);

  for i=1:length(b)-1

    pre2.min_wise_cwt(1,i) =
abs(max(max(pre2.cwt(pre2.band_lim(1,1):pre2.band_lim(1,2),round(b(i)):round(b(i+1))))));

    pre2.min_wise_cwt(2,i) =
abs(max(max(pre2.cwt(pre2.band_lim(1,2):pre2.band_lim(1,3),round(b(i)):round(b(i+1))))));

    pre2.min_wise_cwt(3,i) =
abs(max(max(pre2.cwt(pre2.band_lim(1,3):pre2.band_lim(1,4),round(b(i)):round(b(i+1))))));

  end

  b = linspace(1,size(dur2.coi,1),tt2.dur2_time+1);

  for i=1:length(b)-1

    dur2.min_wise_cwt(1,i) =
abs(max(max(dur2.cwt(dur2.band_lim(1,1):dur2.band_lim(1,2),round(b(i)):round(b(i+1))))));

    dur2.min_wise_cwt(2,i) =
abs(max(max(dur2.cwt(dur2.band_lim(1,2):dur2.band_lim(1,3),round(b(i)):round(b(i+1))))));

    dur2.min_wise_cwt(3,i) =
abs(max(max(dur2.cwt(dur2.band_lim(1,3):dur2.band_lim(1,4),round(b(i)):round(b(i+1))))));
```

```
   end
   b = linspace(1,size(post2.coi,1),tt2.post2_time+1);
   for i=1:length(b)-1
      post2.min_wise_cwt(1,i) =
abs(max(max(post2.cwt(post2.band_lim(1,1):post2.band_lim(1,2),round(b(i)):round(b(i+1))))));
      post2.min_wise_cwt(2,i) =
abs(max(max(post2.cwt(post2.band_lim(1,2):post2.band_lim(1,3),round(b(i)):round(b(i+1))))));
      post2.min_wise_cwt(3,i) =
abs(max(max(post2.cwt(post2.band_lim(1,3):post2.band_lim(1,4),round(b(i)):round(b(i+1))))));
   end
   % find the grand max value from 3 frequency bands and
   % then 1 if brady, 2 if normo, 3 if tachy
   [pre1.max pre1.pos] = max(pre1.min_wise_cwt);      [dur1.max dur1.pos] = max(dur1.min_wise_cwt);
   [post1.max post1.pos] = max(post1.min_wise_cwt);   [pre2.max pre2.pos] = max(pre2.min_wise_cwt);
   [dur2.max dur2.pos] = max(dur2.min_wise_cwt);      [post2.max post2.pos] =
max(post2.min_wise_cwt);
   clear aaa
end
% calculate % time for each band
for aaa=1
   % for pre 1
   brad = 0; norm = 0; tachy = 0;
   for i=1:length(pre1.pos)
      if pre1.pos(1,i)==1
         brad = brad + 1; % if max at 1 then it is brady
      elseif pre1.pos(1,i)==2
         norm = norm + 1; % if max at 1 then it is normo
      else
         tachy = tachy + 1; % if max at 1 then it is tachy
      end
```

```
end
pre1.per_brady = brad/length(pre1.pos)*100; clear brad i % calculate the % time for brady
pre1.per_norm = norm/length(pre1.pos)*100; clear norm % calculate the % time for normo
pre1.per_tachy = tachy/length(pre1.pos)*100; clear tachy % calculate the % time for tachy
% for dur 1
brad = 0; norm = 0; tachy = 0;
for i=1:length(dur1.pos)
   if dur1.pos(1,i)==1
      brad = brad + 1;
   elseif dur1.pos(1,i)==2
      norm = norm + 1;
   else
      tachy = tachy + 1;
   end
end
dur1.per_brady = brad/length(dur1.pos)*100;    dur1.per_norm = norm/length(dur1.pos)*100;
dur1.per_tachy = tachy/length(dur1.pos)*100;
% for post 1
brad = 0; norm = 0; tachy = 0;
for i=1:length(post1.pos)
   if post1.pos(1,i)==1
      brad = brad + 1;
   elseif post1.pos(1,i)==2
      norm = norm + 1;
   else
      tachy = tachy + 1;
   end
end
post1.per_brady = brad/length(post1.pos)*100; post1.per_norm = norm/length(post1.pos)*100;
```

```
post1.per_tachy = tachy/length(post1.pos)*100;
% for pre 2
brad = 0; norm = 0; tachy = 0;
for i=1:length(pre2.pos)
   if pre2.pos(1,i)==1
      brad = brad + 1;
   elseif pre2.pos(1,i)==2
      norm = norm + 1;
   else
      tachy = tachy + 1;
   end
end
pre2.per_brady = brad/length(pre2.pos)*100;     pre2.per_norm = norm/length(pre2.pos)*100;
pre2.per_tachy = tachy/length(pre2.pos)*100;

% for dur 2
brad = 0; norm = 0; tachy = 0;
for i=1:length(dur2.pos)
   if dur2.pos(1,i)==1
      brad = brad + 1;
   elseif dur2.pos(1,i)==2
      norm = norm + 1;
   else
      tachy = tachy + 1;
   end
end
clear i
dur2.per_brady = brad/length(dur2.pos)*100; dur2.per_norm = norm/length(dur2.pos)*100;
dur2.per_tachy = tachy/length(dur2.pos)*100;
```

```
    % for post 2
    brad = 0; norm = 0; tachy = 0;
    for i=1:length(post2.pos)
        if post2.pos(1,i)==1
            brad = brad + 1;
        elseif post2.pos(1,i)==2
            norm = norm + 1;
        else
            tachy = tachy + 1;
        end
    end
    clear i
    post2.per_brady = brad/length(post2.pos)*100; post2.per_norm = norm/length(post2.pos)*100;
    post2.per_tachy = tachy/length(post2.pos)*100;
end
% save the file for each subject
save('after_cwt_and_per_time.mat','-v7.3');
```

C.4 PLOT OF PERCENTAGE TIME CALCULATIONS FOR CHAPTER 2

```
%% load after_cwt_and_per_time.mat
for cwt_time_ana=1
    for load_Data=1
        % each sub groups total of 5 groups: early ivh, early noivh, mid ivh, mid noivh, term
        early_ivh = [19, 20, 28, 31, 32, 34, 35, 36,39,46,59];
        early_noivh = [15,16,18,21,22,23,24,26,33,38,47,58,65,66];   mid_ivh = [17,37,41,54];
        mid_noivh = [25,27,29,30,42,43,44,45,49,50,51,53,55,56,57,62,64];

        % early ivh
```

```
k=1; k1=1; kk=1;
for count_e_i = 1:length(early_ivh)
   cd(strcat('C:\New folder\result_data\POOH0',num2str(early_ivh(count_e_i))));
   load('after_cwt_and_per_time.mat');
   for i=1:length(dur2_all)
      aa = dur1_all(i).dur1;          dur1_use(1,i) = isstruct(aa); clear aa
      aa = dur2_all(i).dur2;          dur2_use(1,i) = isstruct(aa); clear aa
   end
   dur1 = dur1_all(dur1_use);  pre1 = pre1_all(dur1_use);  post1 = post1_all(dur1_use);
   dur2 = dur2_all(dur2_use);  pre2 = pre2_all(dur2_use);  post2 = post2_all(dur2_use);  p=k;
   for i=1:length(pre1)
      e_ivh.dur1(k,1) = dur1(i).dur1.per_brady;
      e_ivh.dur1(k,2) = dur1(i).dur1.per_norm;   e_ivh.dur1(k,3) = dur1(i).dur1.per_tachy;
      e_ivh.pre1(k,1) = pre1(i).pre1.per_brady;
      e_ivh.pre1(k,2) = pre1(i).pre1.per_norm;   e_ivh.pre1(k,3) = pre1(i).pre1.per_tachy;
      e_ivh.post1(k,1) = post1(i).post1.per_brady; e_ivh.post1(k,2) = post1(i).post1.per_norm;
     e_ivh.post1(k,3) = post1(i).post1.per_tachy;k=k+1;
   end
   q=k1;
   for i=1:length(pre2)
      e_ivh.dur2(k1,1) = dur2(i).dur2.per_brady;
      e_ivh.dur2(k1,2) = dur2(i).dur2.per_norm;  e_ivh.dur2(k1,3) = dur2(i).dur2.per_tachy;
      e_ivh.pre2(k1,1) = pre2(i).pre2.per_brady;
      e_ivh.pre2(k1,2) = pre2(i).pre2.per_norm;  e_ivh.pre2(k1,3) = pre2(i).pre2.per_tachy;
      e_ivh.post2(k1,1) = post2(i).post2.per_brady; e_ivh.post2(k1,2) = post2(i).post2.per_norm;
     e_ivh.post2(k1,3) = post2(i).post2.per_tachy; k1=k1+1;
   end

    e_ivh.dur1_sub(kk,:) = mean(e_ivh.dur1(p:end,:));
```

```
    e_ivh.pre1_sub(kk,:) = mean(e_ivh.pre1(p:end,:));
    e_ivh.post1_sub(kk,:) = mean(e_ivh.post1(p:end,:));
    e_ivh.dur2_sub(kk,:) = mean(e_ivh.dur2(q:end,:));
    e_ivh.pre2_sub(kk,:) = mean(e_ivh.pre2(q:end,:));
    e_ivh.post2_sub(kk,:) = mean(e_ivh.post2(q:end,:)); kk = kk+1;
end
    e_ivh.dur1_mean = mean(e_ivh.dur1); e_ivh.pre1_mean = mean(e_ivh.pre1);
    e_ivh.post1_mean = mean(e_ivh.post1);
    e_ivh.dur2_mean = mean(e_ivh.dur2); e_ivh.pre2_mean = mean(e_ivh.pre2);
    e_ivh.post2_mean = mean(e_ivh.post2);
    e_ivh.dur1_std = std(e_ivh.dur1);   e_ivh.pre1_std = std(e_ivh.pre1);
    e_ivh.post1_std = std(e_ivh.post1); e_ivh.post2_std = std(e_ivh.post2);
    e_ivh.dur2_std = std(e_ivh.dur2);   e_ivh.pre2_std = std(e_ivh.pre2);
% early noivh
k=1; k1=1; kk=1;
for count_e_noi = 1:length(early_noivh)
   cd(strcat('C:\New folder\result_data\POOH0',num2str(early_noivh(count_e_noi))));
   load('after_cwt_and_per_time.mat');
   for i=1:length(dur2_all)
      aa = dur1_all(i).dur1;          dur1_use(1,i) = isstruct(aa); clear aa
      aa = dur2_all(i).dur2;          dur2_use(1,i) = isstruct(aa); clear aa
   end
   dur1 = dur1_all(dur1_use);  pre1 = pre1_all(dur1_use);  post1 = post1_all(dur1_use);
   dur2 = dur2_all(dur2_use);  pre2 = pre2_all(dur2_use);  post2 = post2_all(dur2_use); p=k;
   for i=1:length(pre1)
      e_noivh.dur1(k,1) = dur1(i).dur1.per_brady; e_noivh.dur1(k,2) = dur1(i).dur1.per_norm;
     e_noivh.dur1(k,3) = dur1(i).dur1.per_tachy; e_noivh.pre1(k,1) = pre1(i).pre1.per_brady;
     e_noivh.pre1(k,2) = pre1(i).pre1.per_norm; e_noivh.pre1(k,3) = pre1(i).pre1.per_tachy;
     e_noivh.post1(k,1) = post1(i).post1.per_brady; e_noivh.post1(k,2) = post1(i).post1.per_norm;
```

```
    e_noivh.post1(k,3) = post1(i).post1.per_tachy;k=k+1;
  end
  q=k1;
  for i=1:length(pre2)
     e_noivh.dur2(k1,1) = dur2(i).dur2.per_brady; e_noivh.dur2(k1,2) = dur2(i).dur2.per_norm;
     e_noivh.dur2(k1,3) = dur2(i).dur2.per_tachy;  e_noivh.pre2(k1,1) = pre2(i).pre2.per_brady;
     e_noivh.pre2(k1,2) = pre2(i).pre2.per_norm;  e_noivh.pre2(k1,3) = pre2(i).pre2.per_tachy;
     e_noivh.post2(k1,1) = post2(i).post2.per_brady;e_noivh.post2(k1,2) = post2(i).post2.per_norm;
     e_noivh.post2(k1,3) = post2(i).post2.per_tachy; k1=k1+1;
  end
    e_noivh.dur1_sub(kk,:) = mean(e_noivh.dur1(p:end,:));
    e_noivh.pre1_sub(kk,:) = mean(e_noivh.pre1(p:end,:));
    e_noivh.post1_sub(kk,:) = mean(e_noivh.post1(p:end,:));
    e_noivh.dur2_sub(kk,:) = mean(e_noivh.dur2(q:end,:));
  e_noivh.pre2_sub(kk,:) = mean(e_noivh.pre2(q:end,:));
  e_noivh.post2_sub(kk,:) = mean(e_noivh.post2(q:end,:)); kk = kk+1;
end
    e_noivh.dur1_mean = mean(e_noivh.dur1);  e_noivh.post2_std = std(e_noivh.post2);
    e_noivh.pre1_mean = mean(e_noivh.pre1);    e_noivh.post1_mean = mean(e_noivh.post1);
    e_noivh.dur2_mean = mean(e_noivh.dur2); e_noivh.pre2_mean = mean(e_noivh.pre2);
    e_noivh.post2_mean = mean(e_noivh.post2); e_noivh.dur1_std = std(e_noivh.dur1);
    e_noivh.pre1_std = std(e_noivh.pre1);    e_noivh.post1_std = std(e_noivh.post1);
    e_noivh.dur2_std = std(e_noivh.dur2); e_noivh.pre2_std = std(e_noivh.pre2);
% mid ivh
k=1; k1=1; kk=1;
for count_m_i = 1:length(mid_ivh)
  cd(strcat('C:\New folder\result_data\POOH0',num2str(mid_ivh(count_m_i))));
  load('after_cwt_and_per_time.mat');
  for i=1:length(dur2_all)
```

```
    aa = dur1_all(i).dur1;          dur1_use(1,i) = isstruct(aa); clear aa
    aa = dur2_all(i).dur2;          dur2_use(1,i) = isstruct(aa); clear aa
  end
  dur1 = dur1_all(dur1_use);  pre1 = pre1_all(dur1_use);  post1 = post1_all(dur1_use);
  dur2 = dur2_all(dur2_use);  pre2 = pre2_all(dur2_use);  post2 = post2_all(dur2_use); p=k;
  for i=1:length(pre1)
    m_ivh.dur1(k,1) = dur1(i).dur1.per_brady; m_ivh.post1(k,1) = post1(i).post1.per_brady;
    m_ivh.dur1(k,2) = dur1(i).dur1.per_norm;   m_ivh.dur1(k,3) = dur1(i).dur1.per_tachy;
    m_ivh.pre1(k,1) = pre1(i).pre1.per_brady; m_ivh.post1(k,2) = post1(i).post1.per_norm;
    m_ivh.pre1(k,2) = pre1(i).pre1.per_norm;   m_ivh.pre1(k,3) = pre1(i).pre1.per_tachy;
    m_ivh.post1(k,3) = post1(i).post1.per_tachy;k=k+1;
  end
  q = k1;
  for i=1:length(pre2)
    m_ivh.dur2(k1,1) = dur2(i).dur2.per_brady; m_ivh.post2(k1,1) = post2(i).post2.per_brady;
    m_ivh.dur2(k1,2) = dur2(i).dur2.per_norm;  m_ivh.dur2(k1,3) = dur2(i).dur2.per_tachy;
    m_ivh.pre2(k1,1) = pre2(i).pre2.per_brady; m_ivh.post2(k1,2) = post2(i).post2.per_norm;
    m_ivh.pre2(k1,2) = pre2(i).pre2.per_norm;  m_ivh.pre2(k1,3) = pre2(i).pre2.per_tachy;
   m_ivh.post2(k1,3) = post2(i).post2.per_tachy; k1=k1+1;
  end
   m_ivh.dur1_sub(kk,:) = mean(m_ivh.dur1(p:end,:));
    m_ivh.pre1_sub(kk,:) = mean(m_ivh.pre1(p:end,:));
     m_ivh.post1_sub(kk,:) = mean(m_ivh.post1(p:end,:));
    m_ivh.dur2_sub(kk,:) = mean(m_ivh.dur2(q:end,:));
    m_ivh.pre2_sub(kk,:) = mean(m_ivh.pre2(q:end,:));
    m_ivh.post2_sub(kk,:) = mean(m_ivh.post2(q:end,:)); kk = kk+1;
end
    m_ivh.dur1_mean = mean(m_ivh.dur1); m_ivh.dur2_mean = mean(m_ivh.dur2);
    m_ivh.pre1_mean = mean(m_ivh.pre1);     m_ivh.post1_mean = mean(m_ivh.post1);
```

```
    m_ivh.pre2_mean = mean(m_ivh.pre2);     m_ivh.post2_mean = mean(m_ivh.post2);
    m_ivh.dur1_std = std(m_ivh.dur1); m_ivh.pre1_std = std(m_ivh.pre1);
    m_ivh.post1_std = std(m_ivh.post1); m_ivh.post2_std = std(m_ivh.post2);
    m_ivh.dur2_std = std(m_ivh.dur2); m_ivh.pre2_std = std(m_ivh.pre2);
% mid noivh
k=1; k1=1; kk=1;
for count_m_noi = 1:length(mid_noivh)
  cd(strcat('C:\New folder\result_data\POOH0',num2str(mid_noivh(count_m_noi))));
  load('after_cwt_and_per_time.mat');
  for(i=1:length(dur1_all)) aa = dur1_all(i).dur1; dur1_use(1,i) = isstruct(aa); end
  for(i=1:length(dur2_all)) aa = dur2_all(i).dur2; dur2_use(1,i) = isstruct(aa); end
    dur1 = dur1_all(dur1_use);  pre1 = pre1_all(dur1_use);
    post1 = post1_all(dur1_use);    clear pre1_all dur1_all post1_all dur1_use
    dur2 = dur2_all(dur2_use);  pre2 = pre2_all(dur2_use);
    post2 = post2_all(dur2_use);    clear dur2_all pre2_all post2_all dur2_use
  p=k;
  for i=1:length(pre1)
     m_noi.dur1(k,1) = dur1(i).dur1.per_brady; m_noi.pre1(k,1) = pre1(i).pre1.per_brady;
     m_noi.dur1(k,2) = dur1(i).dur1.per_norm;   m_noi.dur1(k,3) = dur1(i).dur1.per_tachy;
     m_noi.pre1(k,2) = pre1(i).pre1.per_norm;   m_noi.pre1(k,3) = pre1(i).pre1.per_tachy;
     m_noi.post1(k,1) = post1(i).post1.per_brady; m_noi.post1(k,2) = post1(i).post1.per_norm;
     m_noi.post1(k,3) = post1(i).post1.per_tachy;     k=k+1;
  end
  q = k1;
  for i=1:length(pre2)
     m_noi.dur2(k1,1) = dur2(i).dur2.per_brady; m_noi.pre2(k1,1) = pre2(i).pre2.per_brady;
     m_noi.dur2(k1,2) = dur2(i).dur2.per_norm;  m_noi.dur2(k1,3) = dur2(i).dur2.per_tachy;
     m_noi.pre2(k1,2) = pre2(i).pre2.per_norm;  m_noi.pre2(k1,3) = pre2(i).pre2.per_tachy;
     m_noi.post2(k1,1) = post2(i).post2.per_brady; m_noi.post2(k1,2) = post2(i).post2.per_norm;
```

```
      m_noi.post2(k1,3) = post2(i).post2.per_tachy; k1=k1+1;
   end
      m_noi.dur1_sub(kk,:) = mean(m_noi.dur1(p:end,:));
     m_noi.pre1_sub(kk,:) = mean(m_noi.pre1(p:end,:));
    m_noi.post1_sub(kk,:) = mean(m_noi.post1(p:end,:));
     m_noi.dur2_sub(kk,:) = mean(m_noi.dur2(q:end,:));
    m_noi.pre2_sub(kk,:) = mean(m_noi.pre2(q:end,:));
    m_noi.post2_sub(kk,:) = mean(m_noi.post2(q:end,:)); kk = kk+1;
end
     m_noi.dur1_mean = mean(m_noi.dur1); m_noi.dur2_mean = mean(m_noi.dur2);
     m_noi.pre1_mean = mean(m_noi.pre1);    m_noi.post1_mean = mean(m_noi.post1);
     m_noi.pre2_mean = mean(m_noi.pre2);    m_noi.post2_mean = mean(m_noi.post2);
     m_noi.dur1_std = std(m_noi.dur1); m_noi.pre1_std = std(m_noi.pre1);
     m_noi.post1_std = std(m_noi.post1); m_noi.post2_std = std(m_noi.post2);
     m_noi.dur2_std = std(m_noi.dur2); m_noi.pre2_std = std(m_noi.pre2);
% term
term_sub = [2 3 4 5]; k=1; kk=1;
for term_count=1:length(term_sub)
   cd(strcat('C:\New folder\result_data\POOH00',num2str(term_sub(term_count))));
   load('after_cwt_and_per_time.mat');
   term.dur1(k,1) = dur1.per_brady; term.pre1(k,1) = pre1.per_brady;
   term.dur1(k,2) = dur1.per_norm;   term.dur1(k,3) = dur1.per_tachy;
   term.pre1(k,2) = pre1.per_norm;   term.pre1(k,3) = pre1.per_tachy;
   term.post1(k,1) = post1.per_brady; term.dur2(k,1) = dur2.per_brady;
   term.post1(k,2) = post1.per_norm;    term.post1(k,3) = post1.per_tachy;
   term.dur2(k,2) = dur2.per_norm;  term.dur2(k,3) = dur2.per_tachy;
   term.pre2(k,1) = pre2.per_brady; term.post2(k,1) = post2.per_brady;
   term.pre2(k,2) = pre2.per_norm;  term.pre2(k,3) = pre2.per_tachy;
   term.post2(k,2) = post2.per_norm;   term.post2(k,3) = post2.per_tachy;
```

```
        term.dur1_sub(kk,:) = term.dur1(k,:);    term.pre1_sub(kk,:) = term.pre1(k,:);
        term.post1_sub(kk,:) = term.post1(k,:);  term.dur2_sub(kk,:) = term.dur2(k,:);
        term.pre2_sub(kk,:) = term.pre2(k,:); term.post2_sub(kk,:) = term.post2(k,:); kk = kk+1; k=k+1;
    end
        term.dur1_mean = mean(term.dur1); term.post2_mean = mean(term.post2);
        term.pre1_mean = mean(term.pre1); term.post1_mean = mean(term.post1);
        term.dur2_mean = mean(term.dur2); term.pre2_mean = mean(term.pre2);
        term.dur1_std = std(term.dur1); term.pre1_std = std(term.pre1);
        term.post1_std = std(term.post1); term.post2_std = std(term.post2);
        term.dur2_std = std(term.dur2); term.pre2_std = std(term.pre2); term.sub_list = term_sub;
  end
    a = term.pre1_mean;     a(2,:) = e_ivh.pre1_mean;       a(3,:) = e_noivh.pre1_mean;
    a(4,:) = m_ivh.pre1_mean;       a(5,:) = m_noi.pre1_mean;
    a(1,:,2) = term.dur1_mean;     a(2,:,2) = e_ivh.dur1_mean;       a(3,:,2) = e_noivh.dur1_mean;
    a(4,:,2) = m_ivh.dur1_mean;       a(5,:,2) = m_noi.dur1_mean;
    a(1,:,3) = term.post1_mean;     a(2,:,3) = e_ivh.post1_mean;       a(3,:,3) = e_noivh.post1_mean;
    a(4,:,3) = m_ivh.post1_mean;       a(5,:,3) = m_noi.post1_mean;
    a(1,:,4) = term.pre2_mean;     a(2,:,4) = e_ivh.pre2_mean;       a(3,:,4) = e_noivh.pre2_mean;
    a(4,:,4) = m_ivh.pre2_mean;       a(5,:,4) = m_noi.pre2_mean;
    a(1,:,5) = term.dur2_mean;     a(2,:,5) = e_ivh.dur2_mean;       a(3,:,5) = e_noivh.dur2_mean;
    a(4,:,5) = m_ivh.dur2_mean;       a(5,:,5) = m_noi.dur2_mean;
    a(1,:,6) = term.post2_mean;     a(2,:,6) = e_ivh.post2_mean;       a(3,:,6) = e_noivh.post2_mean;
    a(4,:,6) = m_ivh.post2_mean;       a(5,:,6) = m_noi.post2_mean;
    b = sta.pre1; b(:,:,2) = sta.dur1; b(:,:,3) = sta.post1; b(:,:,4) = sta.pre2; b(:,:,5) = sta.dur2; b(:,:,6) =
sta.post2;
    % Standard mean: std dev/ sqrt(no of subjects)
    c = term.pre1_std./sqrt(4);     c(2,:) = e_ivh.pre1_std./sqrt(11);
    c(3,:) = e_noivh.pre1_std./sqrt(14);
    c(4,:) = m_ivh.pre1_std./sqrt(4);       c(5,:) = m_noi.pre1_std./sqrt(17);
```

```
    c(1,:,2) = term.dur1_std./sqrt(4);     c(2,:,2) = e_ivh.dur1_std./sqrt(11);
    c(3,:,2) = e_noivh.dur1_std./sqrt(14);
    c(4,:,2) = m_ivh.dur1_std./sqrt(4);       c(5,:,2) = m_noi.dur1_std./sqrt(17);
    c(1,:,3) = term.post1_std./sqrt(4);     c(2,:,3) = e_ivh.post1_std./sqrt(11);
     c(3,:,3) = e_noivh.post1_std./sqrt(14);
    c(4,:,3) = m_ivh.post1_std./sqrt(4);       c(5,:,3) = m_noi.post1_std./sqrt(17);
    c(1,:,4) = term.pre2_std./sqrt(4);     c(2,:,4) = e_ivh.pre2_std./sqrt(11);
    c(3,:,4) = e_noivh.pre2_std./sqrt(14);
    c(4,:,4) = m_ivh.pre2_std./sqrt(4);       c(5,:,4) = m_noi.pre2_std./sqrt(17);
    c(1,:,5) = term.dur2_std./sqrt(4);     c(2,:,5) = e_ivh.dur2_std./sqrt(11);
     c(3,:,5) = e_noivh.dur2_std./sqrt(14);
    c(4,:,5) = m_ivh.dur2_std./sqrt(4);       c(5,:,5) = m_noi.dur2_std./sqrt(17);
    c(1,:,6) = term.post2_std./sqrt(4);     c(2,:,6) = e_ivh.post2_std./sqrt(11);
     c(3,:,6) = e_noivh.post2_std./sqrt(14);
    c(4,:,6) = m_ivh.post2_std./sqrt(4);       c(5,:,6) = m_noi.post2_std./sqrt(17);
%% scatter plot
for gestat_plot=1 % ivh and no ivh together
    cd('C:\New folder');    a = importdata('gestational_age.csv'); % 48 sub we dont have
    gestational_age = 1:66; gestational_age = gestational_age';
    gestational_age(1:47,2) = a.data(1:47,1);   gestational_age(49:66,2) = a.data(48:65,1);
    a = e_ivh.dur1_sub; a(:,:,2) = e_ivh.dur2_sub;  e_ivh.dur_sub = nanmean(a,3); clear a
    a = e_ivh.pre1_sub; a(:,:,2) = e_ivh.pre2_sub;  e_ivh.pre_sub = nanmean(a,3); clear a
    a = e_ivh.post1_sub; a(:,:,2) = e_ivh.post2_sub;  e_ivh.post_sub = nanmean(a,3); clear a
    a = e_noivh.dur1_sub; a(:,:,2) = e_noivh.dur2_sub;  e_noivh.dur_sub = nanmean(a,3); clear a
    a = e_noivh.pre1_sub; a(:,:,2) = e_noivh.pre2_sub;  e_noivh.pre_sub = nanmean(a,3); clear a
    a = e_noivh.post1_sub; a(:,:,2) = e_noivh.post2_sub;  e_noivh.post_sub = nanmean(a,3); clear a
    a = m_ivh.dur1_sub; a(:,:,2) = m_ivh.dur2_sub;  m_ivh.dur_sub = nanmean(a,3); clear a
    a = m_ivh.pre1_sub; a(:,:,2) = m_ivh.pre2_sub;  m_ivh.pre_sub = nanmean(a,3); clear a
    a = m_ivh.post1_sub; a(:,:,2) = m_ivh.post2_sub;  m_ivh.post_sub = nanmean(a,3); clear a
```

```
a = m_noi.dur1_sub; a(:,:,2) = m_noi.dur2_sub;  m_noi.dur_sub = nanmean(a,3); clear a
a = m_noi.pre1_sub; a(:,:,2) = m_noi.pre2_sub;  m_noi.pre_sub = nanmean(a,3); clear a
a = m_noi.post1_sub; a(:,:,2) = m_noi.post2_sub;  m_noi.post_sub = nanmean(a,3); clear a
a = term.dur1_sub; a(:,:,2) = term.dur2_sub;  term.dur_sub = nanmean(a,3); clear a
a = term.pre1_sub; a(:,:,2) = term.pre2_sub;  term.pre_sub = nanmean(a,3); clear a
a = term.post1_sub; a(:,:,2) = term.post2_sub;  term.post_sub = nanmean(a,3); clear a
a = [e_ivh.sub_list e_noivh.sub_list]';
b = gestational_age(a,2);    b(:,2:4) = [e_ivh.pre_sub;e_noivh.pre_sub]; clear a
a = [m_ivh.sub_list m_noi.sub_list]';
c = gestational_age(a,2);    c(:,2:4) = [m_ivh.pre_sub;m_noi.pre_sub]; clear a
e = gestational_age(term.sub_list,2);  e(:,2:4) = term.pre_sub;
title_name = {'Pre feeding Brady','Pre feeding Norm','Pre feeding Tachy'};
figure;set(gcf, 'Position', get(0, 'Screensize'));
for i=1:3
   subplot(2,2,i); scatter(e(:,1),e(:,i+1),'r','filled'); hold on;
   scatter(b(:,1),b(:,i+1),'b','filled'); hold on; scatter(c(:,1),c(:,i+1),'m','filled'); hold on;
   xlabel('Gestational Age (Weeks)','FontSize',20,'FontWeight','bold');
   ylabel('Percantage Time (%)','FontSize',20,'FontWeight','bold');
   title(title_name(i),'FontSize',21,'FontWeight','bold');
   legend('TERM','Early','Mid','FontSize',15,'FontWeight','bold');
end
a = [e_ivh.sub_list e_noivh.sub_list]';  b = gestational_age(a,2);
b(:,2:4) = [e_ivh.dur_sub;e_noivh.dur_sub]; clear a
a = [m_ivh.sub_list m_noi.sub_list]'; c = gestational_age(a,2);
c(:,2:4) = [m_ivh.dur_sub;m_noi.dur_sub]; clear a
e = gestational_age(term.sub_list,2);  e(:,2:4) = term.dur_sub;
title_name = {'Dur feeding Brady','Dur feeding Norm','Dur feeding Tachy'};
figure; set(gcf, 'Position', get(0, 'Screensize'));
for i=1:3
```

```
        subplot(2,2,i); scatter(e(:,1),e(:,i+1),'r','filled'); hold on;
        scatter(b(:,1),b(:,i+1),'b','filled'); hold on; scatter(c(:,1),c(:,i+1),'m','filled'); hold on;
        xlabel('Gestational Age (Weeks)','FontSize',20,'FontWeight','bold');
        ylabel('Percantage Time (%)','FontSize',20,'FontWeight','bold');
        title(title_name(i),'FontSize',21,'FontWeight','bold');
        legend('TERM','Early','Mid','FontSize',15,'FontWeight','bold');
    end
    a = [e_ivh.sub_list e_noivh.sub_list]';
    b = gestational_age(a,2);    b(:,2:4) = [e_ivh.post_sub;e_noivh.post_sub]; clear a
    a = [m_ivh.sub_list m_noi.sub_list]';
    c = gestational_age(a,2);    c(:,2:4) = [m_ivh.post_sub;m_noi.post_sub]; clear a
    e = gestational_age(term.sub_list,2);  e(:,2:4) = term.post_sub;
    title_name = {'Post feeding Brady','Post feeding Norm','Post feeding Tachy'};
    figure;set(gcf, 'Position', get(0, 'Screensize'));
    for i=1:3
        subplot(2,2,i); scatter(e(:,1),e(:,i+1),'r','filled'); hold on;
        scatter(b(:,1),b(:,i+1),'b','filled'); hold on; scatter(c(:,1),c(:,i+1),'m','filled'); hold on;
        xlabel('Gestational Age (Weeks)','FontSize',20,'FontWeight','bold');
        ylabel('Percantage Time (%)','FontSize',20,'FontWeight','bold');
        title(title_name(i),'FontSize',21,'FontWeight','bold');
        legend('TERM','Early','Mid','FontSize',15,'FontWeight','bold');
    end
  end
end
```

C.5 PSD CALCULATIONS FOR CHAPTER 3 AND CHAPTER 4

```
%% Pwelch for PSD calculations
eeglab; close all;     pl_sub = [1 2 3 4 11 13 15 19 21];     led_sub = [5 6 7 8 10 14 16];
%% for sham subjects
```

```
for ii=1:length(pl_sub)
   EEG = pop_loadset('filename','after_component_removal2.set','filepath',strcat('C:\nasa
data2\sub',num2str(pl_sub(ii))));
   %% sepration of data
   final_data = EEG.data(:,1:20*60*512); fs = EEG.srate;   rest1 = final_data(:,1:2*60*512);
   tp_1 = final_data(:,1:5*60*512);              tp_2 = final_data(:,(5*60*512)+1:10*60*512);
   tp_3 = final_data(:,(10*60*512)+1:15*60*512);   tp_4 = final_data(:,(15*60*512)+1:20*60*512);

   %% psd running
   for j=1:64
      [r1_psd_pl(:,j,ii) f_r1_pl(:,j,ii)] = pwelch(rest1(j,:),20*fs,10*fs,4*fs,fs);
      tp1_psd_pl(:,j,ii) = pwelch(tp_1(j,:),20*fs,10*fs,4*fs,fs);
      tp2_psd_pl(:,j,ii) = pwelch(tp_2(j,:),20*fs,10*fs,4*fs,fs);
      tp3_psd_pl(:,j,ii) = pwelch(tp_3(j,:),20*fs,10*fs,4*fs,fs);
      tp4_psd_pl(:,j,ii) = pwelch(tp_4(j,:),20*fs,10*fs,4*fs,fs);
   end
end

%% for led subjects
for ii=1:length(led_sub)
   EEG = pop_loadset('filename','after_component_removal2.set','filepath',strcat('C:\nasa
data2\sub',num2str(led_sub(ii))));
   %% sepration of data
   final_data = EEG.data(:,1:20*60*512); fs = EEG.srate;   rest1 = final_data(:,1:2*60*512);
   tp_1 = final_data(:,1:5*60*512);              tp_2 = final_data(:,(5*60*512)+1:10*60*512);
   tp_3 = final_data(:,(10*60*512)+1:15*60*512);   tp_4 = final_data(:,(15*60*512)+1:20*60*512);

   %% psd running
   for j=1:64
```

```
    [r1_psd_led(:,j,ii) f_r1_led(:,j,ii)] = pwelch(rest1(j,:),20*fs,10*fs,4*fs,fs);
    tp1_psd_led(:,j,ii) = pwelch(tp_1(j,:),20*fs,10*fs,4*fs,fs);
    tp2_psd_led(:,j,ii) = pwelch(tp_2(j,:),20*fs,10*fs,4*fs,fs);
    tp3_psd_led(:,j,ii) = pwelch(tp_3(j,:),20*fs,10*fs,4*fs,fs);
    tp4_psd_led(:,j,ii) = pwelch(tp_4(j,:),20*fs,10*fs,4*fs,fs);
  end
end

%% for saving
cd('C:\nasa data2\fieldtrip trial\matlab pwelch');
save('field_pwelch_0.25_reso.mat');
```

C.6 BRAIN ACTIVATION TOPOPLOTS FOR CHAPTER 3 AND CHAPTER 4

```
clear all; clc; cd('C:\nasa data2\matlab pwelch'); load('pwelch_all_band_no_norm_0.25_reso.mat');
for load_data=1
  [de_low de_high] = [find(f_r1_led(:,1)==1) find(f_r1_led(:,1)==4)];
  [th_low th_high] = [find(f_r1_led(:,1)==4) find(f_r1_led(:,1)==8)];
  [alp_low alp_high] = [find(f_r1_led(:,1)==8) find(f_r1_led(:,1)==13)];
  [beta_low beta_high] = [find(f_r1_led(:,1)==13) find(f_r1_led(:,1)==30)];
  [gamm_low gamm_high] = [find(f_r1_led(:,1)==30) find(f_r1_led(:,1)==70)];
  for sep_bands=1
    de.r1_led = squeeze(mean(r1_psd_led_no_norm(de_low:de_high,:,:)));
    de.r3_led = squeeze(mean(r3_psd_led_no_norm(de_low:de_high,:,:)));
    de.r4_led = squeeze(mean(r4_psd_led_no_norm(de_low:de_high,:,:)));
    de.r1_pl = squeeze(mean(r1_psd_pl_no_norm(de_low:de_high,:,:)));
    de.r3_pl = squeeze(mean(r3_psd_pl_no_norm(de_low:de_high,:,:)));
    de.r4_pl = squeeze(mean(r4_psd_pl_no_norm(de_low:de_high,:,:)));
    de.g3_led = squeeze(mean(g3_psd_led_no_norm(de_low:de_high,:,:)));
```

```
de.g4_led = squeeze(mean(g4_psd_led_no_norm(de_low:de_high,:,:)));
de.g3_pl = squeeze(mean(g3_psd_pl_no_norm(de_low:de_high,:,:)));
de.g4_pl = squeeze(mean(g4_psd_pl_no_norm(de_low:de_high,:,:)));
th.r1_led = squeeze(mean(r1_psd_led_no_norm(th_low:th_high,:,:)));
th.r3_led = squeeze(mean(r3_psd_led_no_norm(th_low:th_high,:,:)));
th.r4_led = squeeze(mean(r4_psd_led_no_norm(th_low:th_high,:,:)));
th.r1_pl = squeeze(mean(r1_psd_pl_no_norm(th_low:th_high,:,:)));
th.r3_pl = squeeze(mean(r3_psd_pl_no_norm(th_low:th_high,:,:)));
th.r4_pl = squeeze(mean(r4_psd_pl_no_norm(th_low:th_high,:,:)));
th.g3_led = squeeze(mean(g3_psd_led_no_norm(th_low:th_high,:,:)));
th.g4_led = squeeze(mean(g4_psd_led_no_norm(th_low:th_high,:,:)));
th.g3_pl = squeeze(mean(g3_psd_pl_no_norm(th_low:th_high,:,:)));
th.g4_pl = squeeze(mean(g4_psd_pl_no_norm(th_low:th_high,:,:)));
alp.r1_led = squeeze(mean(r1_psd_led_no_norm(alp_low:alp_high,:,:)));
alp.r3_led = squeeze(mean(r3_psd_led_no_norm(alp_low:alp_high,:,:)));
alp.r4_led = squeeze(mean(r4_psd_led_no_norm(alp_low:alp_high,:,:)));
alp.r1_pl = squeeze(mean(r1_psd_pl_no_norm(alp_low:alp_high,:,:)));
alp.r3_pl = squeeze(mean(r3_psd_pl_no_norm(alp_low:alp_high,:,:)));
alp.r4_pl = squeeze(mean(r4_psd_pl_no_norm(alp_low:alp_high,:,:)));
alp.g3_led = squeeze(mean(g3_psd_led_no_norm(alp_low:alp_high,:,:)));
alp.g4_led = squeeze(mean(g4_psd_led_no_norm(alp_low:alp_high,:,:)));
alp.g3_pl = squeeze(mean(g3_psd_pl_no_norm(alp_low:alp_high,:,:)));
alp.g4_pl = squeeze(mean(g4_psd_pl_no_norm(alp_low:alp_high,:,:)));
beta.r1_led = squeeze(mean(r1_psd_led_no_norm(beta_low:beta_high,:,:)));
beta.r3_led = squeeze(mean(r3_psd_led_no_norm(beta_low:beta_high,:,:)));
beta.r4_led = squeeze(mean(r4_psd_led_no_norm(beta_low:beta_high,:,:)));
beta.r1_pl = squeeze(mean(r1_psd_pl_no_norm(beta_low:beta_high,:,:)));
beta.r3_pl = squeeze(mean(r3_psd_pl_no_norm(beta_low:beta_high,:,:)));
beta.r4_pl = squeeze(mean(r4_psd_pl_no_norm(beta_low:beta_high,:,:)));
beta.g3_led = squeeze(mean(g3_psd_led_no_norm(beta_low:beta_high,:,:)));
```

```
   beta.g4_led = squeeze(mean(g4_psd_led_no_norm(beta_low:beta_high,:,:)));
   beta.g3_pl = squeeze(mean(g3_psd_pl_no_norm(beta_low:beta_high,:,:)));
   beta.g4_pl = squeeze(mean(g4_psd_pl_no_norm(beta_low:beta_high,:,:)));
   gamm.r1_led = squeeze(mean(r1_psd_led_no_norm(gamm_low:gamm_high,:,:)));
   gamm.r3_led = squeeze(mean(r3_psd_led_no_norm(gamm_low:gamm_high,:,:)));
   gamm.r4_led = squeeze(mean(r4_psd_led_no_norm(gamm_low:gamm_high,:,:)));
   gamm.r1_pl = squeeze(mean(r1_psd_pl_no_norm(gamm_low:gamm_high,:,:)));
   gamm.r3_pl = squeeze(mean(r3_psd_pl_no_norm(gamm_low:gamm_high,:,:)));
   gamm.r4_pl = squeeze(mean(r4_psd_pl_no_norm(gamm_low:gamm_high,:,:)));
   gamm.g3_led = squeeze(mean(g3_psd_led_no_norm(gamm_low:gamm_high,:,:)));
   gamm.g4_led = squeeze(mean(g4_psd_led_no_norm(gamm_low:gamm_high,:,:)));
   gamm.g3_pl = squeeze(mean(g3_psd_pl_no_norm(gamm_low:gamm_high,:,:)));
   gamm.g4_pl = squeeze(mean(g4_psd_pl_no_norm(gamm_low:gamm_high,:,:))); clear sep_bands
end

% normalization
a = de.r1_led;  de.r3_led = de.r3_led./a;   de.r4_led = de.r4_led./a;
de.g3_led = de.g3_led./a;   de.g4_led = de.g4_led./a; clear a
a = th.r1_led;  th.r3_led = th.r3_led./a;   th.r4_led = th.r4_led./a;
th.g3_led = th.g3_led./a;   th.g4_led = th.g4_led./a; clear a
a = alp.r1_led;  alp.r3_led = alp.r3_led./a;   alp.r4_led = alp.r4_led./a;
alp.g3_led = alp.g3_led./a;   alp.g4_led = alp.g4_led./a; clear a
a = beta.r1_led;  beta.r3_led = beta.r3_led./a;   beta.r4_led = beta.r4_led./a;
beta.g3_led = beta.g3_led./a;   beta.g4_led = beta.g4_led./a; clear a
a = gamm.r1_led;  gamm.r3_led = gamm.r3_led./a;   gamm.r4_led = gamm.r4_led./a;
gamm.g3_led = gamm.g3_led./a;   gamm.g4_led = gamm.g4_led./a; clear a
a = de.r1_pl;  de.r3_pl = de.r3_pl./a;   de.r4_pl = de.r4_pl./a;
de.g3_pl = de.g3_pl./a;   de.g4_pl = de.g4_pl./a; clear a
a = th.r1_pl;  th.r3_pl = th.r3_pl./a;   th.r4_pl = th.r4_pl./a;
th.g3_pl = th.g3_pl./a;   th.g4_pl = th.g4_pl./a; clear a
```

```
    a = alp.r1_pl;  alp.r3_pl = alp.r3_pl./a;   alp.r4_pl = alp.r4_pl./a;
    alp.g3_pl = alp.g3_pl./a;   alp.g4_pl = alp.g4_pl./a; clear a
    a = beta.r1_pl;  beta.r3_pl = beta.r3_pl./a;   beta.r4_pl = beta.r4_pl./a;
    beta.g3_pl = beta.g3_pl./a;   beta.g4_pl = beta.g4_pl./a; clear a
    a = gamm.r1_pl;  gamm.r3_pl = gamm.r3_pl./a;   gamm.r4_pl = gamm.r4_pl./a;
    gamm.g3_pl = gamm.g3_pl./a;   gamm.g4_pl = gamm.g4_pl./a; clear a

    % creating tp3 and tp4
    a = de.r3_led;  a(:,:,2) = de.g3_led; de.tp3_led = mean(a,3); clear a
    a = de.r4_led;  a(:,:,2) = de.g4_led; de.tp4_led = mean(a,3); clear a
    a = de.r3_pl;  a(:,:,2) = de.g3_pl; de.tp3_pl = mean(a,3); clear a
    a = de.r4_pl;  a(:,:,2) = de.g4_pl; de.tp4_pl = mean(a,3); clear a
    a = th.r3_led;  a(:,:,2) = th.g3_led; th.tp3_led = mean(a,3); clear a
    a = th.r4_led;  a(:,:,2) = th.g4_led; th.tp4_led = mean(a,3); clear a
    a = th.r3_pl;  a(:,:,2) = th.g3_pl; th.tp3_pl = mean(a,3); clear a
    a = th.r4_pl;  a(:,:,2) = th.g4_pl; th.tp4_pl = mean(a,3); clear a
    a = alp.r3_led;  a(:,:,2) = alp.g3_led; alp.tp3_led = mean(a,3); clear a
    a = alp.r4_led;  a(:,:,2) = alp.g4_led; alp.tp4_led = mean(a,3); clear a
    a = alp.r3_pl;  a(:,:,2) = alp.g3_pl; alp.tp3_pl = mean(a,3); clear a
    a = alp.r4_pl;  a(:,:,2) = alp.g4_pl; alp.tp4_pl = mean(a,3); clear a
    a = beta.r3_led;  a(:,:,2) = beta.g3_led; beta.tp3_led = mean(a,3); clear a
    a = beta.r4_led;  a(:,:,2) = beta.g4_led; beta.tp4_led = mean(a,3); clear a
    a = beta.r3_pl;  a(:,:,2) = beta.g3_pl; beta.tp3_pl = mean(a,3); clear a
    a = beta.r4_pl;  a(:,:,2) = beta.g4_pl; beta.tp4_pl = mean(a,3); clear a
    a = gamm.r3_led;  a(:,:,2) = gamm.g3_led; gamm.tp3_led = mean(a,3); clear a
    a = gamm.r4_led;  a(:,:,2) = gamm.g4_led; gamm.tp4_led = mean(a,3); clear a
    a = gamm.r3_pl;  a(:,:,2) = gamm.g3_pl; gamm.tp3_pl = mean(a,3); clear a
    a = gamm.r4_pl;  a(:,:,2) = gamm.g4_pl; gamm.tp4_pl = mean(a,3); clear a
end
```

```
% preparing for clustering based stats
cd('C:\nasa data2\fieldtrip trial');    load('freq_led2.mat');
start_fr = de_low;      end_fr = de_high;
tp_alpha = max(find(f_r1_led(:,1,1)<=start_fr)); tp_alpha(1,2) = max(find(f_r1_led(:,1,1)<=end_fr));
tp1_led.freq = f_r1_led(tp_alpha(1,1):tp_alpha(1,2),1,1);   base_struc = tp1_led;
tp4_power_led_de = base_struc;   tp4_power_led_de.powspctrm = de.tp4_led;
tp4_power_pbo_de = base_struc;   tp4_power_pbo_de.powspctrm = de.tp4_pl;

start_fr = th_low;      end_fr = th_high;
tp_alpha = max(find(f_r1_led(:,1,1)<=start_fr)); tp_alpha(1,2) = max(find(f_r1_led(:,1,1)<=end_fr));
tp1_led.freq = f_r1_led(tp_alpha(1,1):tp_alpha(1,2),1,1); base_struc = tp1_led;
tp4_power_led_th = base_struc;   tp4_power_led_th.powspctrm = th.tp4_led;
tp4_power_pbo_th = base_struc;   tp4_power_pbo_th.powspctrm = th.tp4_pl;

start_fr = alp_low;      end_fr = alp_high;
tp_alpha = max(find(f_r1_led(:,1,1)<=start_fr)); tp_alpha(1,2) = max(find(f_r1_led(:,1,1)<=end_fr));
tp1_led.freq = f_r1_led(tp_alpha(1,1):tp_alpha(1,2),1,1); base_struc = tp1_led;
tp4_power_led_alp = base_struc;   tp4_power_led_alp.powspctrm = alp.tp4_led;
tp4_power_pbo_alp = base_struc;   tp4_power_pbo_alp.powspctrm = alp.tp4_pl;

start_fr = beta_low;      end_fr = beta_high;
tp_betaha = max(find(f_r1_led(:,1,1)<=start_fr)); tp_betaha(1,2) = max(find(f_r1_led(:,1,1)<=end_fr));
tp1_led.freq = f_r1_led(tp_betaha(1,1):tp_betaha(1,2),1,1);  base_struc = tp1_led;
tp4_power_led_beta = base_struc;   tp4_power_led_beta.powspctrm = beta.tp4_led;
tp4_power_pbo_beta = base_struc;   tp4_power_pbo_beta.powspctrm = beta.tp4_pl;

start_fr = gamm_low;      end_fr = gamm_high;
tp_gammha = max(find(f_r1_led(:,1,1)<=start_fr)); tp_gammha(1,2) =
max(find(f_r1_led(:,1,1)<=end_fr));
tp1_led.freq = f_r1_led(tp_gammha(1,1):tp_gammha(1,2),1,1); base_struc = tp1_led;
```

```
tp4_power_led_gamm = base_struc;   tp4_power_led_gamm.powspctrm = gamm.tp4_led;
tp4_power_pbo_gamm = base_struc;   tp4_power_pbo_gamm.powspctrm = gamm.tp4_pl;

%% permutation test
cfg = [];      cfg.dataset = 'after_component_removal2.set';
cd('C:\nasa data2\sub1');  data12 = ft_preprocessing(cfg);  st_lim = 0.05;
cfg = [];   cfg.channel = 'all'; cfg.method = 'montecarlo';
cfg.statistic = 'ft_statfun_indepsamplesT'; cfg.correctm = 'cluster';
cfg.clusteralpha = st_lim;  cfg.clusterthreshold = 'nonparametric_individual';
cfg.clusterstatistic = 'maxsum'; cfg.minnbchan = 2; cfg.tail = 1; cfg.clustertail = 1;
cfg.alpha = st_lim; cfg.correcttail = 'alpha'; cfg.numrandomization = 10000;
cfg_neighb.method = 'triangulation'; cfg.neighbours = ft_prepare_neighbours(cfg_neighb, data12);

tp4_power_led_de.powspctrm = tp4_power_led_de.powspctrm';
tp4_power_pbo_de.powspctrm = tp4_power_pbo_de.powspctrm';
design = zeros(1,size(tp4_power_led_de.powspctrm,1) + size(tp4_power_pbo_de.powspctrm,1));
design(1,1:size(tp4_power_led_de.powspctrm,1)) = 1;
design(1,(size(tp4_power_led_de.powspctrm,1)+1):(size(tp4_power_led_de.powspctrm,1)+...
   size(tp4_power_pbo_de.powspctrm,1))) = 2;
cfg.design = design;  cfg.ivar = 1;   cfg.avgoverfreq = 'yes';
[stat4_de] = ft_freqstatistics(cfg, tp4_power_led_de, tp4_power_pbo_de);
tp4_power_led_de = ft_freqdescriptives(cfg, tp4_power_led_de);
tp4_power_pbo_de  = ft_freqdescriptives(cfg, tp4_power_pbo_de);
stat4_de.raweffect = mean(tp4_power_led_de.powspctrm',2) -
mean(tp4_power_pbo_de.powspctrm',2);

tp4_power_led_th.powspctrm = tp4_power_led_th.powspctrm';
tp4_power_pbo_th.powspctrm = tp4_power_pbo_th.powspctrm';
design = zeros(1,size(tp4_power_led_th.powspctrm,1) + size(tp4_power_pbo_th.powspctrm,1));
design(1,1:size(tp4_power_led_th.powspctrm,1)) = 1;
```

```
design(1,(size(tp4_power_led_th.powspctrm,1)+1):(size(tp4_power_led_th.powspctrm,1)+...
   size(tp4_power_pbo_th.powspctrm,1))) = 2;
cfg.design = design;  cfg.ivar = 1;   cfg.avgoverfreq = 'yes';
[stat4_th] = ft_freqstatistics(cfg, tp4_power_led_th, tp4_power_pbo_th);
tp4_power_led_th = ft_freqdescriptives(cfg, tp4_power_led_th);
tp4_power_pbo_th  = ft_freqdescriptives(cfg, tp4_power_pbo_th);
stat4_th.raweffect = mean(tp4_power_led_th.powspctrm',2) - mean(tp4_power_pbo_th.powspctrm',2);

tp4_power_led_alp.powspctrm = tp4_power_led_alp.powspctrm';
tp4_power_pbo_alp.powspctrm = tp4_power_pbo_alp.powspctrm';
design = zeros(1,size(tp4_power_led_alp.powspctrm,1) + size(tp4_power_pbo_alp.powspctrm,1));
design(1,1:size(tp4_power_led_alp.powspctrm,1)) = 1;
design(1,(size(tp4_power_led_alp.powspctrm,1)+1):(size(tp4_power_led_alp.powspctrm,1)+...
   size(tp4_power_pbo_alp.powspctrm,1))) = 2;
cfg.design = design;  cfg.ivar = 1;   cfg.avgoverfreq = 'yes';
[stat4_alp] = ft_freqstatistics(cfg, tp4_power_led_alp, tp4_power_pbo_alp);
tp4_power_led_alp = ft_freqdescriptives(cfg, tp4_power_led_alp);
tp4_power_pbo_alp  = ft_freqdescriptives(cfg, tp4_power_pbo_alp);
stat4_alp.raweffect = mean(tp4_power_led_alp.powspctrm',2) -
mean(tp4_power_pbo_alp.powspctrm',2);

tp4_power_led_beta.powspctrm = tp4_power_led_beta.powspctrm';
tp4_power_pbo_beta.powspctrm = tp4_power_pbo_beta.powspctrm';
design = zeros(1,size(tp4_power_led_beta.powspctrm,1) + size(tp4_power_pbo_beta.powspctrm,1));
design(1,1:size(tp4_power_led_beta.powspctrm,1)) = 1;
design(1,(size(tp4_power_led_beta.powspctrm,1)+1):(size(tp4_power_led_beta.powspctrm,1)+...
   size(tp4_power_pbo_beta.powspctrm,1))) = 2;
cfg.design = design;  cfg.ivar = 1;   cfg.avgoverfreq = 'yes';
[stat4_beta] = ft_freqstatistics(cfg, tp4_power_led_beta, tp4_power_pbo_beta);
tp4_power_led_beta = ft_freqdescriptives(cfg, tp4_power_led_beta);
```

```
tp4_power_pbo_beta  = ft_freqdescriptives(cfg, tp4_power_pbo_beta);

stat4_beta.raweffect = mean(tp4_power_led_beta.powspctrm',2) -
mean(tp4_power_pbo_beta.powspctrm',2);


tp4_power_led_gamm.powspctrm = tp4_power_led_gamm.powspctrm';

tp4_power_pbo_gamm.powspctrm = tp4_power_pbo_gamm.powspctrm';

design = zeros(1,size(tp4_power_led_gamm.powspctrm,1) +
size(tp4_power_pbo_gamm.powspctrm,1));

design(1,1:size(tp4_power_led_gamm.powspctrm,1)) = 1;

design(1,(size(tp4_power_led_gamm.powspctrm,1)+1):(size(tp4_power_led_gamm.powspctrm,1)+...
   size(tp4_power_pbo_gamm.powspctrm,1))) = 2;

cfg.design = design;  cfg.ivar = 1;   cfg.avgoverfreq = 'yes';

[stat4_gamm] = ft_freqstatistics(cfg, tp4_power_led_gamm, tp4_power_pbo_gamm);

tp4_power_led_gamm = ft_freqdescriptives(cfg, tp4_power_led_gamm);

tp4_power_pbo_gamm  = ft_freqdescriptives(cfg, tp4_power_pbo_gamm);

stat4_gamm.raweffect = mean(tp4_power_led_gamm.powspctrm',2) -
mean(tp4_power_pbo_gamm.powspctrm',2);


%% plotting

if length(find(stat4_de.prob<st_lim))>1

   cfg = [];

   cfg.alpha  = st_lim; colormap jet; cfg.parameter = 'raweffect';

   cfg.layout = 'biosemi64.lay';cfg.highlightcolorpos = [0 0 0]; cfg.highlightcolorneg = [1 1 0];

   cfg.subplotsize = [1 1]; cfg.colorbar   = 'yes'; cfg.zlim = [-0.3 0.3];

   cfg.highlightsizeseries = [10 10 10 10 10 10]; ft_clusterplot(cfg, stat4_de);

end


if length(find(stat4_th.prob<st_lim))>1

   cfg = [];

   cfg.alpha  = st_lim; colormap jet; cfg.parameter = 'raweffect';

   cfg.layout = 'biosemi64.lay';cfg.highlightcolorpos = [0 0 0];    cfg.highlightcolorneg = [1 1 0];
```

```
   cfg.subplotsize = [1 1];       cfg.colorbar   = 'yes';     cfg.zlim = [-0.3 0.3];
   cfg.highlightsizeseries = [10 10 10 10 10 10]; ft_clusterplot(cfg, stat4_th);
end

if length(find(stat4_alp.prob<st_lim))>1
   cfg = []; cfg.alpha  = st_lim; colormap jet; cfg.parameter = 'raweffect';
   cfg.layout = 'biosemi64.lay';cfg.highlightcolorpos = [0 0 0]; cfg.highlightcolorneg = [1 1 0];
   cfg.subplotsize = [1 1]; cfg.colorbar   = 'yes'; cfg.zlim = [-0.3 0.3];
   cfg.highlightsizeseries = [10 10 10 10 10 10]; ft_clusterplot(cfg, stat4_alp);
end

if length(find(stat4_beta.prob<st_lim))>1
   cfg = [];
   cfg.alpha  = st_lim;    cfg.parameter = 'raweffect'; colormap jet;
   cfg.layout = 'biosemi64.lay';cfg.highlightcolorpos = [0 0 0]; cfg.highlightcolorneg = [1 1 0];
   cfg.subplotsize = [1 1]; cfg.colorbar   = 'yes'; cfg.zlim = [-0.3 0.3];
   cfg.highlightsizeseries = [10 10 10 10 10 10]; ft_clusterplot(cfg, stat4_beta);
end

if length(find(stat4_gamm.prob<st_lim))>1
   cfg = []; cfg.alpha  = st_lim; cfg.parameter = 'raweffect'; colormap jet;
   cfg.layout = 'biosemi64.lay';cfg.highlightcolorpos = [0 0 0]; cfg.highlightcolorneg = [1 1 0];
   cfg.subplotsize = [1 1]; cfg.colorbar = 'yes'; cfg.zlim = [-0.3 0.3];
   cfg.highlightsizeseries = [10 10 10 10 10 10]; ft_clusterplot(cfg, stat4_gamm);
end
```

C.7 GROUP-SVD COMPARISONS CHAPTER 4

Run SVD

```
clear all;  clc; % run svd on combined data of w1 and w4
```

```
cd('C:\nasa data2\SVD'); load('combined_data_w1_raw_norm.mat'); w1_data = all_sub_data;
cd('C:\nasa data2\SVD'); load('combined_data_w4_raw_norm.mat'); w4_data = all_sub_data;
all_sub_data = [w1_data w4_data]; [U,S,V]=svd(all_sub_data',0);
```

Calculate PSD

```
clear all;  clc; cd('C:\nasa data2\SVD'); load('after_svd_w1_w4.mat');
% svd plotting
   a = mean(S);  m = max(a);  m1 = 0.1*m;  x = 1:64; l1 = length(find(a>m1));
   figure;set(gcf, 'Position', get(0, 'Screensize'));
   scatter(x(1,1:l1),a(1,1:l1),500,'.r'); hold on;
   scatter(x(1,l1+1:end),a(1,l1+1:end),500,'.b');
   hold on;yline(m1,'--','LineWidth',1);
   ylabel('Weight of each component','FontSize',20,'FontWeight','bold');
   xlabel('SVD components','FontSize',20,'FontWeight','bold');
   title('Major SVD components','FontSize',20,'FontWeight','bold');

   figure; set(gcf, 'Position', get(0, 'Screensize')); % displaying the SVD components
   for i=1:l1
      subplot(2,6,i);
      topoplot(V(:,i),EEG.chanlocs);  set(gca,'Clim',[-0.25 0.25],'FontSize',15);colorbar;
   end

% for pwelch calculation
   load('w1_pts.mat');   a1 = [];
   for i=1:16
      a = [r1_pts(1,i) g1_pts(1,i) r2_pts(1,i) g2_pts(1,i) r3_pts(1,i) g3_pts(1,i) r4_pts(1,i) g4_pts(1,i)];
      a1 = [a1 a];
   end
   load('w4_pts.mat'); b1= [];
   for i=1:16
```

```
    a = [r1_pts(1,i) g1_pts(1,i) r2_pts(1,i) g2_pts(1,i) r3_pts(1,i) g3_pts(1,i) r4_pts(1,i) g4_pts(1,i)];
    b1 = [b1 a];
  end
  c = [a1 b1];    d = cumsum(c); clear a1 b1 c
  % 128 tps, 64 for w1 and 64 for w4
  fs = 512;k=1; % tpwise pwelch
  for i=2:2:256
    bb = U(d(1,i-2)+1:d(1,i),:);
    all_pwelch(:,:,k) = pwelch(bb,20*fs,10*fs,8*fs,fs);k=k+1; clear bb
  end
  k=1; % rest pwelch
  for i=1:8:256
    bb = U(d(1,i-8)+1:d(1,i),:);
    [rest_pwelch(:,:,k) fre] = pwelch(bb,20*fs,10*fs,8*fs,fs);k=k+1;
  end

a = find(fre==70); li=12;
rest_pwelch2 = rest_pwelch(1:a,:,:);all_pwelch2 = all_pwelch(1:a,:,:);fre2 = fre(1:a,1);
% normalization
k=1;
for i=1:4:128
  all_pwelch_norm(:,:,i:i+3) = all_pwelch2(:,:,i:i+3)./rest_pwelch2(:,:,k);k=k+1;
end
save('w1_w4_pwelch_after_svd.mat','-v7.3');
```

Separate into each frequency bands

```
clear all;clc;
load('w1_w4_pwelch_after_svd.mat'); all_pwelch_norm2 = all_pwelch_norm(:,1:li,:);
fre_lim = [find(fre2==0.5) find(fre2==4) find(fre2==7) find(fre2==13) find(fre2==30) find(fre2==70)];
```

```
% 128 is 4 tps for 16 sub so 64 w1 and 64 w4
w1.all_sub_pwelch = all_pwelch_norm2(:,:,1:64);
w4.all_sub_pwelch = all_pwelch_norm2(:,:,65:128);

for aaan=1 % seprate into tp3,tp4 and bands
   a = 3:4:64; w1.tp3 = w1.all_sub_pwelch(:,:,a); w4.tp3 = w4.all_sub_pwelch(:,:,a); clear a
   a = 4:4:64; w1.tp4 = w1.all_sub_pwelch(:,:,a); w4.tp4 = w4.all_sub_pwelch(:,:,a); clear a

   w1.de_tp3 = reshape(mean(w1.tp3(fre_lim(1,1):fre_lim(1,2),:,:)),12,16);
   w1.th_tp3 = reshape(mean(w1.tp3(fre_lim(1,2):fre_lim(1,3),:,:)),12,16);
   w1.alp_tp3 = reshape(mean(w1.tp3(fre_lim(1,3):fre_lim(1,4),:,:)),12,16);
   w1.beta_tp3 = reshape(mean(w1.tp3(fre_lim(1,4):fre_lim(1,5),:,:)),12,16);
   w1.gamm_tp3 = reshape(mean(w1.tp3(fre_lim(1,5):fre_lim(1,6),:,:)),12,16);

   w1.de_tp4 = reshape(mean(w1.tp4(fre_lim(1,1):fre_lim(1,2),:,:)),12,16);
   w1.th_tp4 = reshape(mean(w1.tp4(fre_lim(1,2):fre_lim(1,3),:,:)),12,16);
   w1.alp_tp4 = reshape(mean(w1.tp4(fre_lim(1,3):fre_lim(1,4),:,:)),12,16);
   w1.beta_tp4 = reshape(mean(w1.tp4(fre_lim(1,4):fre_lim(1,5),:,:)),12,16);
   w1.gamm_tp4 = reshape(mean(w1.tp4(fre_lim(1,5):fre_lim(1,6),:,:)),12,16);

   w4.de_tp3 = reshape(mean(w4.tp3(fre_lim(1,1):fre_lim(1,2),:,:)),12,16);
   w4.th_tp3 = reshape(mean(w4.tp3(fre_lim(1,2):fre_lim(1,3),:,:)),12,16);
   w4.alp_tp3 = reshape(mean(w4.tp3(fre_lim(1,3):fre_lim(1,4),:,:)),12,16);
   w4.beta_tp3 = reshape(mean(w4.tp3(fre_lim(1,4):fre_lim(1,5),:,:)),12,16);
   w4.gamm_tp3 = reshape(mean(w4.tp3(fre_lim(1,5):fre_lim(1,6),:,:)),12,16);

   w4.de_tp4 = reshape(mean(w4.tp4(fre_lim(1,1):fre_lim(1,2),:,:)),12,16);
   w4.th_tp4 = reshape(mean(w4.tp4(fre_lim(1,2):fre_lim(1,3),:,:)),12,16);
   w4.alp_tp4 = reshape(mean(w4.tp4(fre_lim(1,3):fre_lim(1,4),:,:)),12,16);
   w4.beta_tp4 = reshape(mean(w4.tp4(fre_lim(1,4):fre_lim(1,5),:,:)),12,16);
```

```
   w4.gamm_tp4 = reshape(mean(w4.tp4(fre_lim(1,5):fre_lim(1,6),:,:)),12,16);
end
save('w1_w4_band_wise.mat');
```

Bar plots

```
% bar plot them
clear all; clc; cd('C:\nasa data2\SVD');load('w1_w4_band_wise.mat');
for data_segregation=1 % divide into tp3, tp4 and bands
   w1_pl.de_tp3 = w1.de_tp3(:,1:9); w1_pl.th_tp3 = w1.th_tp3(:,1:9);
   w1_pl.alp_tp3 = w1.alp_tp3(:,1:9); w1_pl.beta_tp3 = w1.beta_tp3(:,1:9);
   w1_pl.gamm_tp3 = w1.gamm_tp3(:,1:9);
   w1_led.de_tp3 = w1.de_tp3(:,10:16); w1_led.th_tp3 = w1.th_tp3(:,10:16);
   w1_led.alp_tp3 = w1.alp_tp3(:,10:16); w1_led.beta_tp3 = w1.beta_tp3(:,10:16);
   w1_led.gamm_tp3 = w1.gamm_tp3(:,10:16);
   w1_pl.de_tp4 = w1.de_tp4(:,1:9); w1_pl.th_tp4 = w1.th_tp4(:,1:9);
   w1_pl.alp_tp4 = w1.alp_tp4(:,1:9); w1_pl.beta_tp4 = w1.beta_tp4(:,1:9);
   w1_pl.gamm_tp4 = w1.gamm_tp4(:,1:9);
   w1_led.de_tp4 = w1.de_tp4(:,10:16); w1_led.th_tp4 = w1.th_tp4(:,10:16);
   w1_led.alp_tp4 = w1.alp_tp4(:,10:16); w1_led.beta_tp4 = w1.beta_tp4(:,10:16);
   w1_led.gamm_tp4 = w1.gamm_tp4(:,10:16); clear w1

   w4_pl.de_tp3 = w4.de_tp3(:,1:8); w4_pl.th_tp3 = w4.th_tp3(:,1:8);
   w4_pl.alp_tp3 = w4.alp_tp3(:,1:8); w4_pl.beta_tp3 = w4.beta_tp3(:,1:8);
   w4_pl.gamm_tp3 = w4.gamm_tp3(:,1:8);
   w4_led.de_tp3 = w4.de_tp3(:,9:16); w4_led.th_tp3 = w4.th_tp3(:,9:16);
   w4_led.alp_tp3 = w4.alp_tp3(:,9:16); w4_led.beta_tp3 = w4.beta_tp3(:,9:16);
   w4_led.gamm_tp3 = w4.gamm_tp3(:,9:16);
   w4_pl.de_tp4 = w4.de_tp4(:,1:8); w4_pl.th_tp4 = w4.th_tp4(:,1:8);
   w4_pl.alp_tp4 = w4.alp_tp4(:,1:8); w4_pl.beta_tp4 = w4.beta_tp4(:,1:8);
```

```
    w4_pl.gamm_tp4 = w4.gamm_tp4(:,1:8);
    w4_led.de_tp4 = w4.de_tp4(:,9:16); w4_led.th_tp4 = w4.th_tp4(:,9:16);
    w4_led.alp_tp4 = w4.alp_tp4(:,9:16); w4_led.beta_tp4 = w4.beta_tp4(:,9:16);
    w4_led.gamm_tp4 = w4.gamm_tp4(:,9:16); clear w4 aa bb cc afkj
end

% one sample non parametric t test
for one_sample_testing=1
    w4_tp4_de = w4_led.de_tp4 - w4_pl.de_tp4; w4_tp4_th = w4_led.th_tp4 - w4_pl.th_tp4;
    w4_tp4_alp = w4_led.alp_tp4 - w4_pl.alp_tp4; w4_tp4_beta = w4_led.beta_tp4 - w4_pl.beta_tp4;
    w4_tp4_gamm = w4_led.gamm_tp4 - w4_pl.gamm_tp4;
    for i=1:12
        w4_tp4_st.de(1,i) = signrank(w4_tp4_de(i,:));
        w4_tp4_st.th(1,i) = signrank(w4_tp4_th(i,:));
        w4_tp4_st.alp(1,i) = signrank(w4_tp4_alp(i,:));
        w4_tp4_st.beta(1,i) = signrank(w4_tp4_beta(i,:));
        w4_tp4_st.gamm(1,i) = signrank(w4_tp4_gamm(i,:));
    end

    w1_tp4_de = w1_led.de_tp4 - w1_pl.de_tp4(:,3:9);
    w1_tp4_th = w1_led.th_tp4 - w1_pl.th_tp4(:,3:9);
    w1_tp4_alp = w1_led.alp_tp4 - w1_pl.alp_tp4(:,3:9);
    w1_tp4_beta = w1_led.beta_tp4 - w1_pl.beta_tp4(:,3:9);
    w1_tp4_gamm = w1_led.gamm_tp4 - w1_pl.gamm_tp4(:,3:9);
    for i=1:12
        w1_tp4_st.de(1,i) = signrank(w1_tp4_de(i,:));
        w1_tp4_st.th(1,i) = signrank(w1_tp4_th(i,:));
        w1_tp4_st.alp(1,i) = signrank(w1_tp4_alp(i,:));
        w1_tp4_st.beta(1,i) = signrank(w1_tp4_beta(i,:));
        w1_tp4_st.gamm(1,i) = signrank(w1_tp4_gamm(i,:));
```

```
    end
end

for i=1:12
    w1_bar.led_tp4(i,1) = mean(w1_led.de_tp4(i,:)); w1_bar.led_tp4(i,2) = mean(w1_led.th_tp4(i,:));
    w1_bar.led_tp4(i,3) = mean(w1_led.alp_tp4(i,:)); w1_bar.led_tp4(i,4) = mean(w1_led.beta_tp4(i,:));
    w1_bar.led_tp4(i,5) = mean(w1_led.gamm_tp4(i,:)); w1_bar.pl_tp4(i,1) = mean(w1_pl.de_tp4(i,:));
    w1_bar.pl_tp4(i,2) = mean(w1_pl.th_tp4(i,:)); w1_bar.pl_tp4(i,3) = mean(w1_pl.alp_tp4(i,:));
    w1_bar.pl_tp4(i,4) = mean(w1_pl.beta_tp4(i,:)); w1_bar.pl_tp4(i,5) = mean(w1_pl.gamm_tp4(i,:));

    w1_std.led_tp4(i,1) = std(w1_led.de_tp4(i,:),[],2)./7;
    w1_std.led_tp4(i,2) = std(w1_led.th_tp4(i,:),[],2)./7;
    w1_std.led_tp4(i,3) = std(w1_led.alp_tp4(i,:),[],2)./7;
    w1_std.led_tp4(i,4) = std(w1_led.beta_tp4(i,:),[],2)./7;
    w1_std.led_tp4(i,5) = std(w1_led.gamm_tp4(i,:),[],2)./7;
    w1_std.pl_tp4(i,1) = std(w1_pl.de_tp4(i,:),[],2)./9;
    w1_std.pl_tp4(i,2) = std(w1_pl.th_tp4(i,:),[],2)./9;
    w1_std.pl_tp4(i,3) = std(w1_pl.alp_tp4(i,:),[],2)./9;
    w1_std.pl_tp4(i,4) = std(w1_pl.beta_tp4(i,:),[],2)./9;
    w1_std.pl_tp4(i,5) = std(w1_pl.gamm_tp4(i,:),[],2)./9;

    w4_bar.led_tp4(i,1) = mean(w4_led.de_tp4(i,:)); w4_bar.led_tp4(i,2) = mean(w4_led.th_tp4(i,:));
    w4_bar.led_tp4(i,3) = mean(w4_led.alp_tp4(i,:)); w4_bar.led_tp4(i,4) = mean(w4_led.beta_tp4(i,:));
    w4_bar.led_tp4(i,5) = mean(w4_led.gamm_tp4(i,:)); w4_bar.pl_tp4(i,1) = mean(w4_pl.de_tp4(i,:));
    w4_bar.pl_tp4(i,2) = mean(w4_pl.th_tp4(i,:)); w4_bar.pl_tp4(i,3) = mean(w4_pl.alp_tp4(i,:));
    w4_bar.pl_tp4(i,4) = mean(w4_pl.beta_tp4(i,:)); w4_bar.pl_tp4(i,5) = mean(w4_pl.gamm_tp4(i,:));

    w4_std.led_tp4(i,1) = std(w4_led.de_tp4(i,:),[],2)./8;
    w4_std.led_tp4(i,2) = std(w4_led.th_tp4(i,:),[],2)./8;
    w4_std.led_tp4(i,3) = std(w4_led.alp_tp4(i,:),[],2)./8;
```

```
    w4_std.led_tp4(i,4) = std(w4_led.beta_tp4(i,:),[],2)./8;
    w4_std.led_tp4(i,5) = std(w4_led.gamm_tp4(i,:),[],2)./8;
    w4_std.pl_tp4(i,1) = std(w4_pl.de_tp4(i,:),[],2)./8;
    w4_std.pl_tp4(i,2) = std(w4_pl.th_tp4(i,:),[],2)./8;
    w4_std.pl_tp4(i,3) = std(w4_pl.alp_tp4(i,:),[],2)./8;
    w4_std.pl_tp4(i,4) = std(w4_pl.beta_tp4(i,:),[],2)./8;
    w4_std.pl_tp4(i,5) = std(w4_pl.gamm_tp4(i,:),[],2)./8;
end
clear i

for i=1:12 % led-pl
    w1_diff.tp4(i,1) = mean(w1_led.de_tp4(i,:)) - mean(w1_pl.de_tp4(i,:));
    w1_diff.tp4(i,2) = mean(w1_led.th_tp4(i,:)) - mean(w1_pl.th_tp4(i,:));
    w1_diff.tp4(i,3) = mean(w1_led.alp_tp4(i,:)) - mean(w1_pl.alp_tp4(i,:));
    w1_diff.tp4(i,4) = mean(w1_led.beta_tp4(i,:)) - mean(w1_pl.beta_tp4(i,:));
    w1_diff.tp4(i,5) = mean(w1_led.gamm_tp4(i,:)) - mean(w1_pl.gamm_tp4(i,:));

    w4_diff.tp4(i,1) = mean(w4_led.de_tp4(i,:)) - mean(w4_pl.de_tp4(i,:));
    w4_diff.tp4(i,2) = mean(w4_led.th_tp4(i,:)) - mean(w4_pl.th_tp4(i,:));
    w4_diff.tp4(i,3) = mean(w4_led.alp_tp4(i,:)) - mean(w4_pl.alp_tp4(i,:));
    w4_diff.tp4(i,4) = mean(w4_led.beta_tp4(i,:)) - mean(w4_pl.beta_tp4(i,:));
    w4_diff.tp4(i,5) = mean(w4_led.gamm_tp4(i,:)) - mean(w4_pl.gamm_tp4(i,:));
end

title_name = {'Tp4 Delta','Tp4 Theta','Tp4 Alpha','Tp4 Beta','Tp4 Gamma'};
figure; set(gcf, 'Position', get(0, 'Screensize'));
for i=1:5 % for all bands plot bar
    subplot(3,2,i); a = w1_bar.pl_tp4(:,i); a(:,2) = w1_bar.led_tp4(:,i);
    bar(a);     hold on;
    title(title_name(i),'FontSize',30,'FontWeight','bold'); clear a
```

```
    xlabel('SVD components','FontSize',15,'FontWeight','bold');
    ylabel('nP','FontSize',15,'FontWeight','bold');
end
```